International Scientific-Technical and Production Journal

The Paton WELDING JOURNAL

January 2010 # 1

English translation of the monthly «Avtomaticheskaya Svarka» (Automatic Welding) journal published in Russian since 1948

Founders: *E.O. Paton Electric Welding Institute of the NAS of Ukraine*
International Association «Welding»

Publisher: *International Association «Welding»*

Address:
E.O. Paton Electric Welding Institute,
International Association «Welding»,
11, Bozhenko str., 03680, Kyiv, Ukraine
Tel.: (38044) 287 67 57
Fax: (38044) 528 04 86
E-mail: journal@paton.kiev.ua
http://www.nas.gov.ua/pwj

State Registration Certificate
KV 4790 of 09.01.2001

Subscriptions:
$324, 12 issues per year,
postage and packaging included.
Back issues available.

CONTENTS

NUMERICAL ANALYSIS OF THE PROCESSES OF HEATING AND CONVECTIVE EVAPORATION OF METAL IN PULSE LASER TREATMENT

I.V. KRIVTSUN, I.L. SEMYONOV and **V.F. DEMCHENKO**
E.O. Paton Electric Welding Institute, NASU, Kiev, Ukraine

Mathematical model of the processes of heating, melting and evaporation of metal under the effect of a focused laser beam is suggested. The model allows describing thermal processes in the bulk of metal and gas-dynamic processes in a metal vapour flow occurring in laser treatment by using pulse lasers. Numerical analysis was conducted to study the processes of heating and convective evaporation of metal with a millisecond pulse of the Nd:YAG-laser beam affecting a low-carbon steel sample.

Keywords: *pulse laser, laser radiation, metal, temperature field, evaporation, metal vapour, Knudsen layer, gas-dynamic processes, mathematical model*

Investigation of physical processes occurring in interaction of the high-intensity laser beam with a material plays an important role in development of new technologies for laser welding and treatment of different materials, and first of all the metallic ones [1–4]. Of special interest for upgrading of such technologies as microwelding, engraving, drilling, etc. is investigation into the processes of interaction of the focused pulse and pulse-periodic laser beams with metals [5–8]. Such processes include absorption of the laser beam by metal, its heating, melting and subsequent evaporation accompanied by scattering of the metal vapour into a surrounding gas (convective evaporation mode). Normally, analysis of convective evaporation of metal to determine quantitative characteristics of the evaporation process (density, temperature and velocity of scattering of the vapour) is performed by using a model suggested by C. Knight [9]. This model is based on the assumptions that the vapour flow is unidimensional and stationary. However, both of the above assumptions are known to be invalid in a case of high-rate heating of metal with a focused pulse laser beam, as upon reaching boiling temperature T_b the melt surface at the heat spot centre continues heating up to the temperatures that are much in excess of T_b, and the vapour flowing from the heat spot experiences side unloading, this causing violation of the unidimensional flow pattern assumed in study [9]. The present study is aimed at analysis of applicability of different models describing convective evaporation of metal under the conditions of heating of a metal plate with the focused pulse laser beam (ionisation of vapour and formation of laser plasma being ignored).

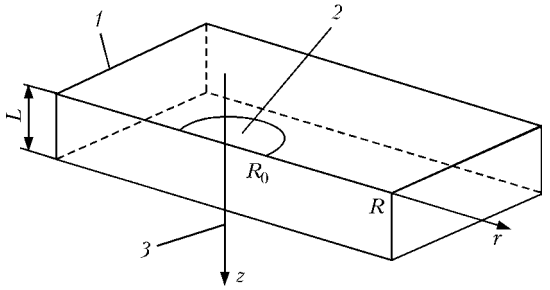

Figure 1. Scheme of heating of metal plate by laser beam: *1* — plate; *2* — heat spot; *3* — laser beam axis

Consider the process of heating of a metal plate with single pulse of the focused laser beam. Assuming the spatial distribution of the radiation intensity to be symmetric about the beam axis, formulate the mathematical model of heating of the plate in the axisymmetric statement. Introduce the cylindrical coordinate system as shown in Figure 1. Assume that radiation intensity I_0 is distributed uniformly over the heat spot with radius R_0 and remains constant during the pulse. Radiation intensity I_0 is determined through total energy W of the pulse, its duration τ and cross section area of the beam on the plate surface, $S = \pi P_0^2$, as follows: $I_0 = W/(\tau S)$.

The volumetric character of absorption of laser radiation can be ignored for the majority of metals. Then the thermal effect by the laser beam on a metal sample can be assumed to be a surface heat source distributed over the plate surface with density $q(r)$:

$$q(r) = \begin{cases} A(T_s)I_0 & \text{at } r \le R_0, \\ 0 & \text{at } r > R_0, \end{cases} \qquad (1)$$

where $A(T_s)$ is the coefficient of absorption of laser radiation, which depends upon the temperature on the metal surface, $T_s(r)$.

Write down the equation of thermal conductivity of a sample in the following form:

$$C(T)\rho(T)\frac{\partial T}{\partial t} = \frac{1}{r}\frac{\partial}{\partial r}\left(r\lambda(T)\frac{\partial T}{\partial r}\right) + \frac{\partial}{\partial z}\left(\lambda(T)\frac{\partial T}{\partial z}\right), \quad 0 < r < R, \quad 0 < z < L, \quad t > 0, \qquad (2)$$

where $C(T)$, $\rho(T)$ and $\lambda(T)$ are, respectively, the effective heat capacity of metal (allowing for the latent melting heat), density and coefficient of thermal conductivity.

Write down the boundary conditions for equation (2) in the following form:

$$\frac{\partial T}{\partial r}\Big|_{r=0} = 0; \quad T(r, L, t) = T(R, z, t) = T_0;$$
$$-\lambda(T_s)\frac{\partial T}{\partial z}\Big|_{z=0} = q - q_{rc} - q_e. \tag{3}$$

Here $q_{rc}(T_s) = \varepsilon\sigma(T_s^4 - T_0^4) + \alpha(T_s - T_0)$ are the losses of heat for radiation and heat exchange between the surface and environment; ε is the emissivity factor of the metal surface; σ is the Stefan–Boltzmann constant; α is the heat exchange coefficient; T_0 is the ambient temperature; $q_e(T_s) = \kappa q_m(T_s)$ is the specific heat flow carried away by the vapour from the melt surface; κ is the specific vaporization heat; $q_m(T_s) = \overline{\rho u}$ is the specific mass flow of the vapour; $\overline{\rho}$ and $\overline{u}$ are, respectively, the density and velocity of the metal vapour near the evaporating surface.

To close problems (2) and (3), it is necessary to use the model of convective evaporation of metal, allowing calculation of velocity $\overline{u}$ and density $\overline{\rho}$. Within the framework of the Knight's model, structure of the unidimensional subsonic flow of the vapour can be described as follows (Figure 2): the shock wave propagates via an ambient gas, followed by a contact discontinuity that is a contact region between the ambient gas and expanding metal vapour.

The Knudsen layer with thickness of an order of several lengths of the free path exists near the evaporating metal surface, outside which (in the gas-dynamic flow region) the equilibrium is established on translational degrees of freedom of the vapour particles. Study [9] suggests the following dependencies relating density $\overline{\rho}$ and temperature $\overline{T}$ of the vapour at the Knudsen layer boundary to saturated vapour density ρ_s and evaporating surface temperature T_s:

$$\frac{\overline{T}}{T_s} = \left[\sqrt{1 + \pi\left(\frac{\gamma-1}{\gamma+1}\frac{m}{2}\right)^2} - \sqrt{\pi}\,\frac{\gamma-1}{\gamma+1}\frac{m}{2}\right]^2, \tag{4}$$

$$\frac{\overline{\rho}}{\rho_s} = \sqrt{\frac{T_s}{\overline{T}}}\left[\left(m^2 + \frac{1}{2}\right)e^{m^2}\operatorname{erfc}(m) - \frac{m}{\sqrt{\pi}}\right] + \frac{1}{2}\frac{T_s}{\overline{T}}\left[1 - \sqrt{\pi}\, m e^{m^2}\operatorname{erfc}(m)\right]. \tag{5}$$

Here $m = \overline{u}/\sqrt{2\Re\overline{T}} = \sqrt{\gamma/2}\overline{\mathrm{M}}$; $\Re$ is the gas constant; $\gamma = 5/3$ is the adiabatic exponent of the vapour, which is assumed to be a monatomic ideal gas; and $\overline{\mathrm{M}}$ is the Mach number at the Knudsen layer boundary.

Pressure of the saturated vapour can be found from the Clausius–Clayperon equation, and density — from the equation of state of the ideal gas, $\overline{p} = \rho\Re\overline{T}$. Velocity $\overline{u}$ and pressure $\overline{p}$ are related to density ρ_0 and pressure in the ambient gas through the shock wave relationship [9]

$$\overline{u} = \frac{\overline{p} - p_0}{\sqrt{\frac{\rho_0}{2}(\overline{p}(\gamma+1) + p_0(\gamma-1))}}. \tag{6}$$

One non-linear equation for determination of velocity $\overline{u}$ can be derived from relationships (4) through (6) (the possibility of using conjugate model (2)–(6) is limited by the Knight assumption of the stationary character of the vapour flow).

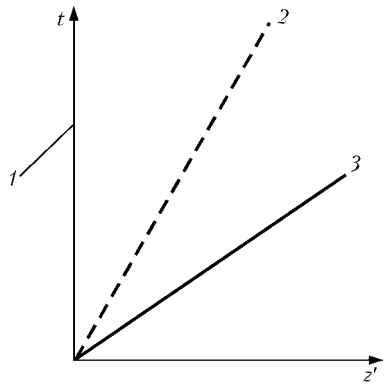

Figure 2. Scheme of unidimensional scattering of vapour [9]: *1* — Knudsen layer; *2* — contact discontinuity; *3* — shock wave

Consider the problem of non-stationary gas dynamics of the metal vapour by keeping, as earlier, to the assumption of a unidimensional flow pattern. Let Oz' be the axis of the cylindrical coordinate system, which is directed normal to the plate surface towards the vapour phase. At a high Reynolds number (velocity of scattering of the vapour is of an order of 500–700 m/s), the Euler equation can be used to describe gas-dynamics of the vapour-gas mixture:

$$\frac{\partial \mathbf{U}}{\partial t} + \frac{\partial \mathbf{F}}{\partial z'} = 0, \quad z' \in [0, H], \tag{7}$$

where $\mathbf{U} = (\rho_m, \rho, \rho_u, E)$; $\mathbf{F} = (\rho_m u, \rho u, \rho u^2 + p)$; $(E + p)u)$; ρ, u and p are the density, velocity and pressure of the mixture, respectively; ρ_m is the density of the metal vapour; $E = \rho e + \rho u^2/2$ is the energy of the mixture; and $e = p/\rho(\gamma - 1)$ is the internal energy.

Integrate equation (7) with respect to the following boundary and initial conditions:

$$\frac{\partial \mathbf{U}}{\partial z'}\Big|_{z'=H} = 0, \quad t > 0, \tag{8}$$

$$u(0, t) = u_{0+} + \frac{p(0, t) - p_{0+}}{\sqrt{\frac{\rho_{0+}}{2}[p(0, t)(\gamma+1) + p_{0+}(\gamma-1)]}},$$
$$\rho_m(0, t) = \rho(0, t), \quad p(0) = p(0, t)RT, \quad t \geq 0; \tag{9}$$

$$p(z', 0) = p_0, \; u(z', 0) = 0, \quad \rho(z', 0) = \rho_0, \quad \rho_m(z', 0) = 0, \quad 0 < z' < H, \tag{10}$$

where $p_{0+} = p(+0, t)$; $\rho_{+0} = \rho(+0, t)$ and $u_{+0} = u(+0, t)$.

Density ρ and temperature T at $z' = 0$ and $t \geq 0$ are determined from conditions (4) and (5), assuming that $\overline{\rho} = \rho$, $\overline{T} = T$, and $\overline{u} = u(0, t)$.

The Peacemen–Rachford method [10] with local non-linearity iterations in difference analogue of the condition of local energy balance on the plate surface was used to find numerical solution for problem (2) and (3). The problem of non-stationary gas dynamics (7) through (10) was solved by the Godunov method of the second order of accuracy [11].

Consider heating of the low-carbon steel plate with single pulse of the focused laser beam having the following parameters: $I_0 = 5\cdot10^6$ W/cm^2, $\tau = 1$ ms, and $R_0 = 0.1$ mm. This corresponds, e.g. to characteristic

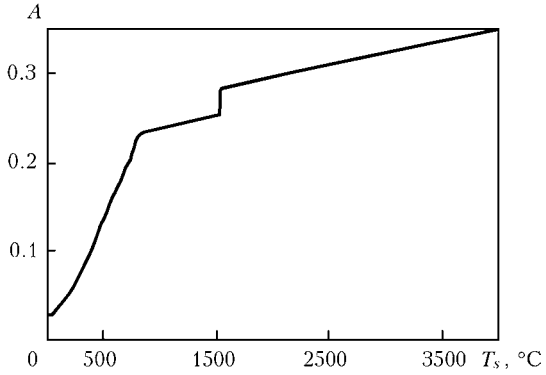

Figure 3. Temperature dependence of coefficient of absorption of Nd:YAG-laser radiation on low-carbon steel sample

operating parameters of the pulse Nd:YAG laser, which is part of the welding, cutting and deep engraving unit [12]. The following values were chosen for plate thickness L and calculation domain radius R (see Figure 1): L = 1 mm and R = 2 mm. Thermal-physical properties of low-carbon steel were taken from study [13], and corresponding temperature dependence of the coefficient of absorption of laser radiation was calculated from the data of studies [14–16] (Figure 3). Iron was used as an evaporating material, and air under normal conditions was used as an atmospheric gas.

Let us conduct comparative analysis of solution of the self-consistent problem of heating (1) through (3)

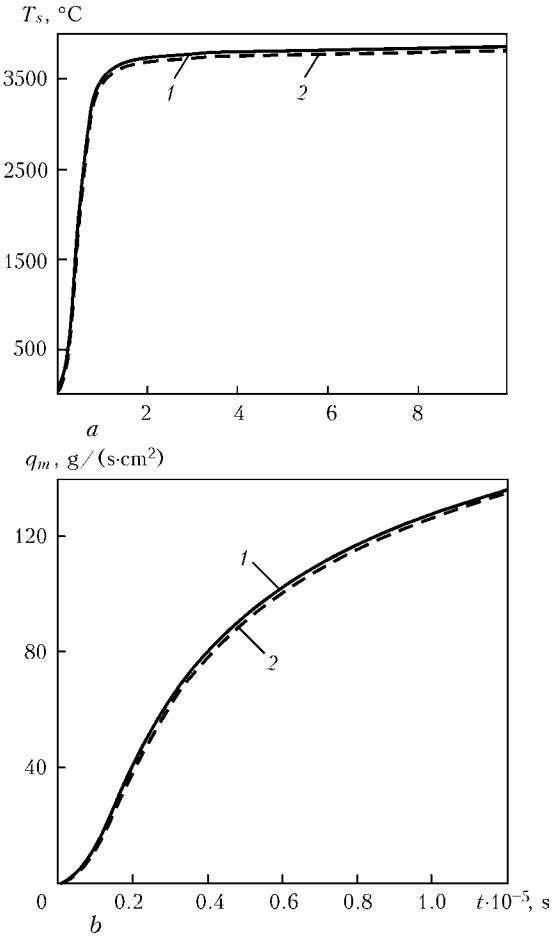

Figure 4. Dynamics of variations in metal temperature at the heat spot centre (*a*) and mass flow from the melt surface (*b*): *1* — non-stationary model; *2* — stationary model

and convective evaporation of metal for two models of gas-dynamics of the vapour: stationary [9] and non-stationary (4), (5) and (7) through (10) for a case of heating of the plate with a laser radiation pulse. The calculation results are shown in Figures 4 and 5 (the time in Figures 4, *b* and 5 is counted out from the beginning of evaporation). At the chosen parameters of the laser pulse, temperature at the centre of the heat spot reaches the boiling point during 7 μs (Figure 4, *a*), and it continues growing to 3800 °C for approximately 80 μs, after which it remains almost constant up to the end of the pulse. In a mode of stabilisation of the metal surface temperature, due to laser heating the heat flow is compensated for by the losses of heat for evaporation and, partially, by the radiant heat exchange between the surface and environment.

By the time moment (with respect to the beginning of evaporation) when the metal surface temperature stops varying with time, the shock wave has moved to a distance that is much in excess of the characteristic size of domain of the gas-dynamic problem solution (e.g. diameter of the heat spot), and no longer affects kinetics of the process of evaporation of metal from the melt surface. If the time during which the molten metal surface reaches the stationary value of temperature tends to zero (infinitely high heating rate), the gas-dynamic characteristics of the flow (velocity and pressure) correspond to the Knight model. In spite of the fact that in the non-stationary model of convective evaporation these characteristics differ from the Knight idealised flow scheme (see Figure 5), the values of the specific mass flow of the vapour at the Knudsen layer boundary calculated from the stationary and non-stationary evaporation models almost coincide (see Figure 4, *b*). This is explained by the fact that the time during which the surface reaches the stationary value of temperature (see Figure 4, *a*) is much shorter than the characteristic time of setting of the gas-dynamic processes. Therefore, it might be expected that a more substantial difference in structure of the flow and, accordingly, in value of the specific mass flow, $q_m(t)$, will occur with decrease in the heating rate.

To illustrate the last statement, consider heating of the plate with laser radiation of lower intensity $I_0 = 7\cdot10^5$ W/cm^2. In contrast to the above heating conditions, differences between the stationary and non-stationary evaporation models at low heating rates become more substantial in terms of the thermal problem solution (Figure 6). Therefore, at lower heating rates it is necessary to allow for the non-stationary character of the gas-dynamic processes.

The above models are valid for evaporation of metal with a developed liquid surface (with unlimited flat surface). In evaporation from the heat spot of a small diameter, as is the case of the focused laser beam affecting the surface, the assumption of a unidimensional structure of the gas-dynamic flow is violated. To study the effect of side scattering of the vapour, consider the two-dimensional problem of gas dynamics for a vapour-gas mixture in the axisymmetric statement. The Euler equations in the cylindrical coordinate system (r, z') have the following form:

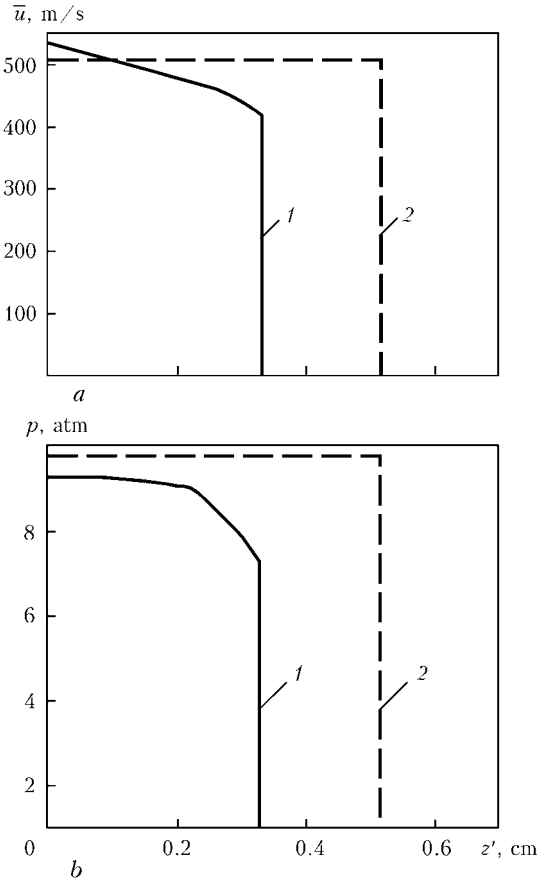

Figure 5. Distribution of velocity of vapour (*a*) and gas-dynamic pressure (*b*) in vapour phase at $t = 6.7 \cdot 10^{-6}$ s: *1*, *2* — same as in Figure 4

$$\frac{\partial \mathbf{U}}{\partial t} + \frac{\partial \mathbf{F}}{\partial r} + \frac{\partial \mathbf{G}}{\partial z'} = -\frac{\mathbf{f}}{r}. \qquad (11)$$

Here $\mathbf{U} = (\rho_1, \rho, \rho u, \rho v, E)$; $\mathbf{f} = (\rho_1 u, \rho u, \rho u, (E + p)u)$; $\mathbf{F} = (\rho_m u, \rho u, \rho u^2 + p, \rho uv, (E + p)u)$; $\mathbf{G} = (\rho_m v, \rho v, \rho uv, \rho v^2 + p, (E + p)v)$; u and v are the axial and radial components of the velocity vector, respectively; $E = \rho e + (\rho u^2 + \rho v^2)/2$ is the mixture energy; and $e = p/\rho(\gamma - 1)$.

Integrate equation (11) in a domain shown in Figure 7.

Boundaries Γ_4 and Γ_5 are the external boundaries of the flow region, Γ_3 is the symmetry axis, and Γ_6 is the metal surface outside the evaporation spot. The Knudsen layer on the surface of the liquid metal pool is modelled by a rectangular protrusion with boundaries Γ_1 and Γ_2. The boundary condition similar to (9) is set at boundary Γ_1. Tangential component of the velocity vector at this boundary is redefined from the flow region by the characteristic relationships. The non-flow boundary condition is set on the metal surface, symmetry condition is set on the flow axis, and non-reflection boundary conditions are set at external boundaries Γ_4 and Γ_5. The initial conditions are set to be as follows: $p = p_0$, $u = 0$, $v = 0$, $\rho = \rho_0$, and $\rho_1 = 0$, where p_0 and ρ_0 are the pressure and density of the atmospheric gas.

The formulated problem of two-dimensional gas dynamics was solved by the Godunov method of the second order of accuracy (TVD scheme). Sizes of the calculation domain were chosen to be as follows: length of boundary Γ_1 was 0.015 cm, and Knudsen layer width Γ_2 was assumed to be 0.006 cm (proceeding from the estimation of mean length of the free path in the atmospheric gas and metal vapours immediately over the melt). Sizes of external boundaries Γ_5 and Γ_6 of the calculation domain were assumed to be equal to $6L_0$. Air under normal conditions was assumed to be the ambient gas, and temperature of the evaporating metal surface was assumed to be constant and equal to 4000 °C.

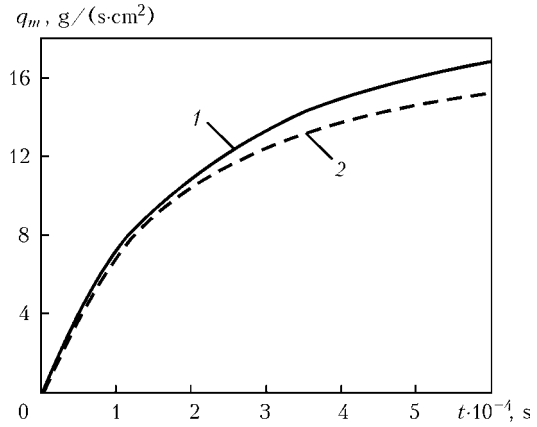

Figure 6. Time variations of mass flow of vapour at $I_0 = 7 \cdot 10^5$ W/cm^2: *1*, *2* — same as in Figure 4

The calculation results are shown in Figures 8 and 9. The qualitatively different flow pattern takes place in a case of side unloading of the vapour flow. Velocity at the Knudsen layer boundary does not reach the stationary value (like in the unidimensional case), but monotonously grows until the Mach number becomes equal to one (Figure 8, *b*). After that a stationary compression shock forms in the vapour flow region with a contact discontinuity propagating behind it at a constant velocity. The compression shock forms because pressure in a region between the Knudsen layer boundary and ambient gas becomes lower than the atmospheric one (region of decreased pressure in Figure 8, *a*). The shock wave at the time moment under consideration is at a distance of 0.075 cm from the Knudsen layer boundary, the decreased pressure region and compression shock being at a distance of 0.05 cm. Such flow pattern was fixed in [5] in investigation of the impact on metal by the pulse laser beam. It should be noted that the similar structure of

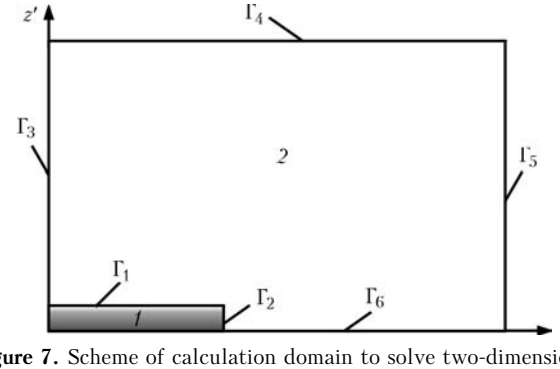

Figure 7. Scheme of calculation domain to solve two-dimensional equations of gas dynamics: *1* — Knudsen layer; *2* — gas-dynamic region

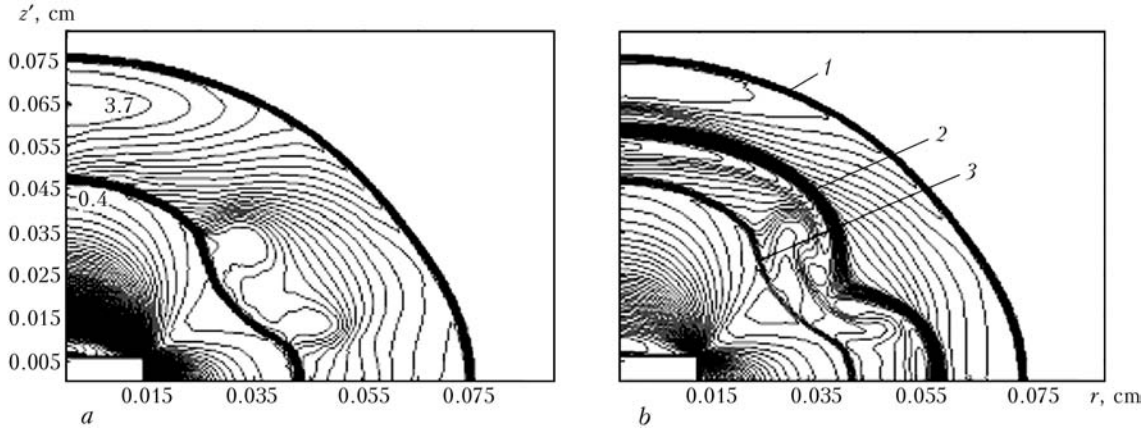

Figure 8. Isolines of pressure p/p_0 (*a*) and density (*b*) at $t = 4 \cdot 10^{-7}$ s: *1* — shock wave; *2* — contact discontinuity; *3* — compression shock

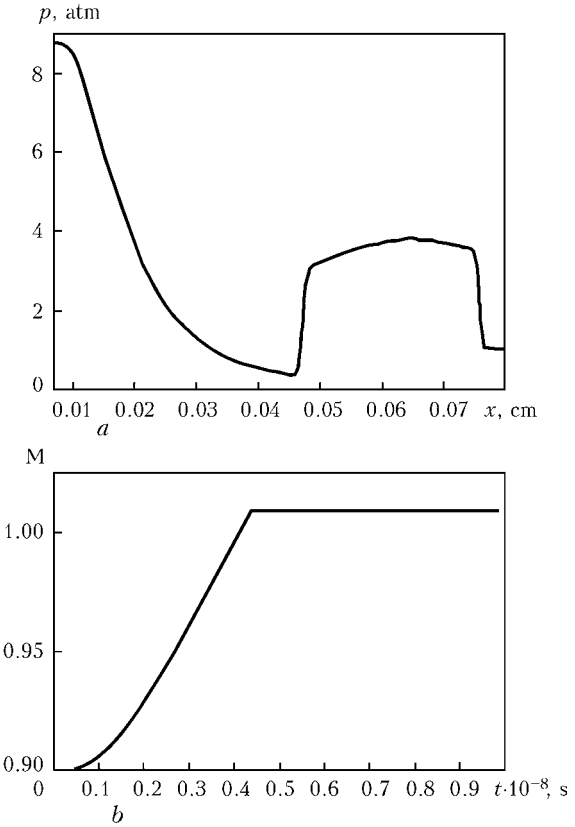

Figure 9. Distribution of pressure along the symmetry axis at $t = 4 \cdot 10^{-7}$ s (*a*) and time dependence of the maximal value of Mach number at the Knudsen layer boundary (*b*)

the flow occurs also in the case of a supersonic outflow of gas from the nozzle in a mode of underexpansion.

Consider the non-stationary conditions of heating of metal with the laser beam. The time of reaching the stationary temperature value by the surface is approximately three orders of magnitude longer than the time during which the Mach number at the Knudsen layer boundary becomes equal to one. Therefore, in the case of side unloading of the vapour the problem of metal heating with the laser beam can be solved with a sufficiently good approximation by assuming the Mach number at the Knudsen layer boundary to be equal to one. In this case, the mass flow can be found from relationships (4) and (5) without solving the gas dynamic problem.

It should be noted in conclusion that such characteristics as the thermal state of metal, density of the mass flow of the metal vapour, its scattering velocity, losses of heat for evaporation and pressure of the vapour recoil reaction, which are important in terms of technological applications, are determined not only by the conditions of metal heating, but also by the gas-dynamic processes occurring in the vapour phase. In a general case, the self-consistent model describing thermal processes in the bulk of metal and processes of heat and mass transfer in the Knudsen layer, as well as gas-dynamic processes in the vapour flow should be used to model the situation under consideration.

1. Arutyunyan, R.V., Baranov, V.Yu., Bolshov, L.A. et al. (1989) *Effect of laser radiation on materials*. Moscow: Nauka.
2. Vedenov, A.A., Gladush, G.G. (1985) *Physical processes in laser treatment of materials*. Moscow: Energoatomizdat.
3. Dulie, U. (1986) *Laser technology and analysis of materials*. Moscow: Mir.
4. *Anisimov, S.I., Imas, Ya.A., Romanov, G.S. et al.* (1970) Effect of high radiation power on metals. Moscow: Nauka.
5. Batarov, V.A., Bunkin, F.V., Prokhorov, A.M. et al. (1970) Stationary shock wave generated in stationary metal evaporation under the effect of laser radiation. *Pisma v Zhurnal Eksperim. i Teoret. Fiziki*, **11**, 113–118.
6. Gusarov, A.V., Gnedovets, A.G., Smurov, I. (2000) Gas dynamics of laser ablation: Influence of ambient atmosphere. *J. Appl. Phys.*, **88**, 4352–4364.
7. Afanasiev, Yu.V., Belenov, E.M., Krokhin, O.N. et al. (1969) Ionisation processes in laser plasma. *Pisma v Zhurnal Eksperim. i Teoret. Fiziki*, **10**, 553–557.
8. Vorobiov, V.S. (1993) Plasma generated in interaction of laser radiation with solid targets. *Ukr. Fizich. Zhurnal*, 163(**12**), 51–82.
9. Knight, C.J. (1979) Theoretical modelling of quick surface evaporation in presence of counterpressure. *Raketnaya Tekhnika i Kosmonavtika*, **5**, 81–86.
10. Peacemen, D.W., Rachford, H.H. (1955) The numerical solution of parabolic and elliptic differential equations. *J. Soc. Ind. Appl. Math.*, **3**, 28–41.
11. Kulikovsky, A.G., Pogorelov, N.V., Semyonov, A.Yu. (2001) *Mathematical problems in numerical solution of hyperbolic equation systems*. Moscow: Fizmatlit.
12. Kirichenko, V., Gryaznov, N., Krivtsun, I. (2008) Experimental facility for research on pulsed laser-microplasma welding. *The Paton Welding J.*, **8**, 26–30.
13. Hu, J., Tsai, H.L. (2007) Heat and mass transfer in gas metal arc welding. Pt 1. The arc. *Int. J. Heat and Mass Transfer*, **50**, 833–846.
14. Kikuo, U. (1972) Reflectivity of metals at high temperatures. *J. Appl. Phys.*, 43(**5**), 2376–2383.
15. Ordal, M.A., Long, L.L., Bell, R.J. et al. (1983) Optical properties of the metals Al, Co, Cu, Au, Fe, Pb, Ni, Pd, Pt, Ag, Ti and W in the infrared and far infrared. *Appl. Opt.*, 22(**7**), 1099–1119.
16. Miller, J. (1969) Optical properties of liquid metals at high temperatures. *Phil. Mag.*, 20(**12**), 1115–1132.

RISK OF FRACTURE OF PRESSURISED MAIN PIPELINE WITH DEFECTS OF THE TYPE OF WALL THINNING DURING REPAIR

V.I. MAKHNENKO, V.S. BUT, S.S. KOZLITINA and **O.I. OLEJNIK**
E.O. Paton Electric Welding Institute, NASU, Kiev, Ukraine

It is shown that welding repair of defects of the type of pipeline wall thinning by compensating the metal lost in the thinning zone by the deposited metal using low-current (~90 A) manual arc weld deposition is a sufficiently efficient technology. Wide application of this technology for repair of pressurised main pipelines is limited by the safety problem. Also, it is shown that the minimum admissible wall thickness in the defect zone under operating pressures depends upon the size of a defect along the generating line and, to a much lesser degree, upon its size on the circumference, as well as upon the thermal parameters of welding and accepted sequence of welding-up (deposition) of the defect.

Keywords: *main pipelines, pressure, thinning defects, minimal thickness, welding repair, welding sequence*

Repair of a linear part of main pipelines without their putting out of operation is a problem of current importance. The most common defects in such structures are caused by corrosion damages on the external surface of a pipe, which are accompanied by decrease in thickness of the wall metal. Normally, such defects are schematised by a certain spatial figure with dimensions S, c and a (Figure 1). In approximate description of this volume in a system of coordinates x, y, z (Figure 2) by the second-order surface in a form of

$$\left(\frac{2x}{S}\right)^2 + \left(\frac{2y}{c}\right)^2 + \left(\frac{z}{a}\right)^2 = 1, \qquad (1)$$

volume V of the filler metal required to weld up such a defect with no allowance for spattering is determined as follows:

$$V = \pi \frac{Sca}{6}. \qquad (2)$$

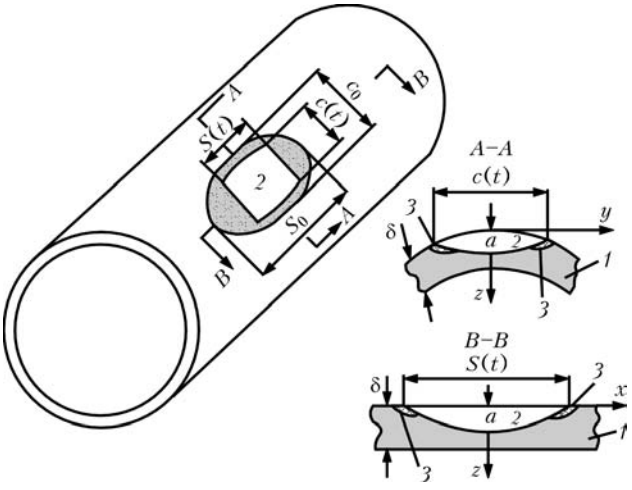

Figure 1. Schematic of pipe with thinning defect $a \times S \times c$: *1* — pipe; *2* — thinning defect; *3* — welded-up regions by time moment t

Time t_r necessary to compensate for the lost volume of metal, V, is equal to

$$t_r = \frac{V\gamma}{\alpha_d I_w} \xi, \qquad (3)$$

where γ is the specific weight of the deposited metal (7.8 g/cm^3 for steel pipes); α_d is the deposition efficiency equal to about 7.8 g/(A·h) for manual arc welding at low currents I_w; and $\xi > 1.0$ is the coefficient allowing for the losses of time for performing auxiliary operations.

At $\xi = 1.5$ and $I_w = 90$ A, one welder per shift (6 h) can fill up the volume of the deposited metal characterised by sizes S, c and a, and by the surface described by expression (1), this volume corresponding to product $Sca = 688 \cdot 10^3$ mm^3. Under the above conditions, sizes of the defects, which can be repaired by one welder per 6 h of operation at rather low operating parameters of manual fusion welding, are given in Table 1. It can be seen from the Table that welding repair of corrosion defects is a very efficient technology. However, its wide application for pressurised pipelines is limited by difficulties associated with ensuring safety in implementing this technology.

The matter of safety can be conditionally subdivided into two groups. The first group includes problems associated with the thermal effect of the welding

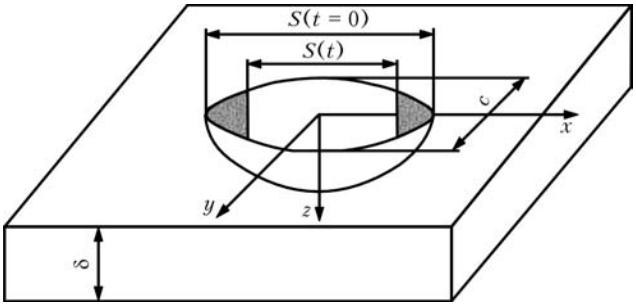

Figure 2. Schematic of welding repair of a defect with passes made on the pipe circumference (direction y) from ends of the defect to the centre

Sizes of thinning defects (mm) which can be repaired by one welder per shift at I_w = 90 A and ξ = 1.5

a = 2		a = 3		a = 4		a = 5		a = 6		a = 7		a = 8	
S	c	S	c	S	c	S	c	S	c	S	c	S	c
100	3440	100	2300	100	1470	100	1380	100	1150	100	980	100	860
200	1720	200	1150	200	735	200	690	200	575	200	490	200	430
400	860	300	575	400	375	400	345	400	290	400	245	400	115
800	430	400	290	800	185	800	172	800	145	800	122	800	60

arc and corresponding risk of burn-through or fracture of the pipeline wall as a result of decrease in its resistance to force loads (internal pressure, bending moments in repair). The second group relates to the problems of weldability of pipe steels under sufficiently rigid welding conditions and force loading, namely with prevention of cold (hydrogen-induced) cracking, as well as unfavourable microstructural changes capable of deteriorating performance of a pipeline region repaired by welding.

Available are publications on both first and second groups of safety issues. However, because of their complex and critical nature they require further investigation, as well as development of methods for prediction of consequences of application of these or those technological solutions.

This study considers the issues of maintaining integrity of a pipeline, which are directly associated with heating of a pipe wall by the welding arc in welding repair of thinning defects on the external surface, i.e. the first group of the safety issues. As applied to welding repair of isolated pit-like defects, these issues are considered in detail in study [1]. As to welding repair of defects of the thinning type, which are extensive both on the circumference and along the pipeline axis, these issues were experimentally investigated in studies [2, 3].

The results obtained provide important references to ultimate bounds of applicability of manual arc welding for repair of the above thinning defects. However, the absence of theoretical generalisation of the results limits their application for the cases outside the considered initial data.

This study suggests a mathematical model for estimation of the risk of violation of integrity of wall of a pressurised pipe under conditions of heating of the thinning zone in welding (see Figure 1). The model is based on tracing the temperature field during welding (weld deposition) of a defect by fixing changes in its dimensions $S(t)$ and $c(t)$ with time. With this calculation, the depth of the defect, $a_r(t)$, is determined at different time moments t from the maximal depth of penetration of temperature, T_r^{max}, at which resistance of a material to deformation is insignificant. For pipe steels, the value of T_r^{max} ranges from 720 to 1000 °C, according to different recommendations. The last value is in a rather good agreement with the experimental data [3], and the first one is more conservative.

According to the data of study [4], the condition of admissibility of a corrosion thinning defect with dimensions $S(t)$, $c(t)$ and $a_r(t)$ in a pipeline at time moment t can be written down as follows:

$$Y(t) = \delta - a_r^m(t) - [\delta]R_j > 0 \quad (j = S, c), \tag{4}$$

where

$$R_S = \begin{cases} 0.2, \text{ if } \lambda = \dfrac{1.285}{\sqrt{D[\delta]}} S \le 0.3475; \\ \left(0.9 - \dfrac{0.9}{\sqrt{1 + 0.48\lambda^2}}\right)\left(1.0 - \dfrac{0.9}{\sqrt{1 + 0.48\lambda^2}}\right)^{-1}, \text{ if } \lambda > 0.3475; \end{cases} \tag{5}$$

$$R_c = \begin{cases} 0.2, \text{ if} \dfrac{c}{D} \le 0.348, \\ \dfrac{-0.7358 + 10.511(c/D)^2}{1.0 + 13.838(c/D)^2}, \text{ if } \dfrac{c}{D} > 0.348; \end{cases}$$

D is the internal diameter of the pipeline; and $[\delta]$ is the admissible calculated thickness of the pipeline wall at the absence of defects, which depends upon the material of the pipe and its force loading, and is known for a given pipeline region.

As noted above, in welding repair of a given defect the $S(t)$, $c(t)$ and $a_r(t)$ values required for the calculation are determined depending upon the welding conditions, initial heating and sequence of deposition of separate passes. In the majority of cases it is enough to determine conditions for maintaining the integrity in deposition of the first layer to weld up the defect for $S(t) = S(0)$, or after deposition of end zones of the defect to substantially decrease the $S(t)$ value, compared with $S(0)$ (Figure 2).

For these purposes, it is possible to use modern methods of mathematical modelling of temperature fields in welding by an appropriate method. Below we will consider such a possibility for the case of arc welding-up of a thinning defect on the surface of a pipe of steel 17G1S with diameter D = 1420 mm, wall thickness δ = 20 mm and $[\delta]$ = 16 mm. Welding parameters were as follows: I_w = 120 A, U_a = 22 V, and v_w = 2 mm/s. The initial heating temperature within the defect zone, T_0, varied from 20 to 150 °C (for walls with thickness δ = 15 and 10 mm, using welding parameters with I_w = 90 A).

Welding repair was performed by depositing beads on the circumference of the pipe (direction y in Figure 2) from the ends of the defect along the generating line (direction x in Figure 2).

While modelling each pass, it was taken into account that the effective power of the welding arc, $q_e = \eta_U I_w U_a$, is introduced partially with the deposited metal, q_1, while the rest of the power, $q_2 = q_e - q_1$, is introduced by the normal law from a heat source moving at speed $v_w = 2$ mm/s.

The value of q_1 is determined from the following dependence:

$$q_1 = \frac{\alpha_d I_w}{3600\gamma}(T_f c\gamma + \kappa), \quad (6)$$

where T_f is the temperature of the filler metal; $c\gamma$ is the volumetric heat capacity of metal, and κ is the latent melting heat.

At $T_f = 2100$ °C, $\alpha_d = 8$ g/(A·h), $\gamma = 7.8$ g/cm^3, $\kappa = 2080$ J/cm^3, $I_w = 120$ A and $c\gamma = 5.2$ J/(cm^3·°C), it yields that $q_1 = 445$ W.

Accordingly, at $\eta = 0.8$ and $U_a = 22$ V, q_2 is equal to

$$q_2 = 2112 - 445 = 1667 \text{ W}.$$

Parameter q_2 has a distribution following the normal-circular law, when

$$g(r) = g_0 e^{-kr^2}, \quad (7)$$

where $g_0 = q_2 k/\pi$; $r^2 = (x - x_s)^2 + (y - y_s)^2$; $x_s = x_s(t)$ and $y_s = y_s(t)$ are the coordinates of the heat source at time moment t, and k is the concentration coefficient equal to 0.05 1/mm^2.

The data on temperature field $T(x, y, z, t)$ were obtained by using the software developed by the E.O. Paton Electric Welding Institute, which realises a corresponding numerical solution of the thermal conductivity problem for a volume limited by surface (1) allowing for the deposited metal, as well as by surfaces $z = \delta$ and $z = 0$, for which the conditions of heat exchange with the environment were set according to the Newton law with heat exchange coefficients α_1 for surface $z = 0$ and α_2 for $z = \delta$. Coefficient $\alpha_2 = 0.05$ W/(cm^2·°C) allows for heat exchange on the internal surface with a gas having a temperature of 40 °C and moving at a speed of 6 m/s, while $\alpha_1 = 0.005$ W/(cm^2·°C) allows for heat exchange on the external surface.

Thermal-physical properties of steel 17G1S were taken from the reference data depending upon the temperature, like in study [1].

Results of the calculations by using the described procedure in the form of minimum admissible thicknesses within the thinning zone

$$\delta_{min} = \begin{cases} \delta - a^{max}(t), \\ \delta - a_0, \end{cases}$$

where a^{max} is the maximal depth of T_f isotherm, starting from surface $z = 0$; and a_0 is the maximal depth according to (4) at c_0 and S_0 (5) with initial dimensions $a_0 \times c_0 \times S_0$ (is shown in Figure 3 depending upon the value of S_0). These data show the effect of wall thickness δ at $\delta = 20$, 15 and 10 mm and diameter $D = 1420$ mm, where admissible thicknesses $[\delta]$ at the absence of a defect were assumed to be 16, 12 and 8 mm, respectively.

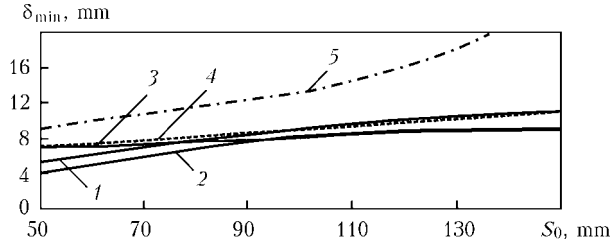

Figure 3. Results of calculation of minimal pipe thickness within the defect zone depending upon defect size S_0 at $c_0 = 70$ mm (see Figure 2), $D = 1420$ mm and welding parameters $I_w = 90$–120 A, $U_a = 22$ V and $v_w = 2$ mm/s: *1, 4, 5* — $\delta = 20$ mm, $[\delta] = 16$ mm; *2* — $\delta = 15$ mm, $[\delta] = 12$ mm; *3* — $\delta = 10$ mm, $[\delta] = 8$ mm; *1–3* — $T_0 = 150$ °C, $T_{cr} = 1000$ °C; *4* — $T_0 = 20$ °C, $T_{cr} = 750$ °C; *5* — $T_0 = 150$ °C, $T_{cr} = 750$ °C; *1, 4, 5* — $I_w = 120$ A; *2, 3* — $I_w = 90$ A

The initial temperature of heating of the defect zone, T_0, was varied from 20 to 150 °C, and critical temperature T_{cr} — from 750 to 1000 °C.

It follows from the data shown in Figure 3 that the minimal wall thickness within the zone of the defect under conditions of its welding repair corresponding to manual fusion arc welding at a current not higher than 120 A for $\delta = 20$ mm, and 90 A for $\delta = 15$ and 10 mm, at the initial heating temperature equal to 150 °C (corresponding to a considerable heating within the welding zone) depends upon defect dimensions S_0 along the pipe axis. However, at low δ and $[\delta]$ (Figure 3, curve *3*), this dependence grows from 6 mm at $S_0 = 50$ mm to about 9 mm at $S_0 = 150$ mm, whereas at $\delta = 20$ mm and $[\delta] = 16$ mm (Figure 3, curve *1*) this dependence grows from approximately 5 mm at $S_0 = 50$ mm to 11 mm at $S_0 = 150$ mm. Curve *2* in Figure 3, corresponding to $\delta = 15$ mm and $[\delta] = 12$ mm, lies between curves *3* and *1*, it being closer to curve *1* in a zone of low S_0 and closer to curve *3* at high S_0.

Curves *4* and *5* in Figure 3 show that critical temperature $T_{cr} = 720$–750 °C postulated in a number of suggestions leads to substantial overestimation of minimal wall thicknesses within the defect zone in terms of application of welding, compared with experimentally verified $T_{cr} \approx 1000$ °C [3], for modern pipe steels used for transportation of hydrocarbons.

It should be noted that in welding repair of the considered defect along the generating line, where length of the defect, $S(t)$, insignificantly varies with time, the minimal thickness within the given defect

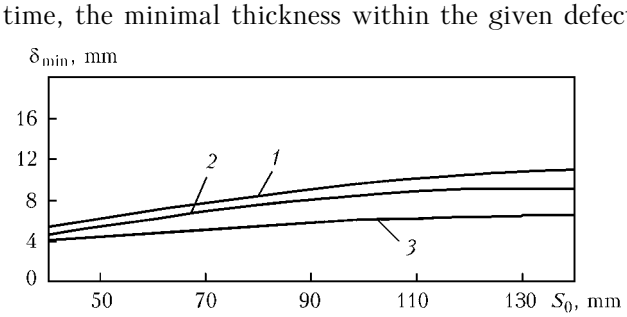

Figure 4. Effect of decrease in operating pressure on minimal thickness within the defect zone at $I_w = 120$ A, $T_0 = 150$ °C, $\delta = 20$ mm, $c_0 = 70$ mm for welding on the circumference: *1* — $p = 7.5$; *2* — 5.6; *3* — 3.75 MPa

zone for the welding parameters under consideration is determined by the depth of penetration of temperature T_{cr} in the zone of a maximal initial depth of the defect, a_0, i.e. approximately 5 mm above the curves in Figure 3, respectively: for curve *1* (δ = 20 mm) the minimal values of thickness within the defect zone will be δ_{min} = 9 mm at S_0 = 50 mm and δ_{min} = 16 mm at S_0 = 150 mm; for curve *2* (δ = 15 mm) it will be δ_{min} = 9.5 mm at S_0 = 50 mm and δ_{min} = 14 mm at S_0 = 150 mm. For δ = 10 mm, this welding sequence is inadmissible in terms of the accepted safety requirements.

Note the possibility of decreasing pressure in the pipeline as a method of improving safety of welding repair of defects of the type of thinning. Figure 4 shows the curves demonstrating the efficiency of this method for a case of large sizes of thinning.

CONCLUSIONS

1. In repair of thinning defects in main pipelines by arc welding, the minimum admissible thickness within the defect zone according to the safety requirements under operating pressures depends upon size S of the defect along the generating line, to a much lesser degree upon size c on the circumference, as well as upon the thermal parameters of welding and accepted sequence of welding-up of the defect.

2. In terms of the safety requirements, the best way of welding repair of defects is to deposit beads on the circumference, starting from the end regions located along the generating line, which allows decreasing the length of a defect in the indicated direction.

3. Worthy of notice from the practical standpoint is development of nomograms to evaluate the possibility of using welding with specific process parameters to repair the considered thinning defects, depending upon the geometric dimensions of the defect, such as S_0, c_0 and a_0, wall thickness δ, pipe diameter D and internal pressure in a pipeline.

1. Makhnenko, V.I., But, V.S., Velikoivanenko, E.A. et al. (2001) Mathematical modelling of pitting defects in active oil and gas pipelines and development of a numerical method for estimation of permissible parameters of arc welding repair of defects. *The Paton Welding J.*, **11**, 2–9.
2. Bruce, W.A., Mishier, H.D., Kiefner, J.F. (1993) *Repair of pipelines by direct deposition of weld metal*: A.G.A. Pipeline Research Committee Project PR-186-9110. Edison Welding Institute.
3. Bruce, W.A., Swatzel, J.F., Dorling, D.V. (2000) Repair of pipeline defects using weld deposition. In: *Proc. of 3rd Int. Pipeline Technology Conf.* (Brugge, Belgium, May 21–24, 2000).
4. *Fitness-for-service*: American Petroleum Institute Recommended Practice 579.

POSSIBILITIES FOR LOWERING DYNAMIC STRESS IN STRUCTURAL ELEMENTS OF MACHINES USING NANOSTRUCTURED COATINGS*

A.I. USTINOV[1], **A.P. ZINKOVSKY**[2], **I.G. TOKAR**[2] and **V.S. SKORODZIEVSKY**[3]
[1]E.O. Paton Electric Welding Institute, NASU, Kiev, Ukraine
[2]G.S. Pisarenko Institute for Problems of Strength, NASU, Kiev, Ukraine
[3]G.V. Kurdyumov Institute for Metal Physics, NASU, Kiev, Ukraine

The paper gives the results of experimental studies of the influence of structural charact eristics on physico-mechanical properties of coating materials and damping capacity of coated structural elements allow ing for such factors as temperature, frequency and amplitude of stress.

Keywords: *coating, material nanostructure, temperature, structural element, vibration frequency, logarithmic damping decrement, dynamic stress*

Progress of modern mechanical engineering leads to high requirements made of the reliability and fatigue life of both individual structural elements and machines as a whole. As most of them are operating under the conditions of a broad spectrum of dynamic loads, which may lead to failure and breaking up of structural elements, and can have catastrophic consequences, ensuring their dynamic strength is one of the key problems in achievement of reliable functioning during the required service life. This is particularly urgent for aviation gas turbine engines (AGTE), most of the defects in which (more than 60 %) detected during design, development and operation, are due to insufficient strength of the components and structural elements, and, primarily, blades. About 70 % of the defects are of vibration-related origin.

One of the most important technico-economic quality indices of mechanical engineering products is ensuring their vibration reliability. In most of the cases, however, it is impossible to eliminate hazardous resonance modes as a result of a considerable density of

*The article was prepared on the basis of results of accomplishment of the NASU targeted integrated program «Problems of Remaining Life and Safe Operation of Structures, Constructions and Machines» (2007–2009).

frequencies of natural and forced vibrations in operation of the considered objects. Therefore, various design-technological methods are used, lowering the risk of their consequences, among which the determinant factor is increase of damping capacity as a means of limitation of maximum resonance stresses of the most stressed structural elements.

In the case of AGTE compressor blades made of high-strength titanium alloys with low values of dissipative properties, one of the effective methods to improve the vibration reliability is deposition of highly-damping coatings on the airfoil [1]. As these alloys are sensitive to surface damage, coatings should also have the required set of physico-mechanical characteristics, namely high values of hardness, fatigue limit, corrosion resistance, etc., i.e. they should simultaneously provide reliable resistance to operating conditions of the structural elements.

Extensive experience has now been accumulated in development of such coatings, which satisfy the conditions of AGTE manufacturing and operation to varying degrees [2]. One the other hand, it should be noted that the parameters of the above characteristics of materials, which can be used as high-damping coatings, are insufficient, and their increase by alloying or thermomechanical treatment as a rule leads to deterioration of the dissipative properties.

Considering the tendencies in development of modern aviation engine construction, manifested in increase of gas temperature and dynamic stress amplitudes, and widening of the external load frequency spectrum, there arises the need to create new materials for coatings. Regarded as the latter can be nanostructured vacuum condensates developed at PWI (further on referred to as condensates) [3], which are deposited on structural elements from the vapour phase by the technology given in [4].

An urgent task from the view point of applicability of such coating materials in manufacture of compressor blades of modern AGTE, is determination of optimum parameters of their material structure and deposition conditions to improve the damping capacity of blades in operation, which is the purpose of this work.

Coating materials and method to produce them. In this work quasicrystalline alloy Al–Cu–Fe characterized by increased values of hardness (10–11 GPa) and corrosion resistance [5, 6], as well as pure copper and with iron additives (up to 4 %) were selected as the main coating material. The latter two materials can be used as a bond coat having a high level of adhesion with the structural element and coating material. In addition, copper presence in the coating composition results in an increase of energy dissipation in the vibration system, as it belongs to highly damping materials in the nanostructured state [7].

Coatings 50–150 μm thick from the selected materials were produced by the technology of electron beam evaporation and deposition in vacuum [4]. The latter was performed on pin samples from VT1-0 titanium alloy characterized by low dissipative properties at up to 450 °C temperature [8]. Initial materials for coatings were copper and iron ingots, as well as tablets of a compacted mixture of aluminium, copper and iron powders. At deposition of Cu–Fe coatings metal was evaporated from two targets simultaneously. Sample surface was first cleaned in a vacuum furnace by an argon ion beam. Coating deposition rate was 2–3 μm/min, and their structural condition was changed by variation of sample temperature in the range from 160 up to 600 °C.

Coating deposition on AGTE compressor blades was performed in the mode of their rotation to ensure coating uniformity. For this purpose the blades were attached to a horizontal shaft, rotating during the process of coating formation.

Coating structure was studied by the methods of scanning and electron microscopy (CanScan4 instrument), and their microhardness was measured on transverse microsections of the samples by Vickers method using PolyvarMet optical microscope at 0.05 N load for 10 s.

Main principles of the procedures of investigation of coating material dissipative properties and structural element damping capacity. Energy dissipation characteristics of coating material were determined by calculation-experimental method. First the amplitude dependencies of the logarithmic damping decrement were derived by the results of testing coated samples supported in cantilever in the damped vibration mode in a unit described in [9]. Then they were used as the basis to determine by the calculation procedure of [10] the amplitude dependencies of the true logarithmic decrement for the coating material, i.e. its energy dissipation characteristics in a uniform stressed state.

Damping capacity of the structural elements was determined using experimental devices developed at G.S. Pisarenko Institute for Problems of Strength of NASU to study the dissipative properties of materials and structural elements both at room and elevated temperature [11], minimizing the energy losses in the articulations, not related to hysteresis losses in materials of the test object or in coatings. Logarithmic damping decrement was determined by the resonance curve method [1].

A cantilever sample of a rectangular cross-section ($h \times b \times 1 = 4 \times 12 \times 150$ mm) was selected as the test object. Coating was deposited only on one surface of the sample test portion across its entire width b, starting from the root section. It had a constant length of 50 mm. Sample was tested at constant thickness $h = 4$ mm and reduction of length l of its test portion from 150 to 50 mm to achieve the required vibration frequency.

In keeping with problem definition, the following range of test parameter variation was established: vibration frequency 150–1000 Hz, temperature 20–400 °C (which, on the whole, corresponds to the main operating modes of AGTE compressor blades).

Structure and properties of coating materials. Structure of copper coatings was changed by variation of deposition temperature T_c in the range of 160–600 °C, which resulted in the size of the columnar

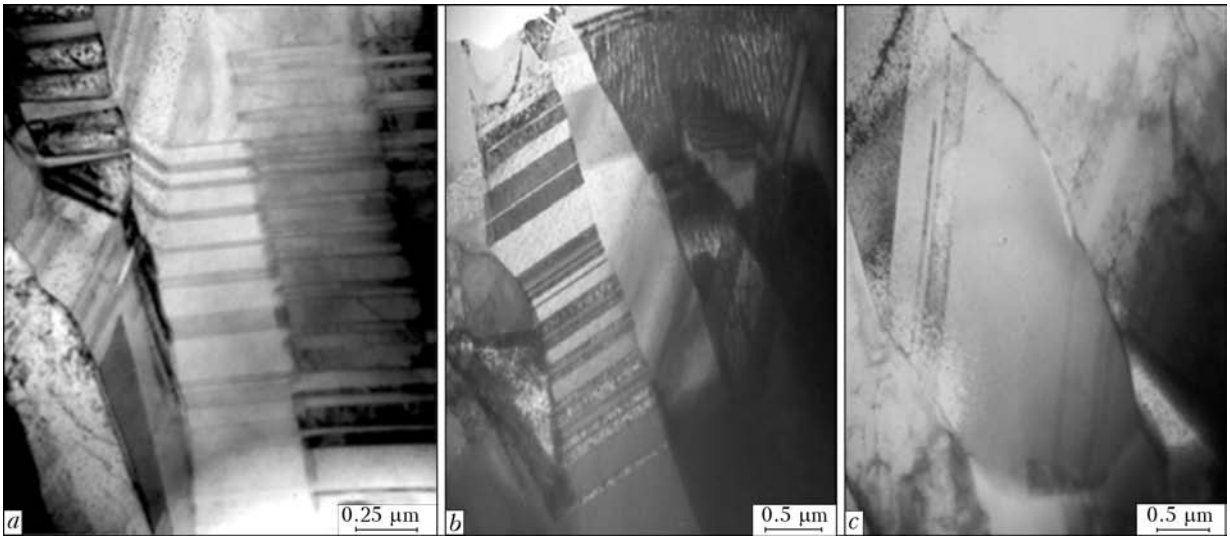

Figure 1. Microstructure of copper condensates (cross-section) deposited on a sample at the temperature of 170 (*a*), 230 (*b*) and 350 (*c*) °C

grain D (of the crystallite) decreasing from 4–5 μm (T_c = 600 °C) to 0.3–04 μm (T_c = 160 °C). A qualitative change of crystallite substructure was found.

From Figure 1 it is seen that the internal structure of the crystallites changes with lowering of deposition temperature, which is manifested in formation of an interlayer of twin domains, located predominantly in parallel to the crystallite growth front (Table). Number of such twins rises abruptly with lowering of the deposition temperature starting from $T_c \approx 350$ °C [7]. At further temperature lowering their quantity rises so much that it leads to formation of a polydomain nanotwinned substructure in the crystallites (Figure 1, *a*).

Transition to a nanotwinned structural state of the copper coatings leads to an abrupt increase of their microhardness from 0.8 up to 1.5 GPa [7], as well as qualitative change of energy dissipation characteristics, which is manifested in an essential weakening of amplitude dependence of the logarithmic damping decrement, inherent to coarse-grained copper with preservation of high values at heating (Figure 2). More over, unlike coarse-grained copper, the energy dissipation characteristics of these coatings are preserved after multiple cyclic deformation.

Additional increase of coating microhardness (up to 2 GPa) is achieved as a result of adding 2–4 % of iron to copper. Energy dissipation characteristics of such a Cu–Fe coating in this case decrease at high deformation amplitudes. On the other hand, they remain quite high and cyclically stable at testing temperature of 20–350 °C. Here an almost complete coincidence of the curves obtained during cyclic deformation of samples at the temperature of 250 °C with the initial curve was registered.

Change of mechanical and dissipative properties of coatings from condensates of copper and Cu–Fe at formation of a nanotwinned substructure in them is due to an essential weakening of the role of intergranular dislocations, both in the process of plastic deformation, and at mechanical energy dissipation.

At approximately 100 nm dimensions of structure components, generation of «fresh» dislocations in metals becomes impossible [12]. On the other hand, the role of grain-boundary surface rises with reduction of grain size, resulting in domination of energy dissipation mechanisms related to thermally activated transformation of atomic configurations on grain boundaries in nanostructured materials.

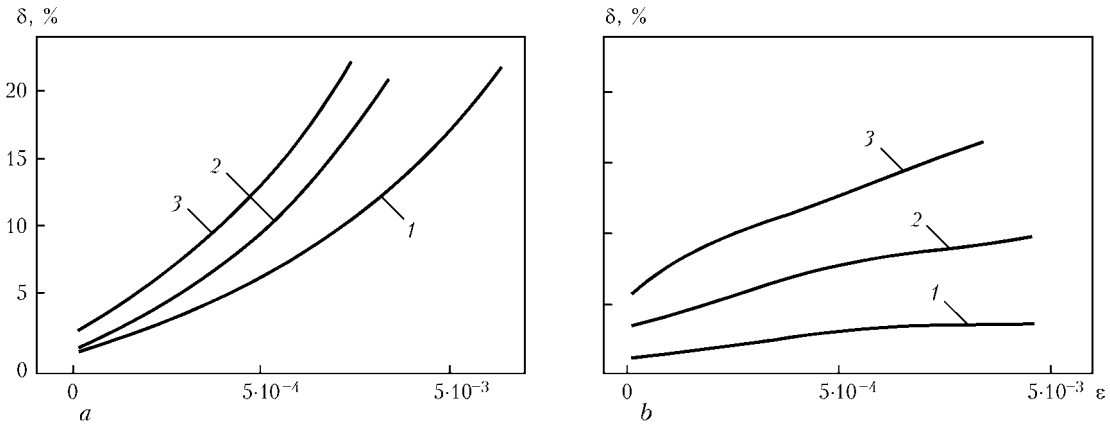

Figure 2. Amplitude dependencies of the logarithmic damping decrement of sample derived for copper condensates with 2.5 μm grain size (*a*) and polydomain nanotwinned substructure (*b*) at the temperature of 20 (*1*), 250 (*2*) and 350 (*3*) °C

Figure 3 gives the results of investigation of the influence of grain size on energy dissipation characteristics for coatings from Al–Cu–Fe composite alloy. In coatings deposited at T_c = 650 °C, average grain size D was equal to 580 nm. At lowering of deposition temperature to 350 and 270 °C, it was reduced to 270 and 30 nm, respectively. For coatings with grain size of 580 and 270 nm the parameters of energy dissipation characteristics in the temperature range of 20–400 °C turned out to be low. However, with grain size reduction to 30 nm, an abrupt increase of the logarithmic damping decrement at 250–400 °C was registered (see Figure 3).

A feature of the considered nanostructured coatings is their amplitude-independent nature right up to relative deformation amplitudes $\varepsilon = 1.2 \cdot 10^{-3}$, which is important from a practical viewpoint. Note also the high hardness of such coatings (15 GPa) and lower value of the modulus of elasticity (177 MPa), compared to a coating of the same composition with grain size equal to 270 and 580 nm, and modulus of elasticity of 207 and 210 MPa, respectively.

Thus, from the results of the above-described investigations it follows that selection of the respective modes of electron beam deposition on the structural element surface allows forming nanostructured coatings with an increased level of dissipative and mechanical properties.

Results of determination of damping capacity of coated structural elements and their analysis. Three kinds of coatings, the characteristics of which are given in the Table, were selected for analysis.

The obtained amplitude-frequency characteristics of the samples were used to determine the values of their logarithmic damping decrement and its respective dependence on maximum stress amplitude σ_{max} at variation of vibration frequency and testing temperature at different values of coating parameters. Note that at resonance testing it is impossible to ensure the same frequency of sample oscillations. As this discrepancy is minor, it did not have any essential influence on test result analysis.

Coating composition and characteristics

Sample #	Coating composition	Deposition temperature T_c, °C	Grain size D/d, nm	Coating thickness h_c, μm
1	Copper	605	3000	97
2	Same	345–350	1400/160	150
3	»	240–245	780/65	170
4	»	600	2800	33
5	»	600	2800	100
6	»	300	1100/105	87
7	»	300	105	72
8	Iron	700	2500	110
9	Same	340	70	102
10	Al–Cu–Fe	500	430	53
11	Same	500	430	62
12	»	300	110	55
13	»	300	110	58

Note. d — twin thickness in copper condensates.

To perform comparative analysis of the influence of particular factors on the damping capacity of samples with the selected coatings, first the amplitude dependencies of the logarithmic damping decrement were determined for an uncoated sample in the specified range of vibration frequencies at room temperature (20 °C), given in Figure 4, *a*. Presented results show that the above dependencies are of a linear nature, while the influence of vibration frequency on the value of the logarithmic damping decrement is negligibly small at small stress amplitudes, and somewhat rises at their increase.

Let us consider the results of the performed testing from the viewpoint of the influence of vibration frequency on damping capacity of samples with the selected coatings.

Analysis of amplitude dependencies of the logarithmic damping decrement of samples with single-component coatings (samples *1–9* were made at room temperature), corresponding to their certain structural condition (Figure 4, *b, c*) showed that in this

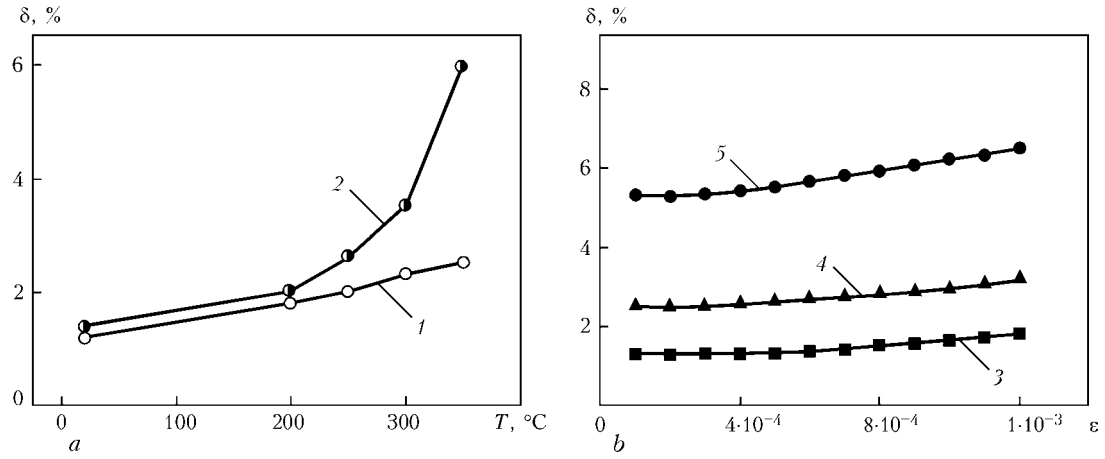

Figure 3. Dependence of logarithmic damping decrement of a sample with Al–Cu–Fe alloy coating on temperature (*a*) at relative deformation amplitude $\varepsilon = 5 \cdot 10^{-4}$ for grains of 580 (*1*) and 30 nm size (*2*) and on relative deformation amplitude (*b*) at grain size of 30 nm and temperature of 20 (*3*), 300 (*4*) and 350 (*5*) °C

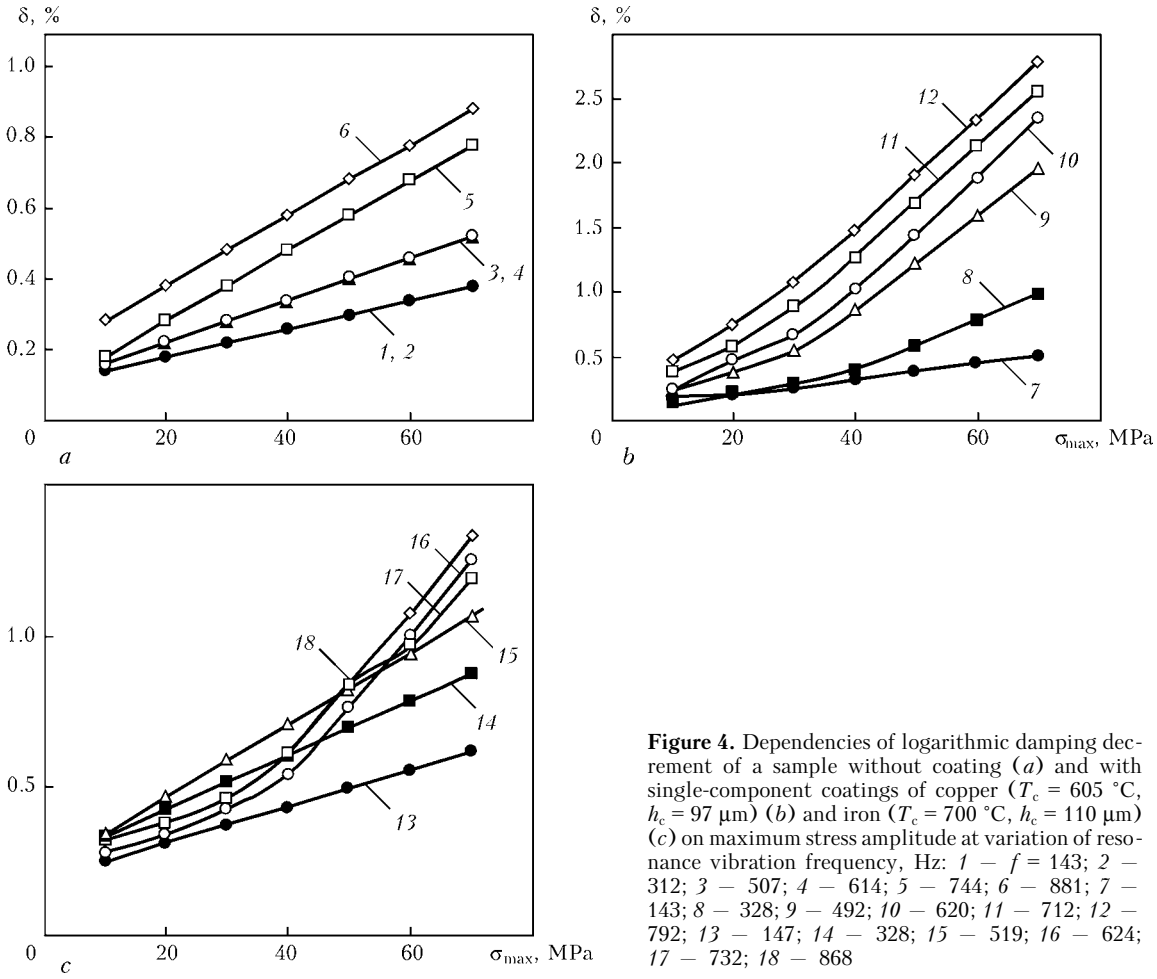

Figure 4. Dependencies of logarithmic damping decrement of a sample without coating (*a*) and with single-component coatings of copper (T_c = 605 °C, h_c = 97 μm) (*b*) and iron (T_c = 700 °C, h_c = 110 μm) (*c*) on maximum stress amplitude at variation of resonance vibration frequency, Hz: *1* — *f* = 143; *2* — 312; *3* — 507; *4* — 614; *5* — 744; *6* — 881; *7* — 143; *8* — 328; *9* — 492; *10* — 620; *11* — 712; *12* — 792; *13* — 147; *14* — 328; *15* — 519; *16* — 624; *17* — 732; *18* — 868

case the influence of vibration frequency on the value of logarithmic decrement depends on coating type. So, the most significant frequency dependence of the logarithmic damping decrement is characteristic for copper coating, particularly, at increased amplitudes of maximum stresses. It is less pronounced for samples with an iron coating.

The influence of frequency on sample damping decrement is visually demonstrated by its frequency dependencies, which for the maximum stress amplitude (σ_{max} = 50 MPa) are given in Figure 5, where the average vibration frequency is plotted along the abscissa axis, allowing for the impossibility of ensuring its constant value during testing.

It follows from the presented test results that damping capacity of the samples essentially depends on their microstructural characteristics.

On the whole, the obtained data lead to the conclusion that frequency dependence of the logarithmic damping decrement of a sample is more characteristic at deposition of a copper coating. The degree of its growth is the most pronounced in coatings with coarse grains and higher values of maximum stress amplitude. For samples with an iron coating the above dependence of the logarithmic decrement on vibration frequency is practically not registered, particularly at lowering of maximum stress amplitude.

In keeping with the problem definition, we will analyze the results of investigations on determination of the joint influence of vibration frequency and operating temperature on the damping capacity of coated samples. Let us consider problem solution in the case of a coating from quasi-crystalline Al–Cu–Fe alloy (more probable) compared to single-component coatings for practical applications, particularly for AGTE compressor blades.

Samples were tested at variation of the same technological and operating parameters, considered for single-component coatings, as well as of the operating temperature. Similar to homogeneous coatings, amplitude dependencies of the logarithmic damping decrement on the maximum stress amplitude were obtained. Their analysis showed that damping capacity of samples with the considered coating at elevated temperature can rise three and more times.

Obtained amplitude dependencies of the logarithmic damping decrement were used to plot the diagram of its variation, depending on the frequency of resonance vibrations of the sample (Figure 6). As follows from the presented data, vibration frequency practically has no influence on damping capacity of a sample with multicomponent coating from quasicrystalline Al–Cu–Fe alloy.

Assessment of cyclic strength of titanium blades with coatings from nanostructured copper. High level and cyclic stability characteristics of energy dissipation by copper-based nanostructured condensates, as well as their good adhesion to titanium alloys allow

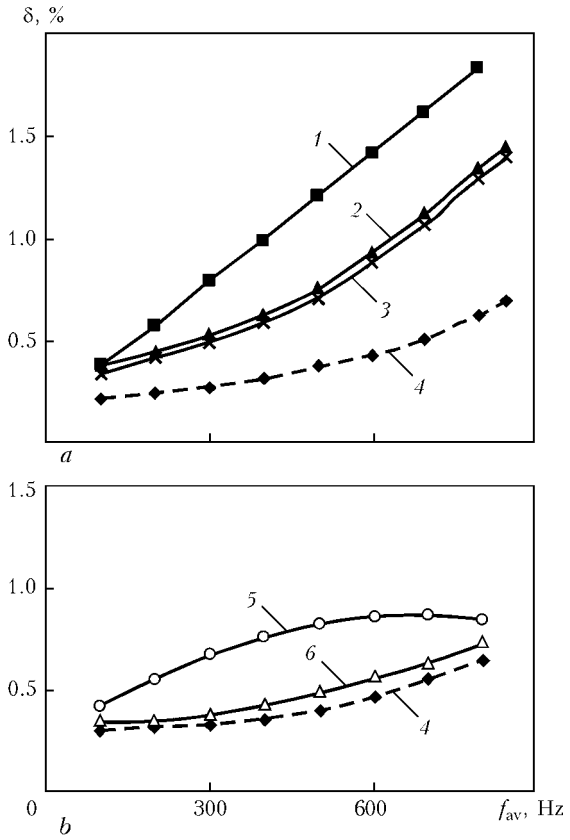

Figure 5. Dependence of logarithmic damping decrement at maximum stress amplitude of 50 MPa for samples with single-component coatings from copper (*a*) and iron (*b*) on average frequency f_{av} of resonance vibrations at different coating parameters: *1* — T_c = = 605 °C, h_c = 97 μm; *2* — T_c = 350 °C, h_c = 150 μm; *3* — T_c = = 245 °C, h_c = 170 μm; *4* — uncoated sample; *5* — T_c = 700 °C, h_c = 110 μm; *6* — T_c = 340 °C, h_c = 102 μm

regarding these condensates as a possible component of the intermediate layer of composite protective coatings for AGTE blades.

Conducted testing was used as the base to establish the technological modes of copper coating deposition on titanium blades, which ensured the coating nanostructured state. The influence of such coatings 5–10 μm thick on fracture strength of titanium blades from VT3-1 alloy was studied. For comparison coatings from copper with microsized grains were deposited on another part of the blade. Testing was conducted at the temperature of 20 °C and vibration frequency of 530 Hz. Cyclic fatigue of the blades was assessed by an accelerated procedure under the conditions of a discrete increase of stress amplitude after every $5 \cdot 10^6$ vibration cycles [13].

Positive influence on vibration stability of blades with coatings with micron-sized grains was noted in 50 % of the samples. Now, in the case of nanostructured coatings positive result was obtained for all the samples, 50 % of them not failing right up to the end of testing.

The given results confirm the assumption that condensates based on nanostructured copper can be used as the components of composite coatings, for instance bond coats between the structural element and the main part of the coating.

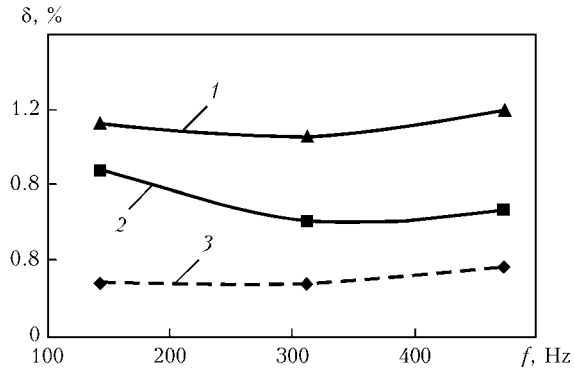

Figure 6. Diagram of variation of the logarithmic damping decrement of a sample with Al–Cu–Fe coating (T_c = 500 °C, h_c = 62 μm) depending on the frequency of resonance vibrations at maximum stress amplitude 45 MPa and testing temperature 350 (*1*) and 20 (*2*) °C and of an uncoated sample (*3*)

CONCLUSIONS

1. It is shown that damping capacity of coated samples essentially depends on their structure and production parameters, primarily coating deposition temperature, as well as vibration frequency.

2. It is established that the logarithmic damping decrement of a sample with a nanostructured coating at elevated temperature can increase by three and more times compared to the room temperature value.

3. A search for further optimum coating nanostructures and their production parameters is necessary to ensure the maximum damping capacity of the structural elements of machines of the type of AGTE compressor blades under service conditions.

1. Matveev, V.V. (1985) *Damping of oscillations of deformable bodies*. Kiev: Naukova Dumka.
2. Yakovlev, A.P. (1985) *Dissipative properties of inhomogeneous materials and systems*. Kiev: Naukova Dumka.
3. Ustinov, A.I., Skorodzievsky, V.S., Kosenko, N.S. (2008) Study of dissipative properties of homogeneous materials deposited as coatings. Report 2: Copper condensates with different microstructure characteristics. *Problemy Prochnosti*, **2**, 149–159.
4. Paton, B.E., Movchan, B.A. (1991) Composite materials deposited from the vapour phase in vacuum. Soviet technologies. *Welding and Surfacing*, **2**, 43–64.
5. Sales, M., Merstallinger, A., Ustinov, A.I. et al. (2007) Effect of the addition of crystalline β-phase in Al–Cu–Fe quasi-crystalline coating on their tribological properties. *Surf. and Coat. Tech.*, **201**, 6206–6211.
6. Milman, Yu.V., Lotsko, D.V., Dub, S.N. et al. (2007) Mechanical properties of quasi-crystalline Al–Cu–Fe coatings with submicron-sized grains. *Ibid.*, 5937–5943.
7. Ustinov, A.I., Skorodzievski, V.S., Fesiun, E.V. (2008) Damping capacity of nanotwinned copper. *Acta Materialia*, **56**, 3770–3776.
8. Pisarenko, G.S., Yakovlev, A.P., Matveev, V.V. (1988) *Reference book on strength of materials*. Kiev: Naukova Dumka.
9. Ustinov, A.I., Movchan, B.A., Skorodzievsky, V.S. (2001) Study of damping capacity of flat specimens of titanium alloy Ti–6 % Al–4 % V with tin and yttrium coatings. *Problemy Prochnosti*, **4**, 55–61.
10. Ustinov, A.I., Skorodzievsky, V.S., Kosenko, N.S. (2007) Study of dissipative properties of homogeneous materials deposited as coatings. Report 1: Method for determination of amplitude relation of true damping decrement of coating material. *Ibid.*, **6**, 134–143.
11. Lebedev, A.A., Troshchenko, V.G., Matveev, V.V. et al. (2005) *Strength of materials and structures*. Kiev: Akademperiodika.
12. Kaschner, G.C., Gibeling, J.C. (2002) Evolution of dislocation glide kinetics during cycling deformation of copper. *Acta Materialia*, **50**, 653–662.
13. Matokhnyuk, L.E. (1988) *Accelerated fatigue testing by high-frequency loading*. Kiev: Naukova Dumka.

MODELLING OF THE PROCESS OF INDUCTION HEATING OF PIPES WITHIN THE WELD ZONE

I.V. CHERNYKH[1] and **S.A. RACHKOV**[2]
[1]Ural State Technical University, Ekaterinburg, Russian Federation
[2]Productive-Scientific Enterprise ELTERM-S Ltd., Ekaterinburg, Russian Federation

Modelling procedure for the process of induction heating of large-diameter pipes before welding is considered. The choice of a software package for modelling is substantiated, and an example of modelling is given. The pattern of temperature field in the weld zone and plots of temperature distribution in the pipe wall are described. An example of embodiment of the induction heating unit is given.

Keywords: *welded pipes, large diameter, weld, induction heating, temperature field, modelling*

Induction heating of the weld zone is widely used now in welding operations performed on large-diameter pipes. The induction heating unit consists of an induction coil and power supply for a medium-frequency (2400 Hz) current. Development of the unit involved mathematical modelling of the heating zone to find geometric parameters of the induction coil and parameters of the power supply for the induction heating unit, and determine the distribution of temperature in the pipe wall. The calculation methods are described in detail in studies [1–3]. The calculation results are temperature field patterns, plots of distribution of power of the heat released in a pipe and temperature, as well as integral indicators, such as power consumption, efficiency, cos φ, etc.

The calculations were performed in two stages.

At the first stage it was assumed that the pipe is continuous (has no discontinuity in the future weld location). The calculations were made by using the Universal 2D software. The software is based on the use of numerical methods (finite differences, finite elements, integral equations and their combinations) for a combined calculation of electromagnetic and temperature fields in 2D regions. This stage made it possible to determine the main energy indicators of the unit and plots of distribution of temperature along and across the pipe wall allowing for the assumption made. The calculations were made for a steel pipe with diameter D = 1420 mm and wall thickness h = = 33.4 mm. The unit has an induction coil consisting of two sections, each having two turns. Distance between the sections is 160 mm, which is sufficient to install an external pipe aligner. The calculations showed that the power consumed by the unit is P = 50 kW, time of heating to a preset temperature is t = 10 min, and electric efficiency of the unit is η = 81.7 %. The curves of distribution of temperature along the pipe wall are shown in Figure 1. Width of the pipe zone heated to a temperature of 100 °C or more is equal to 260 mm.

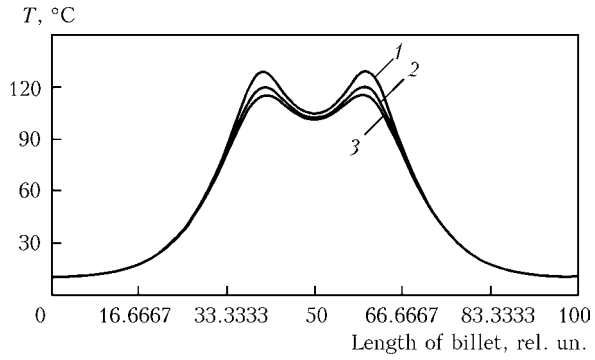

Figure 1. Results of calculations of distribution of temperature along the pipe wall at the first stage: *1, 3* — temperature of external and internal surfaces of the pipe, respectively; *2* — average temperature

The work done at the second stage included checking the calculations allowing for the shape of pipe edge preparation (Figure 2) and solving the electromagnetic and thermal problems. The temperature field pattern, plots of distribution of temperature along the concerned profiles of the pipe, and plots of variations in temperature with time in heating and cooling of the pipe were obtained. The ELCUT software using the finite element method was employed for the calculations [4]. Figure 3 shows the temperature field pattern within the heating zone, as well as location of control point X and profiles A and B. It can be seen from the Figure that the pipe has a maximal temperature of 130 °C in zones of location of the induction coil turns, whereas in the weld zone the temperature is about 100 °C. Figure 4 shows the plots of distribution of temperature along profiles A and B at the end of the heating range. It can be seen that tem-

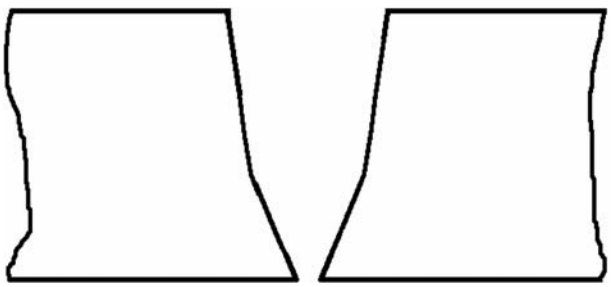

Figure 2. Shape of pipe edge preparation

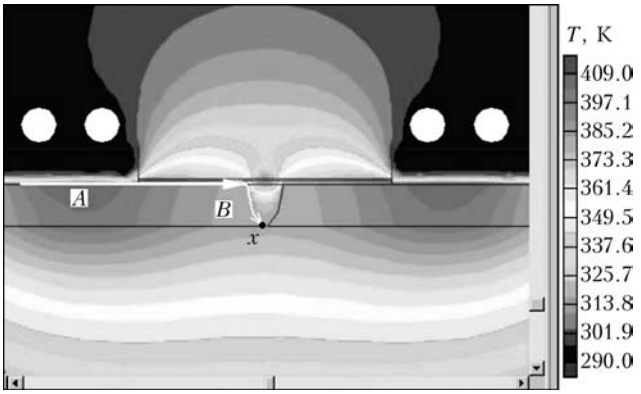

Figure 3. Pattern of distribution of temperature field in the heating zone

perature on the mating surfaces is 100 °C, while on the pipe surface under the induction coil it does not exceed permissible values.

Additionally, parameters of natural cooling of the pipe after switching off of the induction coil from the power supply were calculated at the second stage. As follows from Figure 5, surface within the weld zone remains heated to a temperature of 100 °C for about another 10 min.

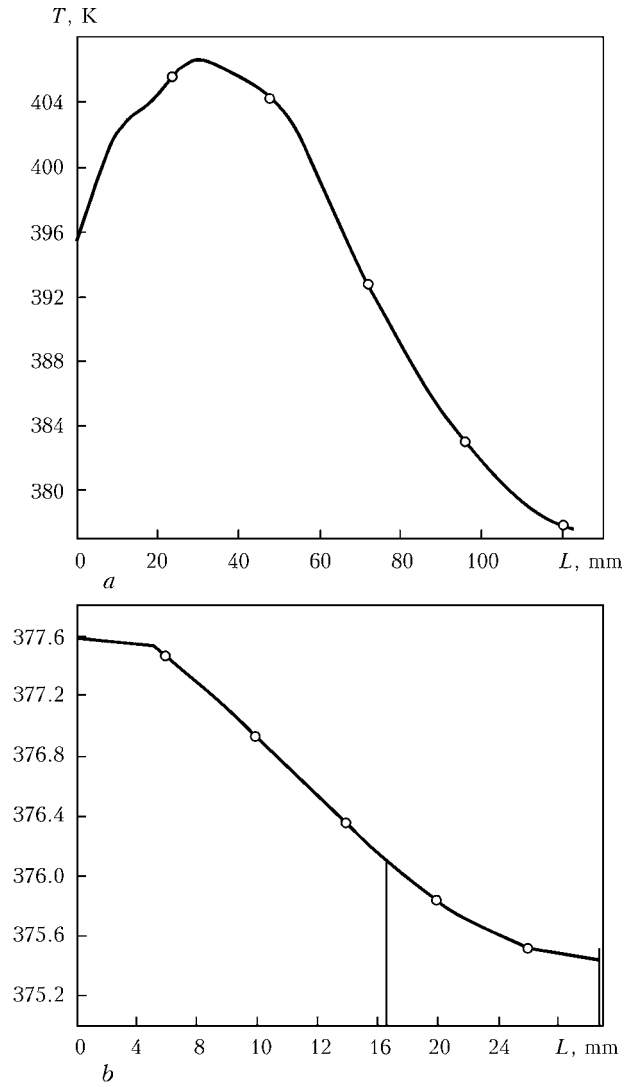

Figure 4. Distribution of temperature at the end of heating range along profiles *A* (*a*) and *B* (*b*)

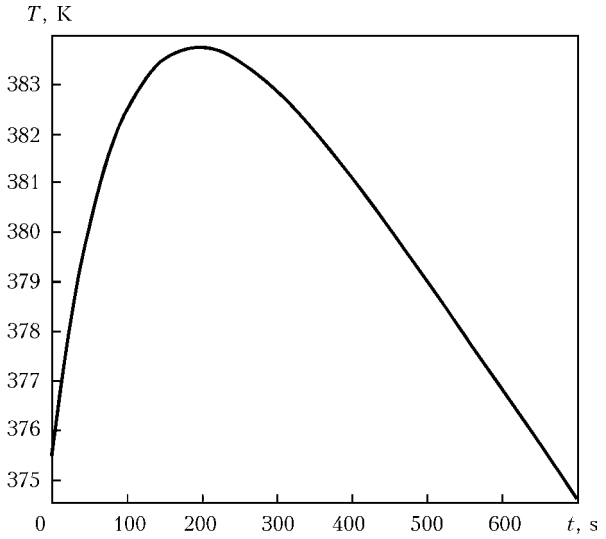

Figure 5. Variations of temperature at control point *X* in cooling

Figure 6. General view of induction heating unit ELTERM-S UINT-50-2.4

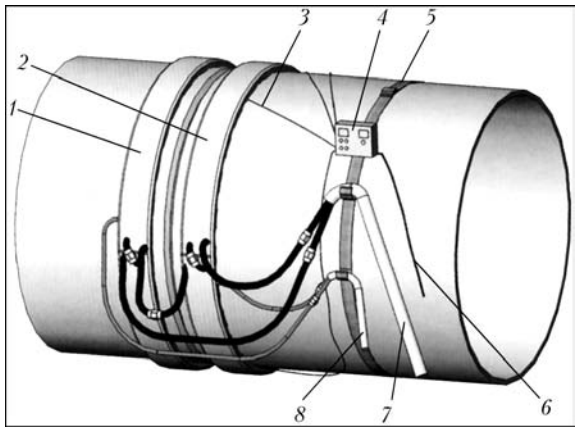

Figure 7. Scheme of arrangement of soft flexible induction coil on the pipe: *1, 2* — 1st and 2nd induction coils, respectively; *3* — connection of thermocouples (4 pcs); *4* — remote control panel; *5* — assembly belt from a set; *6* — control cable; *7* — electric cable; *8* — water hose

Design parameters and operation conditions of induction heating unit ELTERM-S UINT-50-2.4 were optimised using the calculation results. General view of the unit is shown in Figure 6, and arrangement of the induction coil on the pipe heated is shown in Figure 7. Several types of the induction coils were designed on the basis of modelling.

The induction heating units developed and mass produced by ELTERM-S, which were optimised based on the calculation results, are high-efficiency technological units for induction heating to be used prior to and during welding.

The authors suggest using the experience accumulated from electromagnetic and thermal calculations to develop units for induction heating of different objects (pipes, fittings, shafts etc.).

1. Luzgin, V.I., Sarapulov, S.F., Sarapulov, F.N. et al. (2005) *Induction melting complexes based on induction crucible furnaces and their mathematical modelling*. Ekaterinburg: GOU VPO UGTU-UPI.
2. Luzgin, V.I., Petrov, A.Yu., Sarapulov, F.N. et al. (2005) System for induction heating of long-length pipe billets. In: *Proc. of Int. Sci.-Pract. Conf. on Current Problems of Theory and Practice of Induction Heating* (St.-Petersburg, 2005).
3. Luzgin, V.I., Petrov, A.Yu., Sarapulov, F.N. et al. (2001) Induction heating control system for long-length pipe billets. In: *Elektrotekhnika 2010*: Proc. of 6th Symp. Vol. 3. Moscow.
4. Chernykh, I.V. (2003) Software package ELCUT: modelling of induction heating devices. *Exponenta Pro. Mathematics in Appendices*, **2**.

DEVELOPMENT OF THE TECHNOLOGY FOR FORMATION OF MECHANICAL AND GLUED-MECHANICAL JOINTS BY THE PUNCHING METHOD*

Yu.S. VASILIEV, L.S. PARSHUTINA and **A.N. CHUKASHKIN**
E.O. Paton Electric Welding Institute, NASU, Kiev, Ukraine

The processes of formation of mechanical joints in thin-sheet materials with anticorrosive coatings by the punching method using glue compositions of different viscosities between the mating surfaces were investigated. The limiting values of rheological characteristics of the glues that affect formation of the glued-mechanical joints were established. The cold-cured highly filled glue composition on a silicon-polyurethane base, not preventing formation of the glued-mechanical joints, was developed. Press equipment based on a pneumatic actuator, providing a compression force of up to 20 kN, was developed and manufactured.

Keywords: *mechanical joints, glued-mechanical joints, thin-sheet metal structures, forming technologies, hybrid glue compositions, filling compounds, polydisperse filling*

Competition between materials in transport machine building is determined by continuously growing requirements for reduction of weight of structures, improvement of reliability, extension of service life of vehicles, and ensuring comfort and environmental friendliness. The share of aluminium alloys, plastics and composite materials used to produce vehicle bodies constantly increases. Nevertheless, steel continues to be a promising material. It will dominate in transport machine building in the future because of its technological innovation potential, high affordability and environmental friendliness [1]. When using increased- and high-strength steels, reduction of sheet thickness allows maintaining cost characteristics of a vehicle, but leads to a substantial increase in requirements for reliable and durable corrosion protection of a structure.

It is a known fact that galvanising is the most effective method for anticorrosive treatment of thin-sheet steels used to produce vehicle bodies, which is attributable to its peculiar electrochemical mechanism of metal protection. Combined systems containing metallised and polymeric coatings, which are characterised by high deformability, weldability and ageing resistance gain an increasingly wider popularity. Development and application of new materials and coatings require mastering of the advanced methods for joining components of vehicle structures.

Application of the glued joints in components of thin-sheet structures, which do not experience high loads, has been widening lately in a number of industries. The reason is that the glued joints have low reliability characteristics in non-uniform pulling and tear. Moreover, the glued joints have drawbacks related to variations in properties of the glues as a result of ageing, necessity of forming contact pressure and fixation of parts in curing of the glues. Therefore, the trend is to combine the glued joints with joints produced by other methods, providing additional local bonds between the parts.

The combined glued-welded joints made by resistance spot welding (RSW) of parts over the layer of the glue preliminarily deposited on the mating surfaces are widely applied in production of thin-sheet structures from low-alloy steels [2]. However, RSW of coated metal sheets involves some difficulties. Moreover, the high-temperature effect of RSW causes burnout of metallic and organic coatings, this requiring the use of additional operations for corrosion protection.

The glued-riveted and glued-bolted joints are characterised by the highest strength properties, particularly under dynamic loading conditions. However, the presence of holes in the parts joined does not only lead to weakening of a section, but also create some technological difficulties in the process of formation of permanent joints.

Application of the local deformation technology by pressing the metal sheets to be joined into the die with a punch eliminates many problems in formation of the combined joints [3]. Many design and technology solutions to provide formation of the «dovetail» type joints (Figure 1) were patented. It should be noted that, as a rule, the information available on such joining methods is incomplete. Only the flowcharts of the processes used to manufacture the joints can be found, without disclosure of principles of design

*The article was prepared on the basis of results of accomplishment of the NASU targeted integrated program «Problems of Remaining Life and Safe Operation of Structures, Constructions and Machines» (2007–2009).

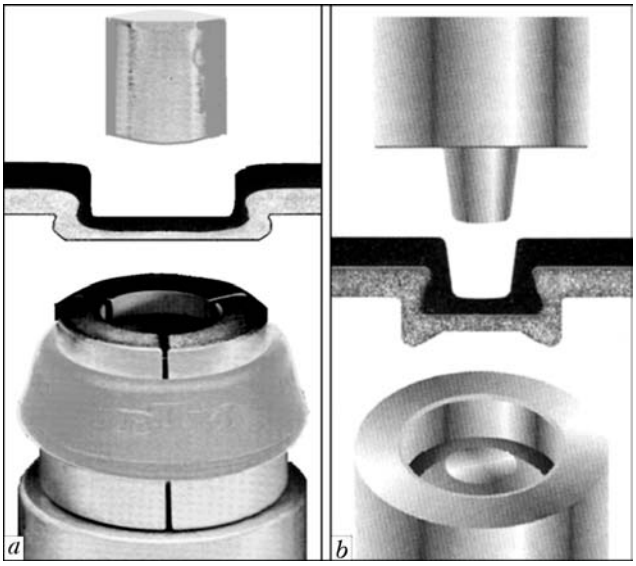

Figure 1. Joints produced by the punching method: *a* — clinch; *b* — TOX

of the equipment and calculation of parameters of forced formation of the joints.

The purpose of this study was to develop recommendations on the technology for formation of mechanical and glued-mechanical joints on galvanised steels by the punching method in order to extend life of thin-sheet structures applied in transport machine building. The problems solved were as follows:

- processes of contact interaction in punching of the metal sheets joined into the die were investigated;
- requirements to rheological and physical-mechanical characteristics of the glues to produce sound joints were identified;
- and technology and experimental equipment were developed for formation of the mechanical and glued-mechanical joints on galvanised metal sheets.

Formation of the joints by the punching method belongs to the category of technologies for pressure treatment of metals and consists of a number of successive operations: fixation of the metal sheets with a clamping element (Figure 2, *a*), punching of the sheets joined until they contact the anvil (drawing) (Figure 2, *b*), upsetting of the sheets with decrease in their thickness and simultaneous increase in their cross-section area (Figure 2, *c*), and removal of a finished joint (Figure 2, *d*) [4, 5].

Analysis of the stress-strain state during the drawing process shows that plastic deformation is mainly concentrated only within the overlap portion of the sheets, which is located on a flat face of the die and its rounded edge. Increase in the radius of rounding of the die, r_d, causes decrease in localisation of plastic deformation in the bent section. Deformation of the sheets on the punch face is characterised by the fact that metal gradually bends over the rounded edge of the punch at the initial moment of drawing, when the load has not yet reached its maximal value. If the radius of rounding of the punch edge is small compared to its diameter, the bend with plastic deformation will not coincide in time with the peak load, and will have no significant effect on the latter.

Investigations of the process of formation of the joints by punching were carried out by using 0.55 and 1 mm thick sheets of cold-rolled low-carbon steel 08kp (rimmed) galvanised by the electrolytic method on both sides. This steel belongs to the materials of deep drawing, and is widely used in formed-welded structures applied in transport machine building.

Rigid TOX-die and opening clinch-die were developed, allowing formation of the joints on metal sheets of different thicknesses due to varying internal diameter and height of a forming bushing (Figure 3, *a, b*). Technological investigations were conducted by loading the punch–die system in a clip (Figure 3, *c*) using testing machine ZD-10, and by recording the compression force depending upon the punch movement.

As established, for the clinch- and TOX-dies it is indicated to use gap z of a different width between the punch and die wall. With a smaller gap than total thickness of the sheets joined ($z < t_0$), thinning of the «sleeve» wall to a preset value occurs at a small decrease in thickness of the metal sheet at the punch face. This approach was used to design the rigid TOX-die. To reduce stresses, the radius of rounding of the leading edge of the die was increased to $r_d \sim (0.25–0.40)t_0$.

In the technology of formation of clinch-joints the drawing stage should be performed without wall thinning at gap $z > 1.1t_0$, as opening of the clinch-die during formation is undesirable. At a minimal value of the radius of rounding of the die, $r_d \sim (0.05–0.10)t_0$, stresses in the dangerous section substantially grow.

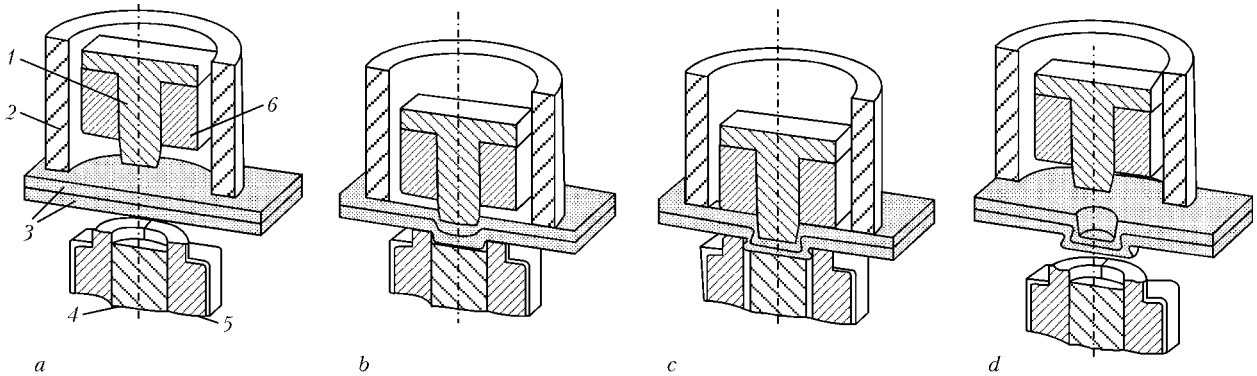

Figure 2. Flowchart of formation joints by punching using an opening die (clinch-joint) [5]: *a–d* — see in the text; *1* — punch; *2* — clamp; *3* — sheets joined; *4* — anvil; *5* — opening die; *6* — limiter

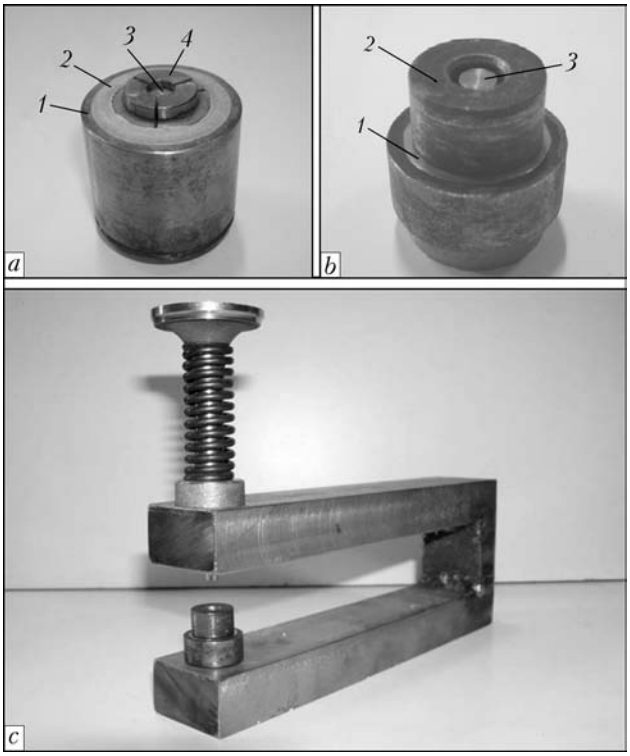

Figure 3. Devices for formation of joints by the punching method: *a* — opening clinch-die (*1* — forming head of the collet type; *2* — anvil; *3* — elastic bushing; *4* — conductor); *b* — mountable-and-dismountable TOX-die (*1* — forming bushing; *2* — adjustment gasket; *3* — anvil); *c* — appearance of clip

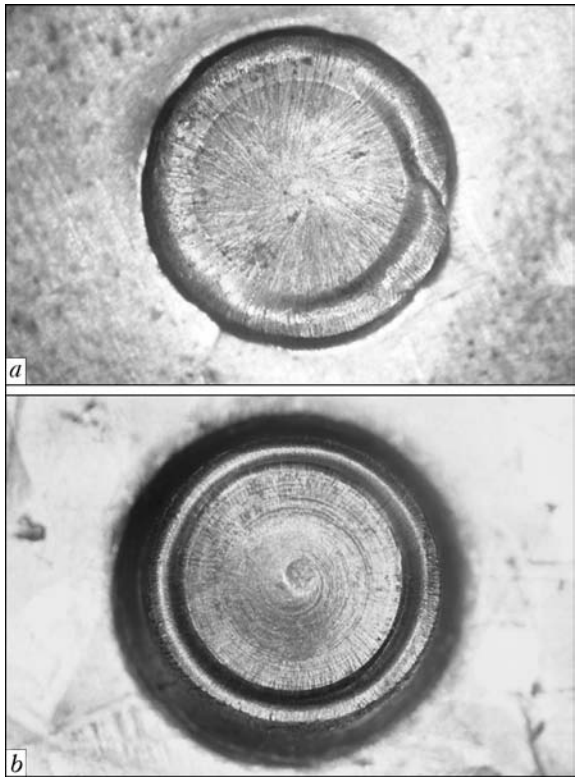

Figure 4. Mechanical lock on the die side in clinch- (*a*) and TOX-joints (*b*)

However, in deep drawing to $1.5t_0$, although tensile bend stresses exceed the values of yield stress of the metal, but displacement of a sheet over the die face prevents opening of the die.

Formation of the «dovetail» takes place in the process of upsetting of the sheets joined between the punch and die anvil. Drawing of the working surfaces together leads to metal flow from centre to periphery, and deformation occurs in a stepwise manner to form riffles at the steel 08kp–zinc coating–die anvil interface. This is accompanied by formation of the so-called collars, where continuity of the zinc coating may be broken (Figure 4, *a*).

Formation of the TOX-joint takes place as a result of the metal flow between the die anvil and punch into the closed volume of cavity on the anvil perimeter. This process corresponds to cold forming with forced drawing of metal. Formation of a «button» joint occurs at a tighter interaction of the metal sheets subjected to orientation thinning. Formation of the joint in a closed volume limits surface deformation of a metal sheet, thus maintaining continuity of the zinc coating (Figure 4, *b*).

It is reported [6] that the use of glue compositions with viscosity of up to 50 Pa·s has no substantial effect on the process of formation of the glued-mechanical joints made by the punching method. However, it makes the entire technological cycle more complicated. There is a problem of dosed deposition of liquid glues on the mating surfaces, while pressing out from the overlap cavity leads to contamination of a workpiece, equipment and process fixture. Viscosity of a glue composition is adjusted by adding various filling agents. While reinforcing the glue interlayer, these agents retain the glue in the overlap gap, help to maintain uniform thickness of the glue layer after deposition of the glue on the curvilinear surfaces, and increase strength characteristics and crack resistance of the glue interlayer.

Investigations of the effect of the glue interlayer on the process of formation of the clinch- and TOX-joints were carried out by using epoxy-polyurethane glue composition EPU with different filling degrees: EPU-K with effective viscosity of about 80 Pa·s, EPU-N — about 200 Pa·s, and EPU-P — paste-like.

As established, composition EPU-K can be readily pressed out from the contact area, and it does not prevent formation of sound joints. At the same time, compositions EPU-N and EPU-P exert different effects at all stages of formation of the joints in the clinch- and TOX-dies. Two variants of accumulation of glue EPU-N were observed in the clinch-joint, where formation occurs without thinning of the sheets joined: in the circumferential zone under a clamp, and in the upset plastic flow zone behind the edge of the working surface of the punch (Figure 5, *a*). The last case is characterised by cracking of the «button» that forms recesses, this leading to contamination of the opening die.

The negative effect of glue EPU-P on formation of the TOX-joint was fixed as early as at the stage of pressing the sheets together and applying load to the punch. The zone of uniform compression forms at the «button» centre. It prevents movement of the paste

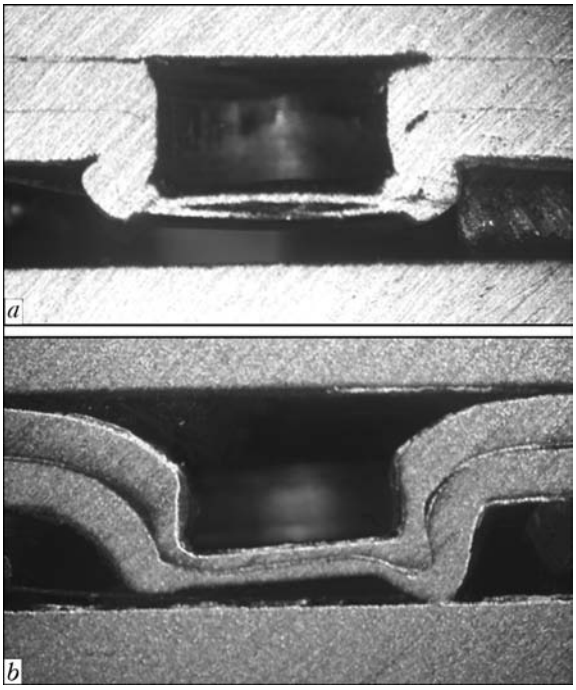

Figure 5. Sections of the glued-mechanical clinch-joint (glue EPU-N) (*a*) and TOX-joint (glue EPU-P) (*b*)

to the circumferential drawing formation zone. The glue appears to be in the closed space and forms a «pocket» that separates the sheets being joined. At the stage of upsetting, the glue is pressed out from the «pocket» to the necking region and hinders formation of the «dovetail» (Figure 5, *b*). The use of glue EPU-N with viscosity of about 200 Pa·s excludes formation of the «pocket» and provides the sound TOX-joint.

In hybrid overlap joints, misalignment of application of load results in their deformation, thus causing redistribution of stresses in the glue layer and their concentration at the overlap end. Upon reaching the level of ultimate stresses, the glue layer fractures and the hybrid joint works as a purely welded or riveted one.

Tensile shear tests of the glued-mechanical specimens showed that strength of the clinch- and TOX-joints with compositions EPU-K and EPU-N is almost identical. Initial fracture occurred in the glue interlayer under the loads twice as high as in the specimens without glue, i.e. the main load is taken up by the glue interlayer, while the rivet functions as a retainer in polymerisation of the glue.

Operation of cars with glued-mechanical joints showed that the cured epoxy glue interlayer is sensitive to surface cracking under dynamic loading and thermal cycling. Intergrowth of cracks leads to their filling up with aggressive media and intensification of crevice corrosion.

Capabilities of formulation methods for regulation of service properties of epoxy glue compositions are limited by narrow ranges of variations in the components making up the system (plasticisers, solvents, filling agents, etc.), the content of which is determined by technological requirements for formation of sound glued-mechanical joints. Therefore, the search for new alternative methods to improve rheological and deformation characteristics of the filled glue compositions is still of current importance.

Investigations were carried out to study a hybrid glue composition (HGC) produced by combining raw rubber and polyurethane, which turned out to be promising in terms of a wider variation of deformation-strength and rheological properties. Organic-silicon elastomer served as a rubber component. The presence of chain-terminal functional groups (Si–OH) in its chain plays an important role in the mechanism of «cold» curing, as the rates of reaction of prepolymer of the urethane matrix with chain-terminal isocyanate groups and silicon are comparable. This made it possible to produce a single-component system in the form of a finished glue composition in the sealed container packing. Curing of this material results from interaction of the atmospheric moisture with hydrolytically unstable groups in molecules of a structuring agent and subsequent reaction with blocked chain-terminal groups of silicon and prepolymer.

Investigation of physical-mechanical properties of the experimental HGC showed their high adhesiveness to aluminium alloys and galvanised steel, as well as to oiled surfaces resulting from the forming process (tensile shear fracture of glued specimens was of a cohesion character). At the same time, high (up to 400 %) elongation is characteristic of elastomeric sealants that effectively protect the overlap joint from crevice corrosion. To use HGC as a structural glue, it is necessary to increase the elasticity modulus and mechanical strength, i.e. the degree of its resistance to external force effects.

Decisive role in physical and, first of all, mechanical properties of the cured glue interlayer is played by the frame of hard particles and fibres, i.e. their packing, orientation and degree of filling of the volume. According to the theory of polydisperse filling [7], the highest effect of strengthening of the glue composition structure is provided by discontinuous granulometry of disperse particles. In this case, fine particles fill up the cavities that inevitably form between coarser particles.

It was established that not only arranging of molecules of the hybrid matrix into a kinetically beneficial position, but also redistribution of intermolecular bonds that catalyse polymerisation reactions occur under the effect of the hard surface of an active filling agent. Here the hydrogen bonds play an important role. Therefore, the non-hydrophobised silicas containing OH-groups on their surface accelerate cross-linking reactions, whereas the hydrophobised ones have no effect.

Hard powders of different chemical nature and degree of dispersion (aerosil, kaolin, aluminium powder, ultra-dispersed silicon carbide powder, high-dispersed iron powder and commercial graphite) were used to investigate filling of the experimental polymeric hybrid matrix.

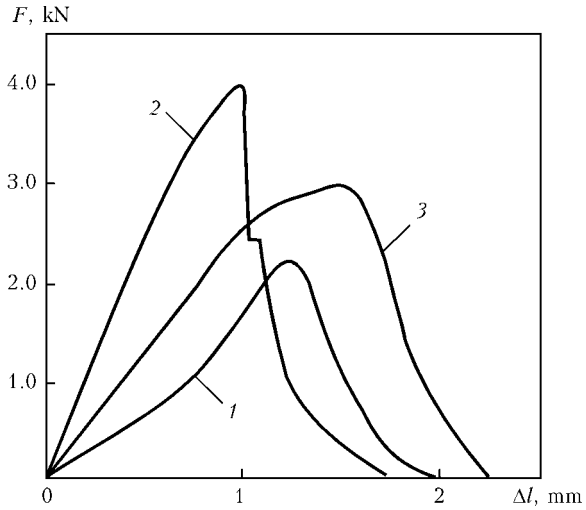

Figure 6. Diagram «force F–deformation Δl» for mechanical (*3*) and glued-mechanical joints with experimental hybrid glued compositions GKK-1 (*1*) and GKK-2 (*2*)

It was found that adding aerosil and kaolin, having on their surface the active groups capable of interacting with the polyurethane component of the hybrid matrix, increases cohesion strength and tightness. Rheological properties of the compositions vary with the concentration of these filling agents.

We used the method of mathematical calculation of the density of packing of the polyfraction loose mixture with simultaneous allowance for the character of interaction of the hybrid polymeric matrix with an inert inorganic surface [8]. This made it possible to solve the following problems: determine the ratio between different fractions of inert filling agents in the polyfraction mixtures, which provided the optimal degree of packing with the highest density and Young modulus; establish the maximum possible doses of the filling agents in the polymeric matrix, which did not prevent formation of the glued-mechanical joints produced by different methods; and provide simultaneous interaction of the glue interlayer and riveting in shear tension with the adhesion-cohesion character of fracture.

Two compositions of HGC were selected, having no effect on the process of formation of the clinch- and TOX-joints. Shear tests of the single-spot glued-mechanical joints showed that the use of GKK-1 increased strength of the clinch- and TOX-joints 1.5 times with simultaneous fracture of the glue interlayer and «button». The use of GKK-2 insignificantly increased strength of the mechanical joint. Fracture of specimens occurred in series — first the separation of the glue interlayer took place to form strands, and then shear or pullout of the «button» followed (Figure 6). Fracture of the glue layer was of a cohesion character. High adhesion strength is indicative of high sealing properties and crevice corrosion resistance.

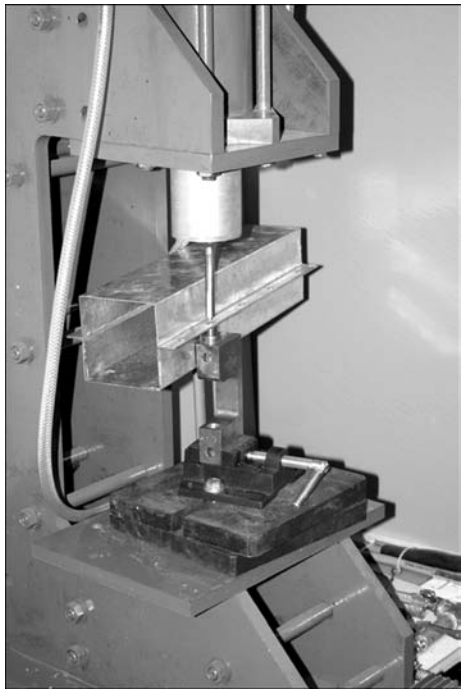

Figure 7. Appearance of pneumatic press for formation of mechanical joints

The investigations conducted resulted in the development of the principles of design of the punch–die system for clinch- and TOX-joints on deep-drawing thin-sheet steel, as well as stationary equipment on the C-frame base with the pneumatic actuator and adjustment of compression in a range of 0–20 kN (Figure 7). The technology for formation of mechanical and glued-mechanical joints produced by the punching method is recommended for manufacture of assemblies of thin-sheet vehicles operating in corrosive environments.

1. Alsman, M. (2001) Modern thin sheets with coatings for automobile construction. *Chyorn. Metally*, **6**, 49–53.
2. Shavyrin, V.N., Ryazantsev, V.I. (1981) *Glued-welded structures*. Moscow: Mashinostroenie.
3. Hahn, O., Budde, L. (1990) Analyse und systematische Einteilung umformtechnischer Fuegeverfahren ohne Hilfsfuegeteil. *Blech Rohre Profile*, 37(**1**), 29–32.
4. Storozhev, M.V., Popov, U.A. (1977) *Theory of pressure treatment of metals*. Moscow: Mashinostroenie.
5. Hahn, O., Peetz, A. (1999) Improvement of the joint element properties through the combination of mechanical fasteners and adhesive bonding. *Welding in the World*, 43(**3**), 38–46.
6. Hahn, O., Wibbeke, T.-M. (2004) Einsatz von warmearmen Hybridfugetechnologien zum Verbinden duennwandiger Blechwerkstoffe. *Schweissen und Schneiden*, **11**, 593–600.
7. Vasiliev Yu.S., Parshutina, L.S., Chukashkin, A.N. (2006) Development of gluing-welding methods for repair and strengthening of elements of industrial and transport structures. In: *Problems of service life and safety of structures, constructions and machines*. Kiev: PWI.
8. Anisimov, I.I., Bochkaryova, S.A., Desyatykh, V.I. et al. (2006) Efficient deformation-strength characteristics of polymer composition with discrete inclusions of different sizes. *Fizich. Mezomekhanika*, **2**, 11–15.

EXPERIMENTAL AND CALCULATION DETERMINATION OF THE CONCENTRATION OF HARMFUL MATERIALS IN THE WORK ZONE AIR IN COVERED-ELECTRODE WELDING

O.G. LEVCHENKO[1], **A.O. LUKIANENKO**[1] and **Yu.O. POLUKAROV**[2]
[1]E.O. Paton Electric Welding Institute, NASU, Kiev, Ukraine
[2]NTUU «Kiev Polytechnic Institute», Kiev, Ukraine

Investigation results are presented on dependence of the concentration of harmful materials in the work zone air in manual rutile-cellulose electrode welding upon the distance to the welding arc under different ventilation conditions (general, local and without ventilation), as well as analytical dependencies of the concentration of harmful materials at different points of the work zone upon the intensity of formation of welding fumes and power of the welding arc.

Keywords: *arc welding, covered electrodes, welding fumes, manganese, ventilation, content of fumes in air, forecast*

Pollution of a work zone air with toxic materials in the form of welding fumes (WF) formed during the electric arc process is one of the main harmful industrial factors in welding engineering. Protection of welders and industrial environment against the WF action is performed by using different ventilation systems, which should provide a content of harmful materials in the work zone air not higher than the maximum allowable concentration (MAC). Experimental data on the content of harmful materials in the work zone air under different ventilation conditions are necessary for selection of the system of ventilation and increase of its efficiency in work places of the welders. Obtaining of such data using conventional methods [1, 2] is a time- and labor-consuming task. Thus, it takes virtually one working shift to take a sample of WF only at one point of the welder's work zone when using a specific welding consumable grade. At that the permissible relative error of the data obtained, in accordance with the requirements [3], is ±25 %. This allows providing a selective determination of the material content at a level of not higher than 0.5 MAC. Taking into account that a large amount of domestic and foreign grades of welding consumables has been used at present in welding engineering, such data are easier to forecast from the index of the WF formation intensity, for the determination of which it is necessary to take no more than 3–5 WF samples during a couple of minutes [1].

The aim of present study is to experimentally investigate dependence of the WF concentration in air of the work zone in covered-electrode welding of low-carbon steel upon the WF formation intensity and/or the arc power, distance to the welding location (welding arc) and type of the ventilation system.

Experiments carried out under laboratory conditions at a typical work place for manual arc welding with and without general and local ventilation. The WF samples were taken around the arc at three points at a different distance from it: 55 cm — welder's breathing zone, 100 and 150 cm — work zone. To compare the efficiency of general and local ventilation systems, its productivity was selected to be the same — 1500 m^3/h. A typical axial fan was used in the system of general ventilation, and a welder's table with built-in exhaust device of the type of a uniform suction inclined panel (Figure 1) was used as a local ventilation system. The samples of WF and gases were taken during the process of deposition of beads by using 4 mm diameter rutile-cellulose electrodes ANO-36 on plates of steel St3sp (killed). The process was performed at the direct current of reverse polarity. The welding current was varied in a range of I_w = = 130–230 A, and arc voltage — in a range of U_a = = 24–40 V to determine dependence of the WF emission intensity upon the arc power. Standard methods [1, 2] were used to take the WF samples in the work zone air and determine the content of manganese as the most toxic component in a composition of WF, formed in low-carbon steel welding, and the WF formation intensity. Reliability of the obtained experimental data was checked according to the accepted instructions [3]. Analytical and statistical processing of the established mathematical dependencies was performed by using the special regression analysis-based software developed by the National Research Institute of the Labor Safety [4, 5].

The investigation results on dependencies of the concentration of WF in the work zone air upon the distance to the welding arc (Figure 2, *a*) showed that this concentration is maximal and decreases with increase in the distance to the arc in welding without ventilation, that it is much lower and increases in the presence of general ventilation, and that it is minimal and hardly changes when using local ventilation. The above-said proves the fact that the local ventilation, which in this case also provides reduction of the manganese concentration below the MAC level (not more

than 0.2 mg/m^3) both in the breathing zone (at a distance of 55 cm from the arc) and at other points of the work zone (Figure 2, *b*), is the most effective. This is explained by the fact that the WF plume is localized by the local exhaust device already in the welding arc zone and does not propagate in the work zone air.

When using general ventilation, the suction port of which is at some distance from the welder's work place, the WF concentration is much higher than in the previous case, and rises even higher with increase in distance from the welding position. This indicates that air, which is polluted with fume in the arc zone, is transferred in a direction to the location of the suction port of the general ventilation system. The manganese concentration in the work zone air at a small (approximately up to 70 cm) distance from the arc is below the MAC level (see Figure 2, *b*).

Dependence on the WF formation intensity and manganese content at different distances from the welding arc and type of applied ventilation was investigated to predict the content of WF and, in particular, manganese as a decisive toxic element formed in general-purpose electrodes welding of low-carbon steel (see Figure 2). Proportionality coefficients (ratios) K_f for WF and K_{Mn} for manganese between the concentration of the given materials at all points of the work zone, where the WF samples were taken, and intensity of their emission were calculated as follows:

$$K_{f(Mn)} = C_{f(Mn)}/V_{f(Mn)}, \quad (1)$$

where $C_{f(Mn)}$ is the concentration of WF and manganese, respectively, in the work zone, mg/m^3; and $V_{f(Mn)}$ is the intensity of emission of WF and manganese, equal to 0.807 and 0.036 g/min, respectively.

Processing of the experimental data shown in Figure 2, performed by using the Lagrange interpolation formula [6], allowed deriving the following dependence of the proportionality coefficients upon distance L to the welding arc:

in welding without ventilation

$$K_{f(Mn)} = 0.0039L^2 - 0.019L + 0.0563; \quad (2)$$

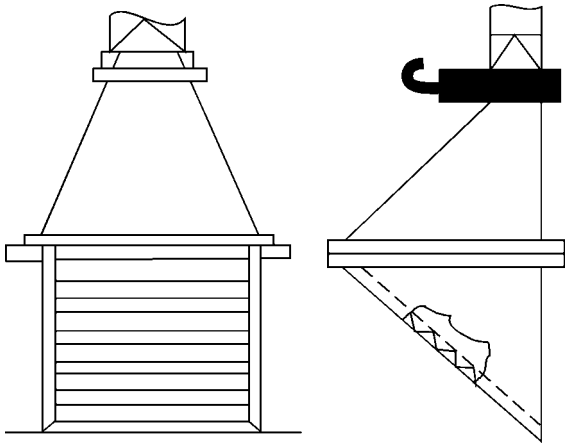

Figure 1. Built-in exhaust device of the type of uniform suction inclined panel over the welder's work table

in welding with general ventilation

$$K_{f(Mn)} = -0.0085L^2 + 0.0295L - 0.011; \quad (3)$$

and in welding with local ventilation

$$K_{f(Mn)} = -0.0005L^2 + 0.0014L - 0.0003. \quad (4)$$

The relative error in the developed mathematical models is no more than 1.8 %.

The C_f and C_{Mn} values are found from formula (1):

$$C_{f(Mn)} = K_{f(Mn)}V_{f(Mn)}. \quad (5)$$

Substituting dependencies (2)–(4) to formula (5) yields the mathematical models for prediction of the concentration of WF and manganese depending upon the intensity of their emission and distance to the welding arc:

in welding without ventilation

$$C_{f(Mn)} = V_{f(Mn)}(0.0039L^2 - 0.019L + 0.056); \quad (6)$$

in welding with general ventilation

$$C_{f(Mn)} = V_{f(Mn)}(-0.0085L^2 + 0.0295L - 0.011); \quad (7)$$

and in welding with local ventilation

$$C_{f(Mn)} = V_{f(Mn)}(-0.0005L^2 + 0.0014L - 0.0003). \quad (8)$$

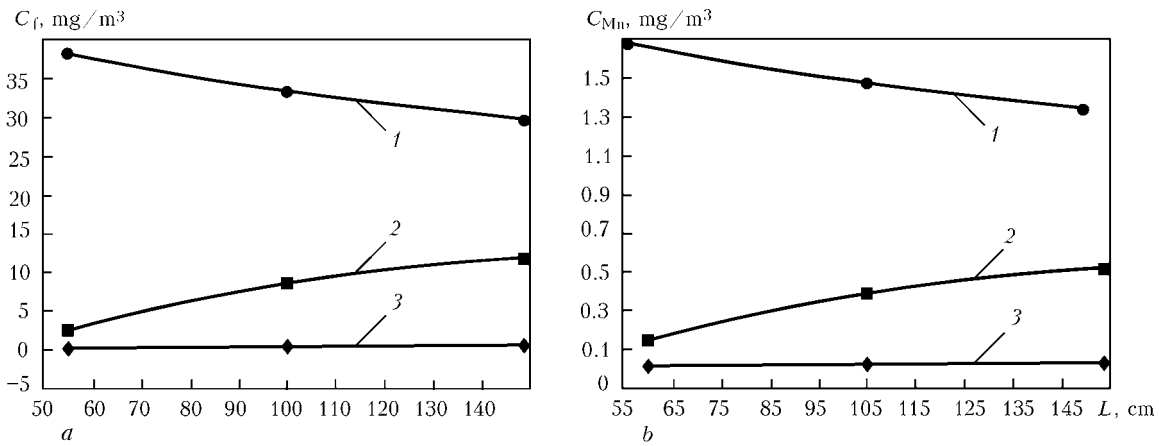

Figure 2. Dependence of WF C_f (*a*) and manganese concentration C_{Mn} (*b*) in the work zone air upon distance L to the welding arc in arc welding without ventilation (*1*), with general (*2*) and local (*3*) ventilation

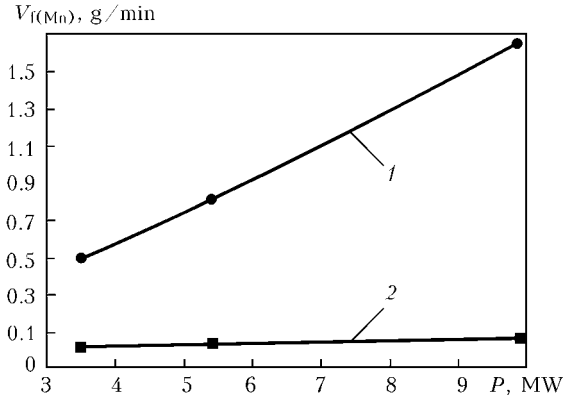

Figure 3. Dependence of the intensity of formation of WF V_f (*1*) and manganese V_{Mn} (*2*) on arc power P

Thus, the concentration of these materials at different points of the welder's work zone with or without ventilation can be easily calculated at a high reliability level from the experimental data on the intensity of emission of WF or manganese, the determination of which involves no particular difficulties [1, 2]. Otherwise, if it is impossible to obtain these data, then other, less accurate method, based on the experimentally established dependence of the intensity of formation of WF and manganese upon the welding arc power, can be employed (Figure 3). Analytical processing of these data by the regression analysis method allowed deriving the following dependencies:

$$V_f = -0.178 + 0.187 I_w U_a, \quad (9)$$

$$V_{Mn} = 0.0014 + 0.0058 I_w U_a, \quad (10)$$

where I_w is the welding current, A; and U_a is the arc voltage, V. The relative errors in dependencies (9) and (10) are 2.1 and 3.7 %, respectively; and the ultimate correlation coefficients are 0.999 and 0.994.

Checking accuracy of the calculation data, compared with the experimental ones, showed that their relative error did not exceed 5.3 % (Table).

Generalization of our experimental and calculation data [7] showed that the intensity of emission of WF did not exceed 0.4 g/min in welding with rutile electrodes and 1.0 g/min in welding with cellulose ones. The content of manganese oxides in WF formed in rutile electrode welding was no more than 10.2 %, and in cellulose electrode welding — 5.5 %. The experimental part of this study was performed with the rutile-cellulose electrodes widely used at present. At the same time, the intensity of WF formation under optimal conditions (I_w = 180 A, U_a = 30 V) was 0.81 g/min (more than for the rutile coverings, but less than for the cellulose ones), and the manganese content was 4.45 % (not more than in study [7]).

Results of verification of the calculation data on the content of manganese in the work zone air in welding with electrode ANO-36

Type of ventilation	L, m	C_{Mn}, mg/m^3		Relative error, %
		Calculation	Experimental	
Without ventilation	0.55	1.700	1.700	0
General	1.00	0.360	0.380	5.3
Local	1.50	0.024	0.023	4.3

Given that the relative error of the WF content in the work zone air, according to the requirements [3], is ±25 %, the developed mathematical models can be applied for an approximate estimation of pollution of the work zone air with manganese in welding of low-carbon steel by using rutile and rutile-cellulose electrodes of different grades.

Considering that manganese is the main harmful component in composition of WF, determining the labor conditions in manual rutile-cellulose electrode welding of low-carbon steels, to decide on the type of ventilation (general or local) it is necessary to use the data on the concentration of manganese in the work zone air, and to calculate the efficiency of ventilation it is necessary to use the data on its emission intensity.

Results of the investigations proved that the local ventilation is much more efficient than the general one. It allows reducing the manganese concentration below the MAC level in the welder's breathing zone and work zone of the production area (see Figure 2).

Prediction of the WF and manganese content in the work zone to select the type of ventilation and its optimum parameters can be performed from formulae (6)–(8), firstly by experimentally determining the intensity of their emission [1, 2] or calculating it depending on the welding conditions (welding current and arc voltage) from expressions (9) and (10).

1. (1980) *Guidelines 1924–78*: Hygienic evaluation of welding consumables and methods for welding, surfacing and cutting of metals. Moscow: Minzdrav SSSR.
2. (1990) *Guidelines 4945–88*: Determination of harmful materials in welding fumes (particulate and gaseous phases). Moscow: Minzdrav SSSR.
3. (1985) *Guidelines 3936–85*: Control of the content of harmful materials in work zone air. Moscow: Minzdrav SSSR.
4. Orlovsky, P.N. (1996) *System analysis*: Training aids. Kiev: ISMO.
5. Ferster, E., Renz, B. (1987) *Methods of correlation and regression analysis*. Moscow: Fin. i Statistika.
6. Myshkis, A.D. (2007) *Elements of the theory of mathematical models*. Moscow: KomKniga.
7. Pokhodnya, I.K., Gorpenyuk, V.N., Milichenko, S.S. et al. (1990) *Metallurgy of arc welding. Processes in arc and melting of electrodes*. Ed. by I.K. Pokhodnya. Kiev: Naukova Dumka.

ASSESSMENT OF THE EFFECTIVENESS OF REPAIR TECHNOLOGIES FOR POWER PLANT OPERATION*

L.V. KRAVCHUK, B.A. LYASHENKO, G.V. TSYBANEV, R.I. KURIAT, K.P. BUJSKIKH and **Yu.S. NALIMOV**
G.S. Pisarenko Institute for Problems of Strength, NASU, Kiev, Ukraine

Tendencies in development of repair technologies in service of gas turbine engines (GTE) are considered. A procedure was developed for qualitative assessment of the influence of part repair technologies on the set of mechanical characteristics of base material in the repair zone. The effectiveness of the technology is determined by the change of mechanical properties.

Keywords: *power plants, repair technologies, gas turbine engine parts, mechanical properties*

Modern tendencies in development of gas turbine construction consist in creation of a service system simultaneously with development of new engines [1]. The most effective element of this system is introduction of advanced technologies of corrective maintenance to extend the operation period with setting up of specialized centers of engine repair. In the USA repair of aircraft equipment is performed by engine manufacturers, large independent repair companies, as well as subdivisions of major carriers [2]. According to predictions, sales of new Boeing aircraft in the next 20 years will amount to 1.7 trln USD, and service income will be 3.1 trln USD. And half of this sum will come from repairs. In 2000 repair income was equal to 44.6 bln USD, and by 2002 it will rise to 110 bln USD [2].

At present the segment of GTE manufacturers in engine service and repair sector is growing. Rolls-Royce has 300 major customers in 50 countries [3, 4], and promotes establishment of subsidiaries specializing in repair. Company's annual contracts amount to 9 bln USD.

GE is developing new repair technologies [5], also for the USA [6], Alstrom is creating CLE system envisaging application of new repair technologies to increase GTE overhaul periods [7]. Leading companies are building enterprises for power equipment repair in different regions of the world [8]. Repair routine for an industrial GTE is being patented [9]. Starting from 2000, Trans Canada Turbines has provided GTE overhaul service. In the next 10 years the sum of orders for repair of GTE of RB 211 type will exceed 250 mln USD [10]. Ever more attention is given to development of repair technologies and repair personnel training [11] in prediction of repair costs [12].

A key issue of repair technologies remains to be assessment of residual life and its extension, so that a number of studies are devoted to development of procedures and mathematical models of damage medium mechanics for theoretical analysis of the processes of life exhaustion of structural element materials, allowing for degradation processes developing under operation conditions [13, 14]. Comparison of strength analysis results with structural changes in the metal proceeding in high-temperature service, allows determination through calculations of the most probable sites of damage accumulation [15].

Practical repair and reconditioning of power equipment components makes use of a broad range of modern technologies. For GTE blade repair MTU Aero Engines GmbH patented a combination of the methods of powder metallurgy, welding and machining of the weld area [16], as well as a repair technology of brazing with nickel alloy based brazing filler metals [17]. The methods of efficient and rational application of brazing for repair of defective blades of GTE hot stage and the main technologies developed for these purposes, are given [18, 19]. Cut-out defective sections are filled with molten powder material, consisting of the braze alloy and filler by argon microplasma spraying [20]. Techniques of laser welding up of defects and laser cladding for repair of spot defects in different combinations of heat and finish treatment are becoming ever wider accepted in practice [21–27].

It is difficult to repair parts from high-temperature nickel alloy with high aluminium and nickel content by regular welding processes. Therefore, the method of electrospark alloying using high-strength filler is promising for repair of unweldable alloys. It is noted [28] that mechanical properties of the repaired section are quite satisfactory, but introduction of the technology of electrospark alloying into industry will require certain efforts in the future. IHI and Mitsubishi developed a new method of electrospark alloying, namely micro spark coating (MSC) [29] for GTE blade repair, which uses the energy of highly-sensitive microelectric discharges, and can replace the traditional repair techniques in a number of cases, namely

*The article was prepared on the basis of results of accomplishment of the NASU targeted integrated program «Problems of Remaining Life and Safe Operation of Structures, Constructions and Machines» (2007–2009).

welding, galvanic, and thermal. Toshiba developed method of hot isostatic pressing (HIP) for reconditioning of GTE blades [30]. Extension of the service life of a part with some fatigue damage is achieved with ion nitriding technology [31].

New integrated technological processes of GTE blade repair, combining various operations, are becoming accepted. Processes of welding and subsequent local heat treatment by the electron beam are efficient [32]. Snecma Moteur SA applies cold rolling after welding of the defective section of blade airfoil. This induces residual compressive stresses in the blade airfoil, which compensate the residual tensile stresses in the weld, thus achieving strengthening of the reconditioned structure. This technique is effective for repair of solid discs with blades, when individual blades cannot be removed for replacement or reconditioning [33].

Most of the repair technologies should be regarded as alternative. In this connection it is necessary to develop procedures of technology assessment and selection.

The effectiveness of repair technologies can be evaluated primarily by the change of the set of mechanical properties of the repaired defect zone compared to properties of unrepaired zone [34].

The purpose of this study is development of the procedure of quantitative assessment of the influence of repair technologies on service properties of base material in the repair zone.

Experimental procedure. Samples from undamaged material and samples with repaired defects — simulators of real damage made from models of GTE blades from EK-9 alloy — were used to perform a series of studies of the influence of the features of repair technology on the characteristics of short-time and long-time static strength, as well as high-cycle fatigue. Repair technologies of arc welding and cladding and microplasma powder cladding developed at PWI were used. Samples were made by spark erosion process. After the cladding cycle the samples were heat-treated according to the accepted repair technology. Two-sided notches of 10×0.5 mm size were made on side surfaces of the flat sample as damage simulators.

A feature of testing was the fact that deformation not of the entire sample, but just of the damaged area was measured using extensometer with 12 mm measurement base. It was also measured in a similar area of an undamaged sample. Diagrams of deformation of such samples at temperatures of 20 and 800 °C were recorded. Investigations were conducted in INSTRON testing system. Programmed loading, thermal condition control and data processing in the numerical and graphic form were provided in the automatic mode.

Two types of samples of EK-9 alloy were made for high-cycle fatigue testing: cylindrical smooth samples for determination in the initial condition and samples with a raiser of 1 mm depth and 2 mm length along sample generatrix. The raiser simulated a defect to be repaired. A sample supported in cantilever was mounted in an electrodynamic tester. During testing the range of oscillations of the cantilever sample free end corresponding to the required level of stress amplitude, was established. The range was monitored by MBS-2 optical microscope, the number and frequency of loading cycles — by data processing frequency meters ChZ-34.

Assessment of the influence of repair technology on the thermal stress and strain state was performed by design-calculation method. Investigations were conducted on wedge-like samples simulating blade edge. Damaged zone cutting out and subsequent repair microplasma powder deposition of a bead were applied to repair the damaged edge. The level of thermal stress state of wedge-like sample edge after repair depending on the technological modes of testing was assessed in a gas-dynamic bench in keeping with the standard [35]. Calculations of thermal and stress-strain state (SSS) of the repaired samples were conducted using SPACE applied software package [36]. Characteristics of EK-9 (base metal) and EP-539 (deposit metal) alloys were used in calculations. The damage stage was considered, when thermal fatigue cracks of up to 0.5 mm length develop on the edge, and edge building-up to 0.7 mm depth is required, which corresponds to the edge rounding-off radius. Results of thermometering of samples in the tester by fixed thermal cycling modes were the basis for analysis of the kinetics of thermal state and SSS of the material. The most stringent mode of GTE blade operation was used, namely 60 s heating and 60 s cooling in the temperature range of 350–1100 °C.

Results and their discussion. *Short-term and long-term static strength*. Analysis of investigation results allows making the following statements.

Deformation curves obtained on undamaged samples (Figure 1, curve *1*) run somewhat lower (≈ 10 %) than the certificate characteristics of EK-9 alloy. This is indicative of the influence of the processes of model blade manufacturing, which lead to certain deviations of mechanical characteristics. Technology of spark erosion treatment of the samples can have additional influence.

Analysis of deformation curves of the sample test portion in the repaired defect zone (Figure 1, *a*, curve *2*) points to 15 % lowering of limit characteristics of strength and significant lowering (more than 50 %) of the ductility margin. However, sample failure at tension occurs beyond the zone of the repaired defect. Therefore, it may be stated that the developed repair technology ensures recovery of material strength to the level not lower than that of the sound region.

Results of long-term strength testing given in Figure 2 show that the nature of failure of sound and repaired samples is practically identical to the given in Figure 1 results of short-term static testing. Similar to short-term testing, the repair zone in the repaired sample is not a weak link.

Prediction of performance by the criterion of resistance to long-term loading was performed using the base diagram method (BDM) suggested by V.V.

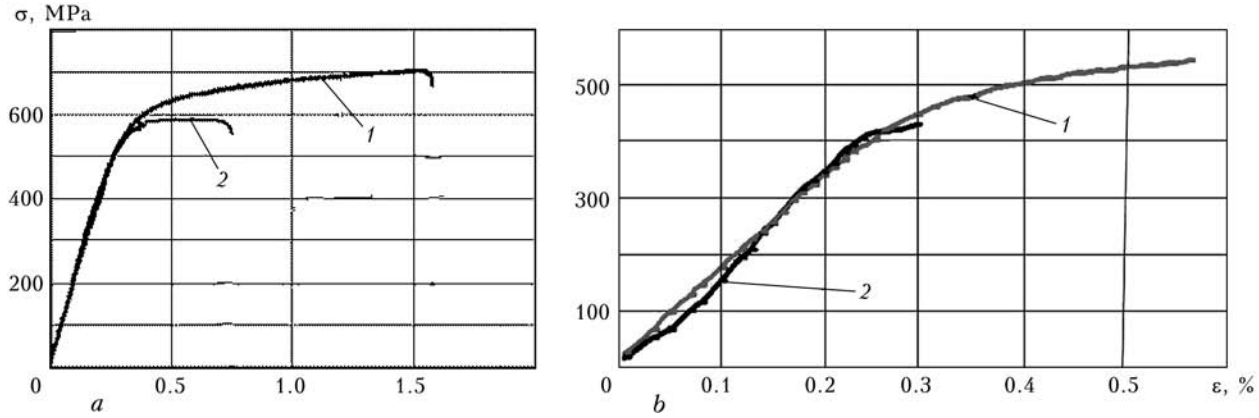

Figure 1. Curves of short-time deformation of a defect-free sample (*1*) and sample with a repaired defect (*2*) at temperature of 20 (*a*) and 800 (*b*) °C

Krivenyuk [37]. This requires information about the behaviour of an analog-material in a certain time interval of prediction; results of static testing (see Figure 1); limited information on the studied material behaviour at long-term loading at a limited cycle number (see Figure 2). If information is available, other data on similar materials as to composition and properties are also used.

Proceeding from the data on the nature of property change allowing for the true scatter of data, coefficients of the base diagram equation were found in the following form:

$$\lg \sigma_t' = \lg \sigma_1 - (3.6 - \lg \sigma_1)(\lg t + 0.11g^2t)/12,$$

where σ_t' is the current value of stress in the base diagram, MPa; σ_1 is the stress leading to fracture within 1 h; t is the time to fracture, h.

Features of individual sections of long-term strength curve are precised using experimental characteristics. A fundamental aspect of application of BDM prediction procedure is determination of correction coefficients, which allow for the kinetics of ductility variation. Tentative calculations by BDM procedure demonstrate a lowering of long-term strength characteristics over considerable time base to the level of about 30 % of the initial values.

High-cycle fatigue. Testing of initial samples was conducted at resonance frequency of 850–900 Hz by the first oscillation mode. Endurance limit was determined on the base of $2 \cdot 10^7$ cycles. Number of loading cycles was recorded during testing. Start of lowering of resonance frequency (1), and lowering of resonance frequency by 1 % (2) were taken to be the limit state criterion. The first of them was taken to be the fatigue life, which corresponds to the moment of fatigue crack initiation, which is followed by the process of crack development to the moment of lowering of resonance frequency by 1 %. The latter fatigue life was taken as the sample final fracture. Testing results are given in Figure 3.

Analysis of the curves is indicative of the fact that in terms of cycle number the process of fatigue crack development is 3 to 4 longer than before crack initiation. A feature of fatigue fracture is presence of several cracks on the surface of sample test part.

After application of repair technology the samples were ground. Resonance frequency was 720 Hz. Fatigue curves after application of repair technology are given in Figure 4. Comparison of testing results shows that samples after repair have lower fatigue characteristics than the initial values (σ_{-1} = 240 MPa — initial; σ_{-1}^{rep} = = 205 MPa — samples after repair). In addition, whereas the fatigue curve of the initial samples has the shape of an inclined curve up to the number of cycles of $2 \cdot 10^7$, the curve for the repaired samples has a steeper slope and physical fatigue limit equal to $2 \cdot 10^7$ cycles with curve break abscissa on the level of $3 \cdot 10^6$ cycles. Fatigue cracks in samples after repair developed not in the weld zone, but in the HAZ metal.

Obtained results were interpreted in terms of limit exhaustion of ductility in keeping with the model proposed in [38, 39].

Thermal-stress state of materials in the repair zone. The main purpose of work in this direction was assessment of the influence of the difference between

Mechanical properties of EK-9 alloy

Temperature, °C	σ_t, MPa	$\sigma_{0.2}$, MPa	δ, %	*E*, MPa
20	704.2 / 597.0	637.3 / 570.0	1.3 / 0.5	180 / 180
800	630.8 / 460.0	536.0 / 450.0	0.6 / 0.3	153.19 / 153.19

Note. The numerator gives the initial values, the denominator — values after repair.

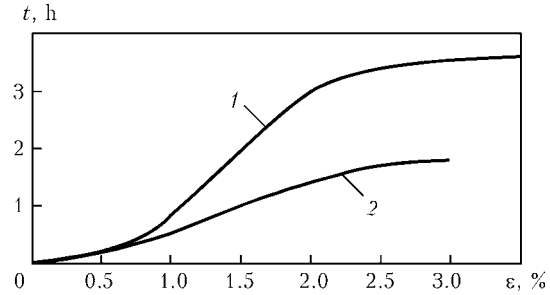

Figure 2. Curves of creep of defect-free samples (*1*) and samples with a repaired defect (*2*) at the temperature of 800 °C

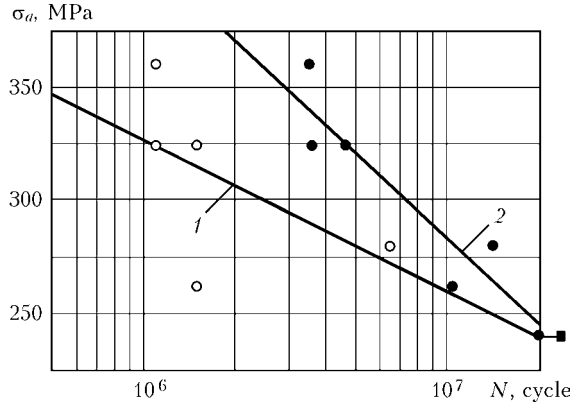

Figure 3. Fatigue curves of samples from EK-9 alloy in the initial state: *1* — start of lowering of resonance frequency; *2* — lowering of resonance frequency by 1 %

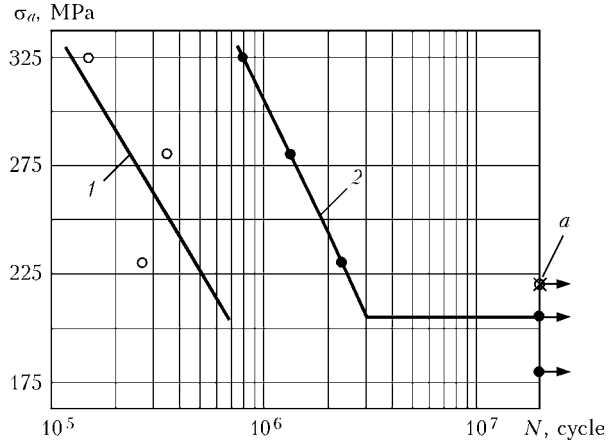

Figure 4. Fatigue curves of samples of EK-9 alloy after repair: *1* — start of resonance frequency lowering; *2* — start of resonance frequency lowering by 1 %; *a* — sample after testing (N = 2·10^7 cycles) first at σ_a = 205, and then at σ_a = 220 MPa

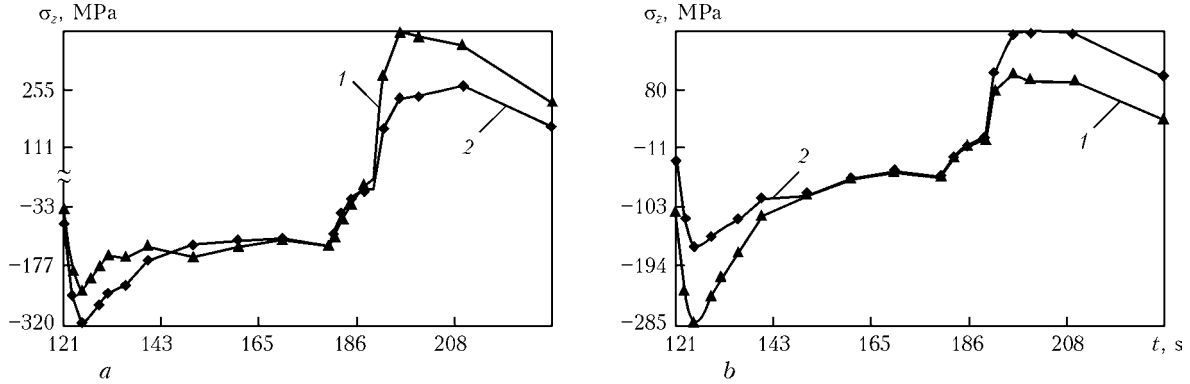

Figure 5. Variation of stresses σ_z in the point of contact of deposit material (*1*) and base metal (*2*) in the thermal load cycle by condition 1 (*a*) and 2 (*b*)

the properties of the base and deposited metals on the level of residual process stresses and kinetics of their variation under the conditions of variable temperatures.

Predominant attention was given to two variants implemented in practice. In the first model problem an assumption was made that the repair technology ensures absence of residual stresses at the temperature of 20 °C, i.e. at this temperature the initial stresses in the wedge are absent. In the second model problem the initial assumption was that the repair deposit was made at the temperature of 1200 °C and at this temperature and uniform thermal state initial stresses are absent. Generalized results of such analysis are given in Figure 5.

Comparing thermal stress states of the wedge-like sample in the thermal load cycle of the two variants of the initial state of materials in the deposit zone, we can note the following. Higher stresses, both compressive and tensile, arise in the case of variant 1. However, while the compressive stresses in the two variants are close in absolute values, tensile stresses, which are particularly hazardous for initiation and development of thermal fatigue cracks, are much smaller for case 2, which gives a more adequate representation of the actual situation. These stresses are as follows: for variant 1 — 400 (on the edge), 380 (deposit metal) and 245 (base metal), and for variant 2 — 145, 110 and 171 MPa, respectively.

In conclusion it should be noted that in practical operation of power plants, including AGTE, a tendency has emerged, when the scopes of repair and reconditioning operations start exceeding the volume of new equipment sales. This discrepancy will increase with time.

Practical repair and reconditioning operations are performed with application of a wide range of modern technologies. A greater effect of ensuring the required level of properties is achieved when using multioperation integrated technologies. Their effectiveness is determined by the level of lowering of the set of mechanical properties of the reconditioned parts.

CONCLUSIONS

1. A procedure is proposed for qualitative assessment of the influence of repair technologies on the service properties of base material in the repair zone. The procedure uses laboratory, bench and numerical methods determining the characteristics of short-time and long-time static strength, high-cycle fatigue, as well as assessment of thermal stress state of the repair zone.

2. Further studies are required on a multifactorial experiment to determine the optimum technological modes of repair technologies. The set of optimization

criteria should include cost indices. Assessment and prediction of the residual life of reconditioned parts are performed by calculation methods based on experimental laboratory testing.

3. It is necessary to develop standard documents specifying introduction in repair plants of the procedures for determination of the set of mechanical properties, depending on the technological modes.

1. Marchukov, E. (1997) New possibilities of engine service. *Aviapanorama*, **5/6**, 53–55.
2. Shifrin, S. (2001) Taking wind. *Airline Bus*, 17(**10**), 61, 63–64.
3. Phillips, E.N. (1999) Rolls-Royce bullish on MRO opportunities. *Aviat. Week and Space Technol.*, 150(**13**), 78–80.
4. Velocci, A.L. (1999) Engine makers target greater MRO share. *Ibid.*, 151(**13**), 27–28.
5. Repair technology breeds success. *Mod. Power Syst.*, 17(**11**), 69, 71.
6. Kandebo, S.W. (1994) USAF GE develop F110 engine plan. *Aviat. Week and Space Technol.*, 141(**24**), 22–23.
7. (1999) Longer engine life with upgrade kits. *Gas Turbine World*, 29(**2**), 46, 48.
8. Jeffs, E. (1999) ESCO would set up repair shop in Thailand. *Turbomach. Int.*, 40(**1**), 32–34.
9. *Gas turbine repair*. Pat. 5575145 USA. Int. Cl. F02C 7/00. Publ. 19.11.96.
10. (2000) RB211 gas turbine repair and overhaul. *Gas Turbine World*, 30(**3**), 30.
11. Pyle, A.S., Rudisel, D.A. (1997) Efficient turbomachinery turnaround. *Chem. Eng.*, 104(**5**), 132–141.
12. Avakyan, A.A., Blinov, A.V., Novikov, N.N. et al. (2001) Prediction of economic costs maintenance and repair of aircraft complex. *Metrologiya*, **8**, 3–14.
13. Kajdalov, V.B., Korotkikh, Yu.G., Panov, V.A. et al. (2006) Mathematical modeling of processes of life exhaustion of structure elements on the base of damaged medium mechanics. In: *Abstr. of 9th All-Russian Meeting on Theor. and Appl. Mech.* (Nizhny Novgorod, 22–28 August 2006). Vol. 3. N. Novgorod: NNGU, 104.
14. Chandra Murthy, R.A., Palani, G.S., Iyer Nagesh, R. (2007) Remaining life prediction of cracked stiffened panels under constant and variable amplitude loading. *Int. J. Fatigue*, 29(**6**), 1125–1139.
15. Danyushevsky, I.A., Kupry, E.B., Malkin, M.R. et al. (2008) Assessment of residual life taking into account the microdamage. *Teploenergetika*, **2**, 17–20.
16. *Process of production and (or) repair of gas turbine engine blades*. Appl. 102005019077 Germany. Int. Cl. B22F 5/04. Publ. 26.10.2006.
17. *Solder alloy, method of its application and method of treatment, in particular, repair of parts, especially of gas turbine blades*. Appl. 10356562 Germany, Int. Cl. B23K 35/28. Publ. 30.06.2005.
18. Kornienko, A.N., Zhadkevich, A.M. (2000) State-of-the-art and problems of brazing application in repair of gas turbine engine blades. *Zagot. Proizv. v Mashinostroenii*, **10**, 9–12.
19. Zhadkevich, A.M. (2005) Brazing of defects of aircraft and ship turbine blades — challenging technology of extension of their life. *Advances in Electrometallurgy*, **1**, 33–39.
20. *Method of repair of machine part surface defects*. Pat. 2310551 Russia. Int. Cl. B23P 6/00, C23C 14/40. Publ. 20.11.2007.
21. Yurkevich, S.N., Fomikhina, I.V. (2004) Laser cladding of local surface defects of 30KhGSN2A steel parts. *Instrum. i Tekhnol.*, **19/20**, 122–126.
22. Popov, V.N., Popova, M.V., Voloshin, D.E. (2007) Study of efficiency of laser systems application at reconditioning of worn parts in repair production. *Trudy Bratsk. Gos. Tekhn. Univers.*, **2**, 238–242.
23. *Method of production and (or) repair of gas turbine parts*. Appl. 10337866 Germany. Int. Cl. C23C 24/10. Publ. 24.03.2005.
24. Yurkevich, S.N., Tomashevich, A.V., Yurkevich, A.S. (2006) Reconditioning of aircraft system parts by laser cladding method. *Remont, Vosstanovlenie, Modernizatsiya*, **3**, 31–33.
25. *Method and device for repair of structure parts*. Appl. 102004002551 Germany. Int. Cl. B23K 26/34. Publ. 18.08.2005.
26. Yurkevich, S.N. (2005) Repair without dechromizing of spot and local defects on aircraft system parts of high-strength steels 30KhGSN2A and 30KhGSA with chromium coating. *Metalloobrabotka*, **3**, 39–41.
27. Blackshire, J.L., Dosser, L., Hix Ken (2004) Laser processing of microcracks for structural life extension. *Proc. of SPIE*, **5392**, 168–178.
28. Xie Yu-Jiang, Wang Mao-Cai. (2005) Unweldable superalloy component repair using electro-spark deposition with high strength filler material. *Transact. on Nonferrous Metals Soc. China*, 15, Spec. Issue 3, 359–364.
29. Ochiai, H., Watanabe, M., Arai, M. et al. (2005) Development of technology of coating deposition and cladding by MSC method using electric discharge energy. *Harima Eng. Rev.*, 45(**2**), 72–79.
30. Saito, D., Yoshika, Y., Ishibashi, K. et al. (2004) Study on the HIP technology for the life extension of gas turbine buckets. *Schiff und Hafen*, 56(**4**), 42.
31. Alsaran, A., Kaymaz, I., Celik, A. et al. (2004) A repair process for fatigue damage using plasma nitriding. *Surface and Coat. Technol.*, 186(**3**), 333–338.
32. Sharonova, N.I. (2006) *Technology of repair of rotor and case structures of gas turbine engines by electron beam treatment*: Syn. of Thesis for Cand. of Techn. Sci. Degree of MATI. Moscow: RGTU.
33. *Method of repair of damaged blade airfoil of aircraft turbo-jet engine*. Appl. 2871399 France. Int. Cl. B23P 6/04, B23P 15/02. Publ. 16.12.2005.
34. Yushchenko, K.A., Kravchuk, L.B., Lyashenko, B.A. et al. (2009) Technological processes for repair of GTE blading with different types of damage. In: *Proc. of 9th Int. Sci.-Techn. Conf. on Surface Engineering and Renovation of Products* (25–29 May 2009, Yalta, Crimea). Kiev: ATM Ukraine, 246–248.
35. *DSTU 2367–94*: Unified system of corrosion and ageing protection. Metals, alloys, heat-resistant coatings. Method of testing for high-temperature corrosion and thermal fatigue in a flow of combustion products.
36. Software «Three-dimensional final element modeling of thermal and thermal-stressed state of elements in machine-building structures (SPACE)». In: *Certification system Ukr-SEPRO*.
37. Krivenyuk, V.V. (1990) *Prediction of long-term strength of refractory metals and alloys*. Kiev: Naukova Dumka.
38. Tsybanev, G.V., Tsybanev, M.V. (2005) Model of limit strengthening of material as a criterion of crack initiation in high-cycle loading. In: *Abstr. of Int. Sci.-Techn. Conf. on Dynamics, Strength and Service Life of Machines and Structures*. Vol. 2. Kiev: IPP, 361–362.
39. Tsybanev, G.V., Novikov, A.I. (2008) Application of limit strengthening model for assessment of fatigue life of materials under alternating conditions of cyclic loading. In: *Proc. of Int. Sci.-Techn. Conf. on Materials and Mechanisms of Sea Transport. Methods of Testing and Strengthening. Technology of Production*. Sevastopol: UMI, 149–160.

INCREASE OF RESISTANCE OF WELDS TO FORMATION OF CRYSTALLINE CRACKS IN REPAIR OF BANDS OF KILN FURNACES USING ELECTROSLAG WELDING

S.M. KOZULIN[1], **I.I. LYCHKO**[1] and **M.G. KOZULIN**[2]
[1]E.O. Paton Electric Welding Institute, NASU, Kiev, Ukraine
[2]Toliatti State University, Toliatti, Russian Federation

The results of study of causes of appearance of crystalline cracks in central parts of layers of multi-layer electroslag weld are given. The method of increase of resistance of such welds to formation of crystalline cracks applied to repair of damaged bands of rotary kiln furnaces at the site of their operation is developed.

Keywords: *multi-layer electroslag welding, rotary furnaces, bands, carbon steels, crystalline cracks, repair, weakness area*

The most critical parts of rotary kiln furnaces are bearing bands of solid rectangular section, which are mounted on the furnace body with a definite radial gap, and bands of solid shaped section, welded-in into the furnace body [1]. The bands are manufactured of medium-carbon steels of the type 35L, 30GSL and 34L-ESh. The sizes of cross sections of butts being welded of bands are (355–500) × (900–1350) mm, outer diameter is up to 8450 mm.

Through cross cracks, often initiated in the bands of rotary furnaces during operation, result in forced and durable stop of the whole machine for replacement by a new band or repair of the band which came out of order [2].

In most cases the rewelding of cracks is performed without removing of a band from the furnace body. To realize this method of repair a band is set in a way that damaged place was positioned strictly in upper position by rotation of the furnace body. To repair the non-through cracks the groove is made using drilling of holes of 50 mm diameter with a pitch of 0.8–0.9 of diameter, and welding is performed using non-consumable nozzle with a feed of single wire of 5 mm diameter [3]. However due to the high rigidity of fastening of edges in re-welding of holes of the depth of more than 100 mm the crystalline cracks are formed in welds (Figure 1). Besides, the re-welding of through cracks is complicated by the requirements of limitation of residual deformations, distorting the initial geometric sizes of a band.

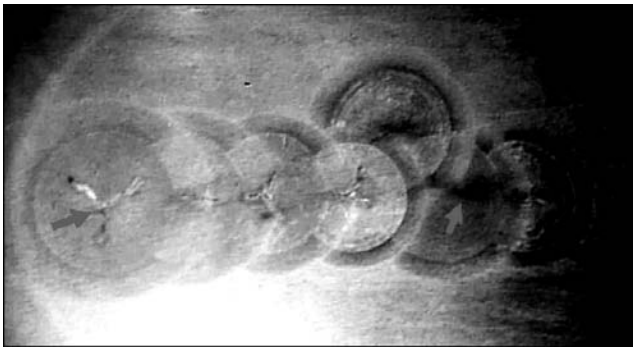

Figure 1. Transverse macrosection of specimen of steel 35L of 500 × × 300 × 500 mm size with hot cracks formed after ESW of holes of 50 mm diameter and 500 mm depth

The comparative analysis of efficiency of application of existing methods of repair of similar defects using fusion welding showed that the most promising technological process for repair of fractured bands directly at the site of their operation (at the furnace) is the multi-layer electroslag welding (MESW) [2, 3]. However its application is limited by the number of factors, one of which is a low resistance of weld layers to formation of crystalline cracks in the central part of the weld layers.

To study causes of initiation of these defects and to develop the technological methods of improving resistance of layers of multi-layer weld to formation of crystalline cracks, the number of experiments was carried out. The investigation was performed according to the procedure, including comprehensive study of experience of application of MESW, analysis of obtained results, development of new methods of welding and their practical realisation at making the MESW of specimens.

The sizes and material of specimens were selected similar to specimens-witnesses applied at manufacturing of bands of rotary furnaces (Figure 2). The welding machines of the type A-645 and A-1304 with power source TShS-3000-3, electrode wires of grades Sv-08GA and Sv-10G2 of 3 mm diameter, and also flux AN-8M were used. In the process of welding the main parameters of conditions were recorded using information-recording system ISU-150 [4]. The welded specimens were cut into templates, from which transverse and longitudinal macrosections were produced, the prints were taken according to Bauman.

Considering the peculiarities of electroslag welding (ESW) of large workpieces in thickness and sizes it turned out to be impossible to apply known methods of quantitative evaluation of resistance of a weld to formation of crystalline cracks [5–7]. Therefore, to obtain qualitative evaluation of metal resistance against hot cracks formation the so-called rigid sam-

ples were investigated [8]. According to these methods the specimens, similar by sizes and their mass to production workpieces (full-scale specimens), are welded. To increase rigidity, the fixing distance gaskets were placed into a welding gap (see Figure 2). As the criteria of evaluation of weld metal resistance against hot crack formation the specific heat input of welding was taken E_w, providing guaranteed fusion at minimal required penetration depth without hot crack formation.

With the purpose of providing the sufficient resistance margin of a weld metal to crystalline crack formation the preheating of full-scale specimens (rigid samples) was intentionally not performed before welding.

In MESW using vertical welds the rigidity of edges fastening was caused by mounting of transverse metallic bridges, forming the groove (see Figure 2). The rigidity of joint increases with layout of layers (increase of obstacle to free shrinkage of crystallizing metal). As far as decrease of rate of tensile deformation of weld metal by decrease in welding speed failed due to the loss of steadiness of electroslag process [5, 9] it was decided to change the conditions of formation of a multi-layer weld.

According to the selected methods the specimens (Figure 2) of the steels 30L and 34LESh were re-welded. The holes formed at mounting of plates of rolled metal were re-welded successively using dual electrode consumable nozzle at specific heat input E_w = 110–170 kJ/cm^2.

The study of transverse macrosections of welded joints of performed specimens showed that after re-welding of holes of rectangular shape the lines (areas) of fusion have an elliptical shape. The crystallites grow from the edges of parent metal in the direction of a centre, where meeting each other, they form a weld area with the least ductility (plane of weakness) [5, 10]. The plane of weakness is positioned along the large axis of ellipsis, thus parallel to the edges being welded. It is known [11] that development of a hot crack mainly occurs in the direction perpendicular to the action of the largest component of deformation (Figures 3, *a* and 4, *a*). Considering high rigidity of elements being welded and the fact that in the weld metal area of high temperature the transverse deformations are mainly developed, the most favourable conditions to hot crack formation are formed at this position of weakness area. It was also proved by carried out investigations.

Basing on the results of carried out experiments the suggestion was made about the possibility of decrease of negative influence of the area of the smallest ductility on technological strength using positioning of weakness plane parallel to the vector of the maximal tensile forces appeared at crystallisation of a weld metal (Figure 3, *b*). In order to check it, the groove of edges was formed using plates-spacers after mounting of which the rectangular holes appeared between the edges being welded. The largest side of the hole

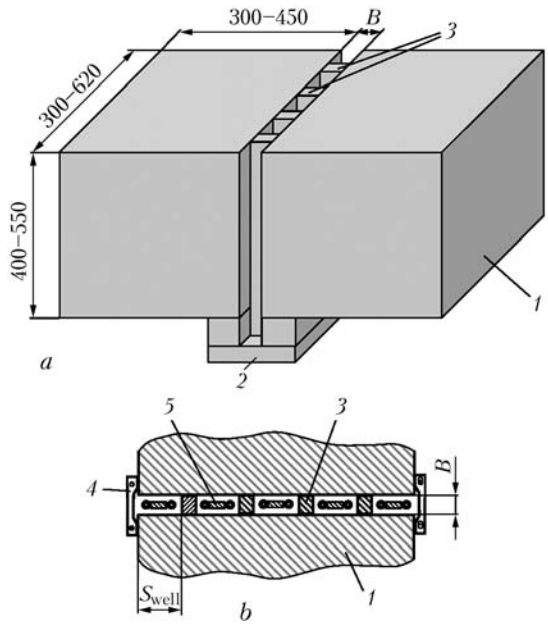

Figure 2. Scheme of assembly (*a*) and MESW (*b*) of pilot samples with longitudinal arrangement of consumable nozzles: *1* — parts being welded; *2* — input pocket; *3* — forming plates-spacers; *4* — water-cooled cover plate; *5* — consumable nozzle; *B* — width of welding gap; S_{well} — thickness of well metal

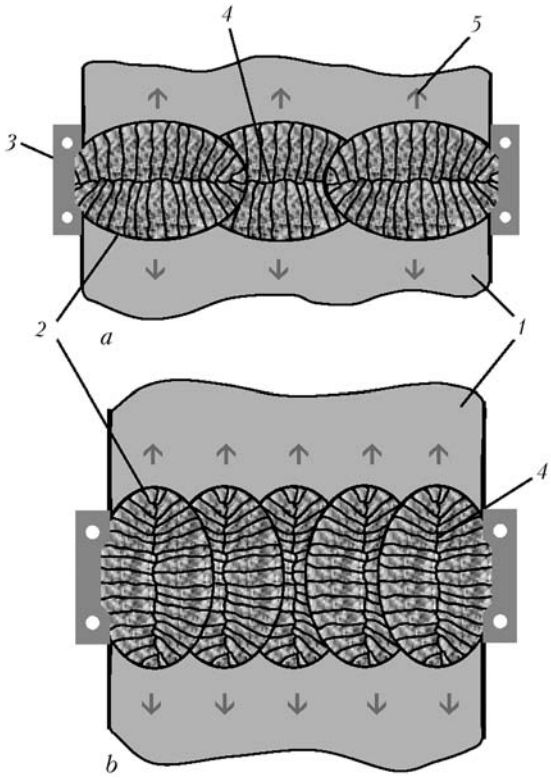

Figure 3. Schemes of positioning of zones (planes) of weakness in metal of layers of multi-layered weld in ESW with consumable nozzle with arrangement of consumable nozzles along the axis of edges preparation (*a*) and across (*b*): *1* — edge being welded; *2* — shape of layer of a weld in a cross section; *3* — forming cover plate; *4* — weakness zone (plane); *5* — vector of shrinkage forces

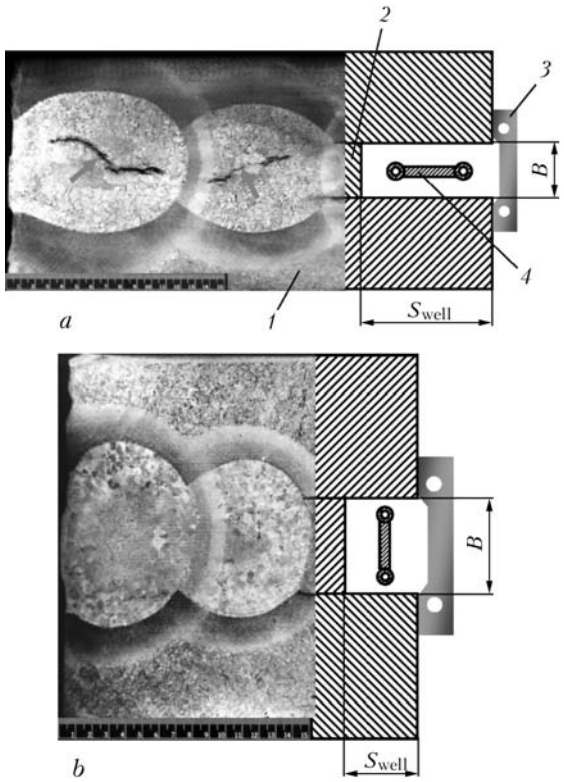

Figure 4. Transverse macrosections of multi-layer electroslag welds performed with longitudinal (*a*) and transverse (*b*) arrangement of consumable nozzles in a gap: *1* — billets being welded; *2* — forming plate-spacer; *3* — forming water-cooled device; *4* — consumable nozzle

(well) was positioned not parallel, but perpendicularly to the edges being welded (Figure 4).

ESW of the holes was performed using consumable dual electrode nozzles mounted across the welding gap according to the scheme in Figure 4, *b* at the specific power within the above-mentioned limits. The results of investigations of macrosections and Bauman's prints of transverse and longitudinal sections of welds performed according to the offered scheme showed that hot cracks in weld layers were not detected.

Thus, it was established that by changing the direction of weakness plane of single layers relative to the vector of tensile forces of multi-layer weld it is possible to achieve increase of its resistance against formation of crystalline cracks.

At the repair of through cracks in bands of rotary kiln furnaces the shape of groove of edges and pitch of layers being re-welded should be determined depending on the configuration and sizes of defects.

1. *OST 22-170–87*: Bands of rotary kilns. Specifications. Moscow: TsNIITEstrojmash.
2. Kozulin, S.M., Lychko, I.I., Kozulin, M.G. (2007) Methods of reconditioning rotary kilns (Review). *The Paton Welding J.*, **10**, 33–39.
3. Kozulin, M.G., Filchenkov, D.I. (1977) Reconditioning of rotary kiln bands using electroslag welding. *Avtomatich. Svarka*, **3**, 64–65.
4. Zvezdin, S.M., Bondarenko, O.P., Popovsky, V.Yu. (1985) Information-measuring system for control of welding and surfacing process parameters. *Ibid.*, **12**, 54–56.
5. (1959) *Electroslag welding*. Ed. by B.E. Paton. Kiev: Mashgiz.
6. Semenov, V.M., Eregin, A.P., Gelman, A.S. et al. *Method of examination of welded joint*. USSR author's cert. 421910. Int. Cl. B 23 K 25(00). Publ. 19.12.74.
7. Yakushin, B.F., Bashev, L.F. *Method of welded joint testing on hot cracking resistance*. USSR author's cert. 998062. Int. Cl. B 23 K25(00). Publ. 23.02.83.
8. Sushchuk-Slyusarenko, I.I., Lychko, I.I., Semenov, V.M. (1981) *Base materials and consumables for electroslag welding*. Kiev: Naukova Dumka.
9. Sushchuk-Slyusarenko, I.I., Lychko, I.I. (1974) *Technique of electroslag welding execution*. Kiev: Naukova Dumka.
10. (1974) *Vocabulary-handbook on welding*. Ed. by K.K. Khrenov. Kiev: Naukova Dumka.
11. Prokhorov, N.N. (1968) *Physical processes in metals during welding*. Vol. 1. Moscow: Metallurgiya.

PECULIARITIES OF TECHNOLOGY OF WELDING PIPELINES OF DISSIMILAR STEELS IN NUCLEAR POWER ENGINEERING*

O.G. KASATKIN, A.K. TSARYUK, V.Yu. SKULSKY, A.R. GAVRIK and **S.I. MORAVETSKY**
E.O. Paton Electric Welding Institute, NASU, Kiev, Ukraine

The main factors promoting corrosion cracking of welded joints of pipelines from dissimilar steels are analyzed. Welding consumables and technologies allowing improvement of welded joint resistance to local corrosion damages are proposed.

Keywords: *arc welding, pipelines, austenite and carbon steels, dissimilar welded joints, structure of welded joints, brittle interlayers*

In the pipelines of the second circuit of power units of nuclear power stations the welded joints of pipes of dissimilar steels (austenite and low-alloyed) are mostly subjected to corrosion fracture [1]. During repair of a pipeline the site welding is usually not applied. Instead of a removed defect area a specially manufactured insert is welded-in, which has also a limited life.

The investigations carried out earlier showed that corrosion cracking and fracture of mentioned joints is caused by heterogeneity of metal of welded joints, presence of brittle and weakened interlayers, stressed state and hydrogen embrittlement of metal.

The main factors influencing the life of welded joints of dissimilar steels are their chemical and structural heterogeneity in the places of joining of austenite and pearlite steels due to mixing of these metals in a weld pool and diffusion of different elements, especially carbon.

In mentioned areas of a welded joint the formation of alloyed martensite with sufficiently high carbon content is possible. It is characterised by high hardness and also low plasticity.

The residual stresses in similar and dissimilar welded joints are considerably differed after performance of heat treatment. During cooling in the process of tempering of dissimilar welded joints the new residual stresses occur due to different thermal expansion of steels.

Tensile stresses arise in an austenite part of welded joint. In welding of butts of pipes of dissimilar steels the stresses at the inner surface of austenite pipe are tensile and in the pipe of a perlite steel — compression. During evaluation of stressed state of the joint it is necessary to take into account the structural stresses. In martensite interlayers they can much exceed the residual stresses.

The main factor influencing the serviceability of dissimilar welded joints is hydrogen. The combination of three factors (diffusion-mobile hydrogen, martensite structure and stressed state) can result in delayed fracture of the welded joint [2]. Here the local defects and microcracks are formed on the grain boundaries of former austenite grains. The development of delayed fracture process can result in a rapid intercrystalline corrosion cracking of the welded joint.

The increase in life of dissimilar welded joints can be achieved as a result of development of different technological measures providing minimal penetration

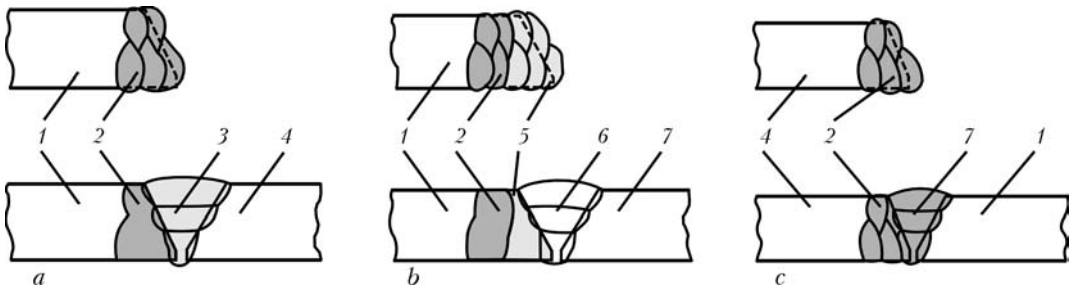

Figure 1. Schemes of first (*a*), second (*b*) and third (*c*) technologic variants of welded joints of dissimilar steels: *1* — base metal (steel 20); *2* — hard-facing of Armco-iron; *3* — weld made using filler metal Sv-10Kh16N25AM6; *4* — base metal (steel 08Kh18N10T); *5* — hard-facing of filler metal Sv-10Kh16N25AM6; *6* — weld made using filler metal Sv-04Kh19N11M3; *7* — weld made using Armco-iron as a filler metal

*The article was prepared on the basis of results of accomplishment of the NASU targeted integrated program «Problems of Remaining Life and Safe Operation of Structures, Constructions and Machines» (2007–2009).

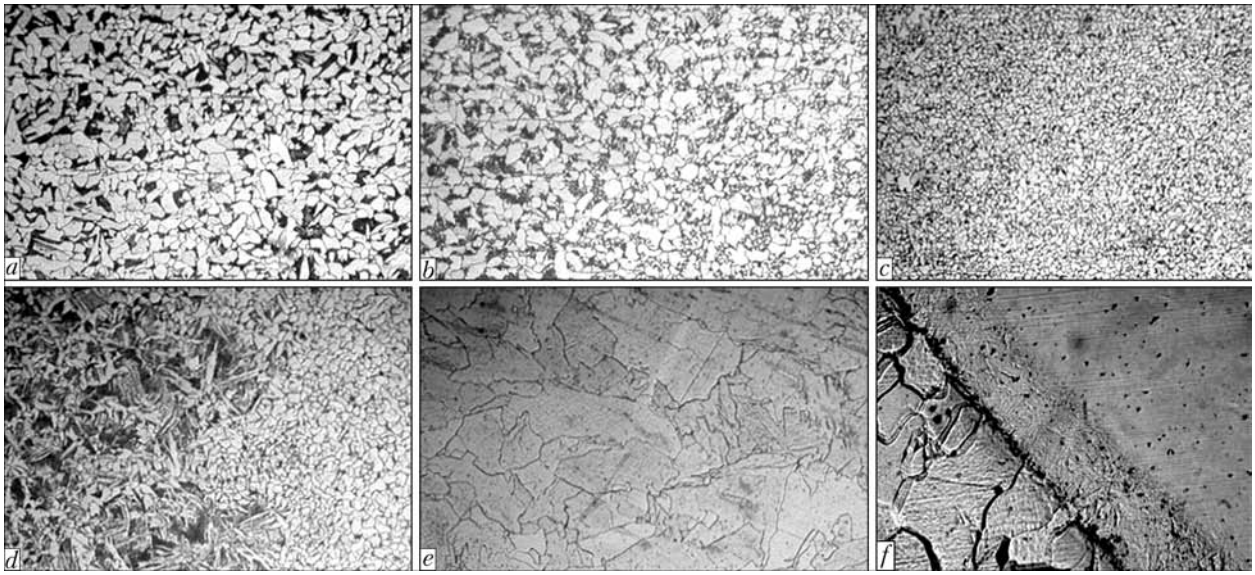

Figure 2. Microstructures (*a–e* — ×200; *f* — ×1000) of different zones in metal of welded joints of dissimilar steels: *a* — steel 20; *b* — steel 20, area of incomplete recrystallisation; *c* — steel 20, area of normalisation; *d* — zone of fusion of steel 20 with Armco-iron; *e* — hard-facing of Armco-iron; *f* — zone of fusion of deposited metal with austenite weld

of base metal and prevention of formation of brittle and decarbonized interlayers.

The analysis of existing domestic and foreign high-alloyed welding consumables showed that they do not allow complete prevention of formation of chemical and structural heterogeneity in dissimilar welded joints as well as formation of martensite and decarbonized interlayers.

To prevent formation of martensite interlayers it is necessary to exclude the possibility of mixing pearlite and austenite metals in welding. For this purpose it is possible to line the edge of pearlite steel with commercially pure iron (Armco-iron) with a low carbon content. During hard-facing the share of base metal should be small. In this case it is possible to prevent the formation of alloyed metal with carbon content of more than 0.05 %. In the iron with a low carbon content no hard martensite with a high density of dislocations is formed.

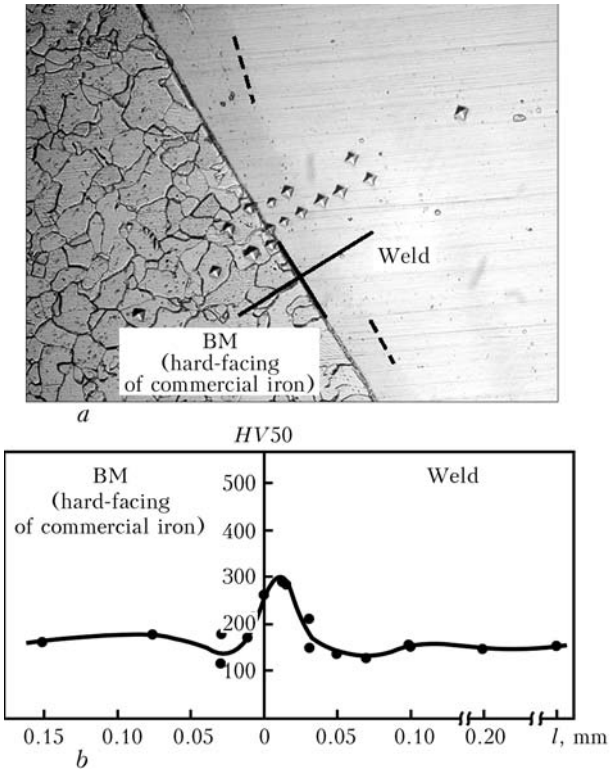

Figure 3. Microstructure (*a* — ×250) and change of microhardness (*b*) at the area of fusion of commercial iron layer deposited on steel 20 and weld metal made using wire Sv-10Kh16N25AM6

The universal method of decrease of diffusion movement of carbon is nickel adding to weld metal or lining of edges with this metal. Necessary concentration of nickel in a weld should be increased with increase of operating temperature of the welded joint.

In the work the following technological variants of welding dissimilar steels using interlayer of commercially pure iron are evaluated:

- preliminary argon arc hard-facing of two layers of Armco-iron on edge of steel 20 (Figure 1, *a*). After mechanical treatment of edges the welding of austenite steel using wire Sv-10Kh16N25AM6 was performed;
- argon arc hard-facing of Armco-iron layer, then two layers with filler wire Sv-10Kh16N25AM6 on the edge of steel 20. After mechanical treatment of edges the welding of joint was performed using filler wire Sv-04Kh19N11M3 (Figure 1, *b*);
- argon arc hard-facing of Armco-iron layer on the edge of steel 08Kh18N10T. After mechanical treatment of deposited edge the argon arc welding of a joint was performed using filler of commercial iron (Figure 1, *c*).

The welded joints of steels 20 and 08Kh18N10T, made according to different technological variants, were cut into transverse templates to perform mechanical and metallographic investigations.

The values of strength, bend angle and impact toughness, obtained as a result of investigations, satisfied the requirements set forth to welded joints of steels 20 and 08Kh18N10T.

Figure 2 shows microstructures of metal of characteristic areas of welded joint of dissimilar steels:

• area of complete recrystallization or normalization (Figure 2, *c*) where after phase recrystalization the metal acquired a fine-grain structure;

• area of overheating, where along with hard-facing of Armco-iron layer (Figure 2, *d*) the coarse structure of large areas of ferrite and pearlite (Widmanstaetten structure) was formed on steel 20. The deposit of Armco-iron near steel 20 has a fine-grain structure, and due to its mixing with base metal single pearlite areas were present in it;

• the metal of hard-facing of commercial iron (Figure 2, *e*) has a purely ferrite structure with a relatively coarse grain;

• area of fusion of Armco-iron layer with austenite weld metal (Figure 2, *f*), where coarse grains of ferrite and layer of Armco-iron melt, not mixed with weld metal, are seen.

Depending on conditions of mixing metal in weld pool the transition from Armco-iron can be abrupt or have a layer with a fine-dispersed structure. This is a metal formed as a result of incomplete melting of grain fragments of commercial iron and absence of mixing such melted metal with austenite weld metal (or deposited metal).

It is obviously that formation of such interlayers is influenced by higher temperature of technical iron melting (about 1530 °C as compared to 1380 °C in austenite metal) and narrow range of crystallization temperatures facilitating its rapid solidification at changes of temperatures in the process of welding and also difficulty of mixing with an austenite melt.

The joint metal at the transition area from the layer of commercial iron to the layer of deposited metal of the type Sv-10Kh16N25AM6 has a similar microstructure (Figure 3).

It is seen from results of measurements that in austenite weld metal or deposited metal at the area of changing composition in base metal (commercial iron) the microareas are formed with increased hardness, much lower than that of martensite due to different volume participation of melted unalloyed and surfaced high-alloyed metals. Due to non-uniform mixing of melts of iron and austenite metal, except areas with increased hardness, the microareas with hardness of austenite are formed.

The obtained results showed the following:

• in hard-facing of transient unalloyed carbon-free iron layer and next welding using the austenite weld the migration of carbon and formation of carbide interlayers, characteristic of the zone of fusion of steel 20 with austenite weld metal, were revealed;

• migration of carbon and formation of decarbonized interlayer in steel 20 does not occur at the area of its fusion with underlayer of commercial iron;

• at the areas of the commercial iron–deposited weld austenite metal fusion the microareas with variable hardness are formed due to additional alloying of iron melt by alloying elements and carbon of austenite wire.

The investigations of technological variant with hard-facing of Armco-iron layer on the edge of steel 08Kh18N10T and next argon arc welding of a joint with Armco-iron filler showed that at the area of fusion of the first hard-facing layer of Armco-iron on austenite steel no areas with high hardness of metal, characteristic of hardened structures, were formed. At this area of welded joint no redistribution of carbon and formation of carbide interlayers were observed.

The results of investigations of flat specimens showed that boundary of fusion of austenite and low carbon steel is more homogeneous if to perform hard-facing of low carbon steel on austenite and to fill a weld with ferrite metal. However filling of a weld with low carbon unalloyed metal leads to the decrease in strength of the welded joint.

Later to fill a weld, the Armco-iron, alloyed with a small amount of strengthening elements, was used as a filler material. As a whole, the values of mechanical properties of dissimilar welded joints performed according to suggested technology meet completely requirements regulated by PNAE G-7-010–89 for equipment of nuclear power stations.

CONCLUSIONS

1. In the course of preliminary corrosion tests of welded joints of dissimilar steels 20 and 08Kh18N10T it was established that their welded joints represent complex multi-electrode element with difference of potentials between base metals in a welded joint of up to 0.5 V in neutral medium of sodium chloride (pH 6.5–7.0), thus causing intensive fracture of metal in a fusion zone.

2. In the process of tests of welded joints at the loading of up to $0.9\sigma_y$ in boiling solution of mixture of calcium nitrite and nitrite of ammonium in the specimens welded both according to conventional technology, and also in hard-facing of commercial iron on the edges of steel 08Kh18N10T, corrosion cracking occurs. Under similar conditions of testing specimens with hard-facing of edges of carbon steel by Armco-iron the corrosion cracking was not observed.

3. The developed technology of welding of the second circuit pipelines of dissimilar steels is supposed to be certified at Khmelnitskaya nuclear power station.

1. Zemzin, V.N. (1981) Welded joints of dissimilar steels. In: *Welding and consumables*. Vol. 1. Moscow: Metallurgiya.
2. Makarov, E.L. (1981) *Cold cracks in welding of alloy steels*. Moscow: Mashinostroenie.

INFLUENCE OF WELD METAL IMPACT TREATMENT ON WELDED JOINT STRENGTH

A.S. PISMENNY and **V.M. KISLITSYN**
E.O. Paton Electric Welding Institute, NASU, Kiev, Ukraine

The paper gives the results of experiments on qualitative assessment of the influence of thermomechanical treatment on the strength of spot welded joint. Rationality of shock application of the compressive force at the temperature close to the recrystallisation point of the metal being welded is shown.

Keywords: *resistance spot welding, welded joint, thermomechanical treatment, shock application of compressive force, crystalline structure refinement, mechanical strength*

As is known, the most widely accepted cause for lowering of welded joint strength is development of tensile stresses in the weld zone, caused by metal shrinkage during cooling.

The level of residual mechanical stresses is lowered using thermal, thermomechanical [1,2] and shock-mechanical kinds of weld zone treatment, which is conducted after completion of welding operation. For instance, performance of strengthening by the method of high-frequency mechanical peening [3, 4], hammer peening [5] or shot blasting [6] allows several times increase of cyclic fatigue life of the welded structure due to redistribution of residual mechanical stresses in the weld zone. The above strengthening methods are characterized by multiple shock application of the compressive force, which is performed at the speed of about a hundred meters per second.

«Peening» term characterizes a process of welding at a much lower speed of compressive force application (not more than a dozen meters per second) and one-time action, which is due to the inertia of the pneumatic drive assembly of electrode displacement both at the stage of welding, and peening.

This led to the need to reject the term «peening» from resistance welding area and use a term from a related area of engineering, namely «impact treatment of metal» [3–6], which characterizes high-speed and multiple treatment of metal directly during the welding process at the stage of spot weld cooling.

The disadvantages of welded joint heat treatment include the need for either long-term (for several hours) heating by a certain cycle of the entire welded product in furnaces, or not less long-time local heating of the weld zone.

In some cases, however, it turned out to be possible to replace the expensive and power-consuming heat treatment of the entire product by additional surface melting of welds by arc heating in argon. This technology was developed at PWI. Results of the conducted studies showed that argon-arc surface melting of welds allows recovering the weld metal impact toughness, improving the welded joint fatigue limit, which, as was explained by the author of [7], is related to structural changes in the weld metal.

Lowering of the level of residual tensile stresses in welded joints can be achieved also through application of special filler materials, characterized by low temperature of interphase transfer in the weld metal [8].

Compressive stresses in welded joints form directly during the welding process, for instance, at spot resistance welding with a peening cycle envisaging the impact of an additional and higher force of metal compression at the stage of cooling of the formed spot weld. This treatment variant was accepted in welding metals prone to cracking and porosity formation, in order to lower residual stresses and improve the fatigue strength of welded joints [9, 10]. This treatment variant, however, is characterized by a low level of compressive stresses induced in the spot weld metal, because of the low speed of peening force application and inertia of the compressive mechanism; moreover, it excludes the possibility of variation of the moment of peening pulse application relative to the temperature of spot weld metal heating.

Shock-mechanical kinds of welded joint treatment include peening with a pneumatic vibration tool, shot blasting and ultrasonic peening. Technical literature gives information about improvement of cyclic fatigue life of welded joints by several times after performance of the operation of metal peening with a pneumatic hammer or its shot blasting. Ultrasonic treatment also allows an improvement of mechanical strength, for instance, in treatment of welded joints of 20KhGSA steel and some aluminium alloys [11, 12].

In view of the technological disadvantages inherent to the above treatment techniques, high-frequency mechanical peening became widely accepted now. Conducted studies [3, 4] showed that application of this kind of treatment, even without metal preheating, allows achieving a more favourable redistribution of residual stresses in the metal surface layers and forming a sufficiently high level of compressive stresses, in particular in the base-to-weld metal transition zone.

Proceeding from the above said, it may be anticipated that the joint action of heat treatment and mechanical peening can turn out to be an effective means of improvement of both the mechanical strength, and

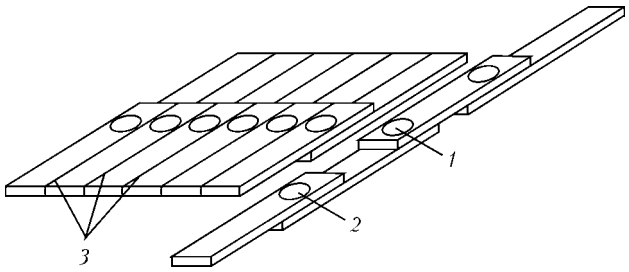

Figure 1. Schematic of sample preparation to rupture testing: *1, 2* — spot welds with peening and without it, respectively; *3* — cut lines

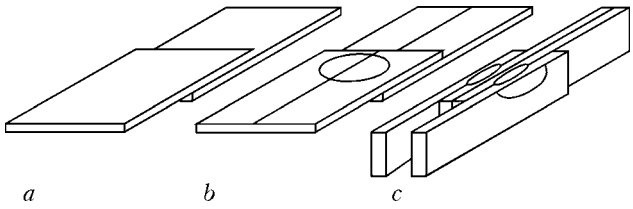

Figure 2. Schematic of welded sample preparation to microsection cutting out: *a* — before welding; *b* — after welding with the line of the cut along the spot weld; *c* — for microsection preparation

endurance limit of welded joints. Action of impact treatment at increased temperature certainly should increase the depth of the surface layer of metal where plastic deformation takes place, and, therefore, also the dimensions of the zone of residual (post-weld) mechanical stress.

This gives rise to the following questions, requiring experimental verification of the possibility of improvement of welded joint mechanical strength, namely determination of the optimum temperature range, in which the shock impact of the compressive force is favourable, optimum ratio of thermal and mechanical impact energy, and optimum speed of compressive force application.

Solution of these problems is of theoretical and practical interest not only for improvement of the methods of welding metals and joining new structural materials, but also during performance of repair-maintenance operations on welded structures. It is also necessary to assess the effectiveness of application of different kinds of heating, namely electric contact, arc, flame heating, for this purpose.

This work is an attempt at a qualitative evaluation of the attractiveness of impact treatment of weld metal in resistance welding of sheet steel.

In order to perform technological verification of the anticipated positive effect of shock application of the compressive force on mechanical strength due to refinement of the spot weld metal crystalline structure we have performed investigations by the following procedure. St3 steel plates of $100 \times 30 \times 1$ mm size were used as the samples. Selection of St3 steel 1 mm thick was supported by the generally accepted current practice of application (for the sake of lowering product cost at the expense of reducing item service life from dozens of years to dozens of months) of low-alloyed sheet steel with unspecified content of impurities for mass-produced items (for instance, automotive products, electrical equipment, household appliances).

The laboratory resistance spot welding machine used for this experiment included the module for adjustment of the number of welding current pulses (from 1 to 8 half-periods) and module of setting the moment of sending the voltage pulse to the solenoid of the assembly of shock application of the compressive force, adjusted in the range from 1 up to 12 half-periods.

After mechanical and chemical cleaning to remove contamination, samples were resistance welded in two modes: with the use of the device to provide the shock application of the compressive force and without thermomechanical treatment. To perform comparative evaluation of the strength of welded joints made in the above modes, the welded plates were cut into 5 mm wide strips, which were joined in pairs to each other by resistance spot welding, as shown in Figure 1.

Thus, during rupture testing the rupture load was simultaneously applied to three spot welds made with one power source mode, but differing by the impact or absence of shock application of compressive force at the temperature close to metal recystallization point.

To assess the effect of peening on welded joint strength, instead of measuring the breaking force it turned out to be sufficient to record the fracture of one of the spot welds, having minimum strength, i.e. the weakest link in joints of four strips welded in three points.

Such a preparation of welded joint samples allowed elimination of a number of negative factors, namely possible influence of fluctuations of initial metal properties on its strength; differences in the thickness and composition of oxide films on the surfaces being joined; random deviations of welding mode and tem-

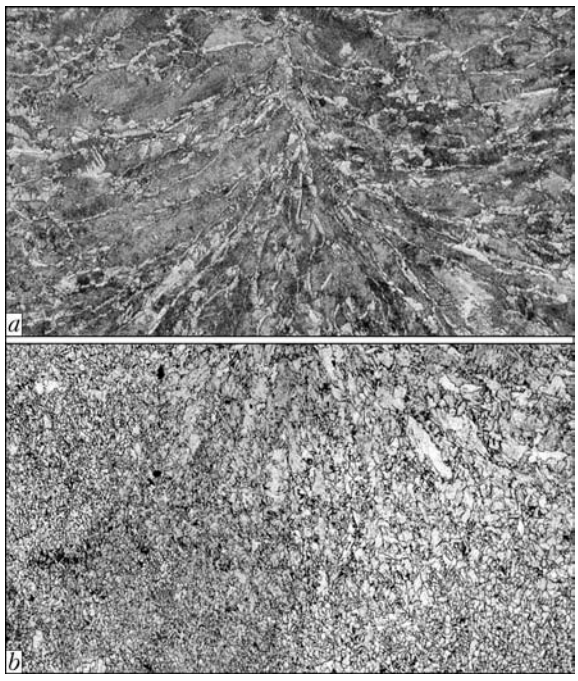

Figure 3. Microstructure (×100) of spot weld metal before thermomechanical impact (*a*) and metal of mirror half of the same spot weld after thermomechanical impact (*b*)

perature, at which the shock application of the compressive force is applied.

The proposed comparative assessment of welded joint strength can be regarded as a procedure of qualitative evaluation of the effectiveness of the impact of the modes heating and subsequent thermomechanical action. Despite a limited scope of information on joint strength, obtained with application of the proposed testing procedure, it has the advantage of the possibility of evaluation of the results for a specific technological sample in minimum time, which is particularly valuable during adjustment operations.

Results of the conducted rupture testing of samples showed that more than 97 % of welded joints fail through the spot welds, not treated by shock application of the compressive force.

In order to asses the influence of shock peening on the change of spot weld metal structure, samples were made by spot welding (Figure 2, *a*), which were cut along the strips and through the spot weld (Figure 2, *b*). One of the spot weld halves was reheated to the temperature of (600 + 50) °C (near the steel recrystallization point) and shock compressive force was applied starting from the moment of the thermocouple recording the specified temperature. Then the two halves of the spot weld were joined to produce a macrosection as shown in Figure 2, *c*.

As the time of cooling of spot weld metal in the selected samples is equal to about 0.5 s, the spot weld can be subjected to one or several dozens of shocks even at pulse repetition rate of 50 Hz.

As is seen from Figure 3, the microstructures of mirror halves of one spot weld differ significantly both by the crystallite size, and homogeneity of metal structure near the spot weld. Microstructures of peened joints show a significant refinement of the largest crystallites, which grew out of the spot weld central zone.

In addition, the spot weld metal shows a lowering of the content of foreign particulates and porosity, i.e. the difference between the structure of metal of the spot weld, HAZ and base metal becomes smaller.

Thus, the conducted technological studies of the influence of shock thermomechanical treatment performed directly during welding, showed the possibility of an essential improvement of welded joint mechanical strength.

Proceeding from the existing interrelation between the parameters of the metal crystalline lattice and its operating properties, it can be anticipated that impact treatment of the weld at the temperature close to recrystallization point will allow improvement of welded joint fatigue limit.

1. (1976) *Principles of materials*: Manual. Ed. by I.I. Sidorin. Moscow: Mashinostroenie.
2. Gulyaev, A.P. (1951) *Materials science*. Moscow: Oboron. Promyshlennost.
3. Knysh, V.V., Solovej, S.A., Kuzmenko, A.Z. (2008) Accumulation of fatigue damage in tee welded joints of 09G2S steel in the initial condition and after strengthening by high-frequency mechanical peening. *The Paton Welding J.*, **10**, 10–15.
4. Knysh, V.V., Kuzmenko, A.Z., Solovej, A.S. (2009) Increase of cyclic fatigue life of tee welded joints with surface cracks. *Ibid.*, **1**, 29–33.
5. Branko, C., Infante, V., Bartista, R. (2004) Fatigue behavior of the weld joints with cracks repaired by hammer peening. *Fatigue & Fract. of Eng. Materials and Struct.*, **27**, 785–798.
6. Turnbull, A., Los Rios, E.R., Tait, R. et al. (1998) Improving the fatigue crack resistance of wespalloy by shot peening. *Ibid.*, **21**, 1513–1524.
7. Asnis, A.E. (1983) Argon-arc treatment as a reserve in strength increase of welded joints. In: *Argon-arc treatment of welded joints*. Kiev: PWI.
8. Mazel, Yu.A. (2003) Martensite welding wire on the base of 10 % Cr and 10 % Ni with low temperature of transition. *Welding Int.*, 17(**5**), 386–389.
9. Moravsky, V.E., Vorona, D.S. (1985) *Technology and equipment for spot and projection capacitor welding*. Kiev: Naukova Dumka.
10. Moravsky, V.E. (1963) *Welding with accumulated energy*. Kiev: Gostekhizdat.
11. Polotsky, I.G., Nedoseka, A.Ya., Prokopenko, G.I. et al. (1974) Lowering of residual welding stresses by ultrasonic treatment. *Avtomatich. Svarka*, **4**, 74–75.
12. Kholopov, Yu.V. (1973) Ultrasonic treatment of metal welded joints for the purpose of residual stress relieving. *Svarochn. Proizvodstvo*, **12**, 20–21.

PROCEDURE OF EVALUATION OF TRANSPORTATION LAGS IN WELD FORMATION ACS

V.V. DOLINENKO, V.A. KOLYADA, T.G. SKUBA and **E.V. SHAPOVALOV**
E.O. Paton Electric Welding Institute, NASU, Kiev, Ukraine

A method is suggested for determination of transportation lags in feedback circuit of automatic system for control of weld reinforcement formation process in MAG welding. Mechanism of emergence of two different transportation lags, i.e. formation of weld reinforcement height and width, which are revealed by measurements of its geometric parameters by a laser TV-sensor, has been investigated. To estimate the transportation lags, it is suggested using the regression formulae derived on the basis of computational experimental results. A mathematical model of the weld pool developed for conditions of item heating with the movable normal-circular heat source has been used as an object of the computational experiments.

Keywords: *arc welding, welded joints, weld shape, ACS, transportation lag, laser-TV sensor*

The problem of closed-loop control of formation of the weld in arc welding has for a long time attracted the attention of specialists in the field of welding process automaton. One of the main challenges in solving this problem is realization of feedback by parameters determining the weld shape. In [1] it is proposed to perform closed-loop control of the process of weld formation using weld pool observation with a special sensor, the functioning of which is based on the method of two-colour pyrometry. Such an approach allows obtaining only indirect assessments of weld parameters, which can essentially differ from actual values. Of great interest is the method, proposed in [2], which suggests using direct measurement of geometrical parameters of weld reinforcement with a laser-TV sensor (LTVS). The fact that the presence of several transportation lags between LTVS and weld pool sections is not taken into account can be regarded as one of the disadvantages of the known schematics of closed-loop control of weld formation. Therefore, control stability can deteriorate at the change of the welding mode parameters.

This work proposes a procedure of assessment of transportation lags for automatic control systems (ACS) of MAG welding, in which the feedback is provided using LTVS [3].

It is known from the theory of welding processes that bead width and height correspond to pool solidification front in its middle and tail parts [4]. Figure 1 shows the schematic of formation of two transportation lags in ACS using LTVS (separately for measurement of height g and width e of weld reinforcement). The dashed line outlines the contour of an imaginary weld pool at the moment of time, when the projection of the electrode axis was in point O. Weld shape corresponds to the direction of welding from left to right. Point A indicates the extreme point of the solidification front of the weld pool tail part. Its coordinate along the abscissa axis determines the start of formation of the height of weld reinforcement. Points B and B' indicate the points of the weld pool solidification front in its middle part. Their coordinates along the abscissa axis determine the start of formation of weld reinforcement width. Distance between the electrode (welding torch axis) and LTVS light trace L_{TV} determines the base value of transportation lag at the change of bead parameters. Distance between point A (B) and point O along the abscissa axis is equal to $L_g(L_e)$. Thus, the values of portions of transportation lags of following width ΔL_e and height ΔL_g of weld bead are calculated as follows: $\Delta L_e = L_{TV} - L_e$, $\Delta L_g = L_{TV} - L_g$. Hence, the formulas for calculation of time parameters of transportation lags become:

$$\tau_g = \frac{L_{TV} - L_g}{v_w}; \quad \tau_e = \frac{L_{TV} - L_e}{v_w}, \qquad (1)$$

where τ_e, τ_g are the time parameters of transportation lags of measurements of bead width and height, respectively, s; v_w is the welding speed, cm/s.

It is seen from the Figure that in order to determine the value of transportation lags between the weld pool and LTVS light trace, it is necessary to know coordinates of points A, B, B' relative to the current coordinate of the projection of electrode axis O. However,

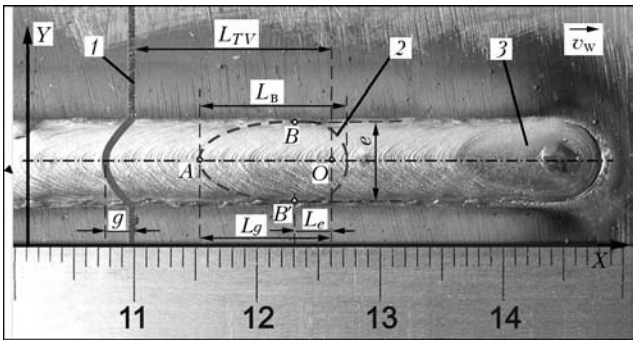

Figure 1. Schematic of emergence of transportation lags between the weld pool and LTVS in MAG welding: *1* — LTVS light trace; *2* — imaginary contour of weld pool; *3* — surface of solidified weld pool

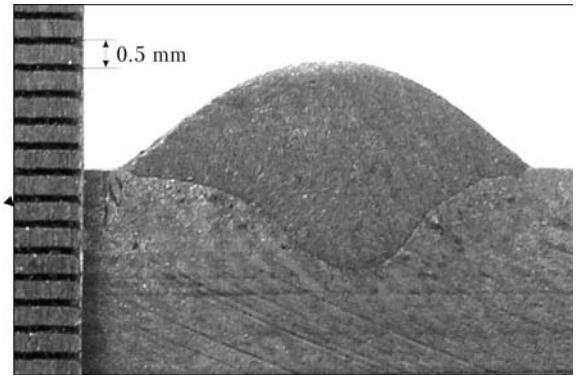

Figure 2. Weld macrosection (U_a = 19 V; I_w = 160 A; v_w = = 0.75 cm/s)

for a symmetrical bead shape, abscissas of points B and B' are equal, so that calculation is required only for points A and B.

In order to solve this problem, a mathematical model was synthesized, which allows calculation of weld pool geometrical parameters based on heat transfer in the welded items. Equation describing the process of heat propagation in a semi-infinite body at its heating by a moving normal-circular source [5], has the following form:

$$T(x, y, z, t) = \frac{2q}{c\gamma(4\pi a)^{3/2}} \exp\left(-\frac{v_w x}{2a}\right) \int_0^t \frac{dt''}{\sqrt{t''(t_0 + t'')}} \times \times \exp\left[-\frac{z^2}{4at''} - \frac{r^2}{4a(t_0 + t'')} - \frac{v_w^2}{2a}(t_0 + t'')\right], \quad (2)$$

where $r^2 = x^2 + y^2$, cm^2; x, y, z are the coordinates of the current calculation point of the temperature field, cm; $a = \lambda/c\gamma$ is the thermal diffusivity, J/m^2; $c\gamma$ is the bulk heat content, J/(m^3·K); $q = 0.24\eta U_a I_w$ is the effective heat power, J/m; U_a, I_w are the average values of welding voltage and current; $t_0 = 1/(4ak_t)$ is the duration of propagation of a fictitious source, s; k_t is the coefficient of heat concentration of the arc, cm^{-2}; t is the time interval of the action of a continuous mobile heat source, s; $t'' = t - t'$, s; t' is the auxiliary moment of time, in which the source applied heat in the initial section of its motion, s.

Numerical solution was fulfilled with sampling increment of 0.01 cm. Ignoring the processes of mass transfer into the weld pool, can be regarded as one of the disadvantages of such a solution.

Welding experiments were performed to precise the values of the main energy parameters of the thermal model. Reverse polarity welding was performed in shielding gas (Ar + 15 % CO_2) in the downhand position. Carbon steel plates 0.8 mm thick (butt welding) were welded with Sv-08G2S electrode wire of 0.12 cm diameter. Rated parameters of welding mode were as follows: I_w = 160 A, U_a = 19 V, v_w = 7.5 cm/s. Figure 2. shows a macrosection of the weld bead used to verify the adequacy of the thermal model. Results of welding experiments were used to more precisely determine the values of thermal model parameters: effective efficiency of welding η = 0.75 and coefficient of concentration of the arc thermal action k_t = 8.3 cm^{-2}. Other parameters of the thermal model have the following values: a = 0.0718 J/m^2, $c\gamma$ = 0.975 J/(m^3·K).

The computational experiment was performed in keeping with the full factorial plan of second order experiments [6]. The following variables were considered: U_a = 17–21 V, I_w = 145–175 A and v_w = 0.5–1.0 cm/s. Calculation of such weld pool parameters, as width e of weld pool, maximum penetration depth h, weld pool length L_p, distances L_e and L_g, was performed. The following ranges of parameters variation were obtained: h = 0.15–0.25 cm, e = 0.70–0.91 cm, L_p = 0.98–1.22 cm, which corresponds to the welding experiment. Results of the computational experiment are given in the Table. Normalized factors x_1, x_2 and x_3 correspond to factorial variables U_a, I_w and v_w.

Matrix of computational experiment and calculation results

#	x_1	x_2	x_3	U_a, V	I_w, A	v_w, cm/s	L_g, cm	L_e, cm
1	0	0	0	19.0	160	0.75	1.08	0.59
2	−1	−1	−1	17.8	151	0.60	0.95	0.48
3	−1	−1	1	17.8	151	0.90	1.04	0.57
4	−1	1	−1	17.8	169	0.60	1.02	0.47
5	−1	1	1	17.8	169	0.90	1.11	0.68
6	1	−1	−1	20.2	151	0.60	1.04	0.51
7	1	−1	1	20.2	151	0.90	1.13	0.59
8	1	1	−1	20.2	169	0.60	1.13	0.48
9	1	1	1	20.2	169	0.90	1.22	0.68
10	−1.68	0	0	17.0	160	0.75	0.99	0.59
11	0	−1.68	0	19.0	145	0.75	1.01	0.60
12	0	0	−1.68	19.0	160	0.50	0.99	0.50
13	1.68	0	0	21.0	160	0.75	1.16	0.51
14	0	1.68	0	19.0	175	0.75	1.16	0.63
15	0	0	1.68	19.0	160	1.00	1.14	0.65

The following regression formulas are obtained:

$$L_g = -0.69 + 0.041U_a + 0.0048I_w + 0.3v_w \text{ (cm)}; \quad (3)$$

$$L_e = 0.08 + 0.004U_a + 0.0016I_w + 0.4v_w \text{ (cm)}. \quad (4)$$

Mean root square error of approximation for regression model (3), (4) does not exceed 5 %.

According to the proposed procedure, a priori information about value L_{TV} and ranges of variation of welding variables I_w, U_a and v_w is used to calculate the ranges of variation of distances L_e and L_g, and then formula (1) is used to calculate minimum and maximum evaluations of transportation lags τ_e and τ_g.

Let us consider as an example a practical case with L_{TV} = 7.5 cm. Comparing maximum changes of transportation lags for a constant and varying welding speed at variation of welding mode in the following range: U_a = 17–21 V and I_w = 145–175 A. In the first case, for v_w = 0.75 cm/s calculation yields the range

of variation of τ_e = 9.0–9.1 s (relative change is equal to 1 %) and τ_g = 8.4–8.8 s (5 %). In the second case for the range of variation v_w = 0.5–1.0 cm/s changes of transportation lags are as follows: τ_e = 6.7–13.8 s (relative change of 78 %) and τ_g = 6.2–13.3 s (83 %). Thus, in the second case, the model of control object is a non-stationary dynamic system which requires more sophisticated control algorithms.

The proposed procedure of calculation of transportation lags in weld reinforcement formation ACS with feedback allows correct selection of time parameters and type of automatic regulator.

1. Zhang, H., Pan, J., Lao, B. (1999) The real-time measurement of welding temperature field and closed-loop control of isotherm width. *Sci. in China Press*, 21(**2**), 129–135.
2. Doumanidis, C., Kwak, Y.-M. (2002) Multivariable adaptive control of the bead profile geometry in gas metal arc welding with thermal scanning. Intern. *J. Pressure Vessels and Piping*, **79**, 251–262.
3. Kiselevsky, F.N., Shapovalov, E.V., Kolyada, V.A. (2006) System of laser following of weld reinforcement bead. *The Paton Welding J.*, **1**, 42–44.
4. Erokhin, A.A. (1973) *Fundamentals of fusion welding. Physico-chemical principles*. Moscow: Mashinostroenie.
5. Rykalin, N.N., Uglov, A.A. (1951) *Calculations of thermal processes in welding*. Moscow: Mashgiz.
6. Johnson, I., Lion, F. (1981) *Statistics and experiment planning in engineering and science: methods of experiment planning*. Moscow: Mir.

THESIS FOR A SCIENTIFIC DEGREE

E.O. Paton Electric Welding Institute of the NAS of Ukraine

On December 10, 2009, **A.V. Yarovitsyn** (PWI) defended his Candidate of Sciences Thesis on subject «Microplasma Powder Cladding of Heat-Resistant Nickel Alloy with 45–65 % γ-phase Content».

The thesis is dedicated to investigation of the energy, thermal and technological peculiarities of microplasma powder cladding with the aim of development of a commercial technology for repair of blades from heat-resistant nickel alloys.

The thesis substantiates requirements to a welding heat source for microplasma powder cladding. It shows that a combination of low specific heat inputs of 100–650 W, low heat power density in an equivalent heat spot equal to 150–1500 W/cm^2 and low speed of the microplasma arc provides slow cooling of the base metal in the brittle temperature intervals at a rate of 3–10 °C/s. In this case the strain growth rate does not exceed the critical values, and initiation of hot cracks is hardly possible in the most dangerous zone of the base metal. The microplasma arc stability at a current of 2–35 A with portioned feed of a powder to the arc column, depending on the level of constriction of the arc by plasma nozzles, was investigated. It was determined that destabilization of the microplasma arc at currents of less than 22–25 A is caused by the influence on the arc by the carrier gas dosing pulses moving in a flow-through gas-powder system at a speed of up to 60 m/s. Proportion of a carrier gas dosing pulse speed of 5–15 m/s and specific plasma gas flow rate of 2–4 m/s was experimentally found to provide the stable arc.

It was established, based on experimental calorimetry data, that at currents of 5–35 A the effective methods for control of the heat power density in the microplasma arc heating spot include the effective heat power of the arc equal to 100–600 W, constriction of the arc due to changes in diameters of the plasmatron nozzle channels and shielding gas types (Ar or a mixture of Ar + 10 % H_2), and concentrated powder feed. In microplasma powder cladding the heat power density in the equivalent heat spot is 100–250 W/cm^2, which is 3–8 times lower in comparison with the arc for the low-current TIG process. Such heat characteristics of the microplasma arc provide a more uniform metal cooling and, combined with its speed of about 1 m/h, efficiently limit the strain rate.

The thesis determines that in microplasma powder cladding of heat-resistant nickel alloys the oxygen content of the deposited metal varies in a range of 0.0068–0.0220 %, and the nitrogen content — in a range of 0.0026–0.0080 %. It was experimentally proved that it is necessary and efficient to limit the oxygen content in the deposited metal of heat-resistant nickel alloys to 0.006–0.009 % by providing the following process parameters: plasmatron-to-workpiece distance of 2.5–5.0 mm, using powders with a low oxygen content, and using a mixture of Ar + 10 % H_2 as a shielding gas.

The thesis established the feasibility of microplasma powder cladding at currents of 5–35 A on a narrow substrate, and at currents of 17–35 A on a wide substrate.

The technology was developed for repair of ends of band flanges of blades from heat-resistant nickel alloy JS32-VI for aircraft engine D18T. The technology is based on application of one-layer cladding at currents of 8–20 A using additive powder of JS32 alloy. The feasibility was proved of repair of polycrystalline blades by microplasma powder cladding using additives with a composition identical to that of the base metal of JS6U-VI alloy, as well as less heat-resistant additives with a specified level of properties for alloys JS6K-VI and ChS70-VI.

O.V. Makhnenko (PWI) defended thesis for a Doctor's degree on the subject «Prediction of Deformations in Welding and Thermal Straightening of Structures Based on Methods of Thermal Ductility and Functions of Shrinkage».

The thesis is devoted to development of general approach to prediction of deformations in welding (hard-facing, thermal straightening) of large-sized structures based on complex application of methods of thermal ductility and functions of shrinkage, and also development of appropriate calculation algorithms of realization of a combined approach.

Suggested are the calculation methods of determination of parameters of shrinkage function for the characteristic cases of welding heating based on the geometric typification of object.

Designed are the calculation algorithms for girder structures and the investigation of kinetics of general deformations of welded girders in laser welding at multi-supporting fastening is carried out which allowed solution of problem of positioning the laser heat source in the process of welding with account for welding deformations. The distinctive feature of developed mathematical model is consideration of static indeterminateness connected with the sites of intermediate fastening of a girder in the process of welding performance, possibility of prediction of forces for maintaining of a girder on supports during welding and also providing the preliminary bending or mechanical straightening after welding.

Designed are the calculation algorithms for prediction of welding deformations of tube plates of heat exchangers in the process of welding-in of a big amount of heat exchanger tubes and new practical results were obtained based on carried out calculated investigations. The type of welded joint was defined for tube plate with the tubes of five considered ones providing the least deformation of a tube plate. It was established that application of austenite steel for tubes and fillers as compared to the variant of ferrite steel allows obtaining lower residual general stresses of the tube plate. It was defined that for the structures with two tube plates and short straight tubes the welding-in in a certain sequence of two tube ends simultaneously can considerably decrease deformations of tube plates especially at limited thicknesses of the latter. The estimation of risk of buckling at axial compression of tubes welded in the first turn was made.

Designed are the calculation algorithms for prediction of general deformations connected with multipass surfacing large-sized plates using wear-resistant alloy. It was established that the variant of surfacing along the long edge of a plate at the minimum heat input modes, providing necessary microstructure in HAZ metal is most favourable from the point of view of decrease of deformations. The significant effect of decrease of deformations (nearly by 3 times) was revealed in application of fastening in the surfacing area, i.e. pressing of this area against the plate with subsequent release after cooling.

Designed are the calculation algorithms for modelling the process of thermal straightening of thin-walled structures with buckling deformations using heating spots of different shape. Basing on the developed algorithms the study of possibility of increase of efficiency of thermal straightening process was carried out. It was established that due to optimisation of heating parameters it is possible to increase considerably the straightening efficiency that is connected with significant economy in power and labour consumption. The fundamental regularities of thermal straightening process of thin-walled structures with buckling deformations, defined by geometric parameters of buckling and arrangement of heating spots, were revealed for the first time. It was established that the process of thermal straightening of buckling deformations has a complete number of objective factors limiting the efficiency of this technological operation especially at large thicknesses of lining sheet.

On the basis of developed calculation algorithms the controlling software was created to automate the process of thermal straightening of thin-walled structures with buckling deformations, which found its application in automated complexes of equipment for laboratory tests and tests under conditions of manufacture of welded shipbuilding panels.

Designed are the calculation algorithms and methods of determination of optimal parameters of thermal straightening of distortion deformations of axis of cylindrical shell allowing in-process obtaining of solution on the selection of parameters of thermal effect in the real time mode. The experimental approbation of thermal straightening general distortion deformations of a long axis of cylindrical shell and long screw shafts showed a high efficiency of the developed method.

V.Yu. Skulsky (PWI) defended thesis for a Doctor's degree on the subject «Weldability of Heat-Resistant Chromium Steels for Boiler Units of High Parameters».

The thesis is devoted to investigation of regularities of formation of a structure, properties of welded joints of chromium heat-resistant steels, nature of formation of cold and tempered cracks in welded joints of these steels and development of scientifically-grounded approaches towards technology of producing quality joints of welded pipe systems of boiler units of new generation with supercritical parameters of a steam for power units of thermoelectric power stations.

The concepts of influence of alloyed elements on the peculiarities of high-temperature $\delta \rightarrow \gamma$ transformation and phase composition of martensite chromium steels were expanded. It was shown that exclusion of

δ-ferrite formation and obtaining of one-phase martensite structure of complex-alloyed chromium steels (as conditions of providing their high technological properties and durable strength) is achieved at chromium content at the level of 8.15–9.75 % which is grounded by practicability of application of steels with 9 % Cr with alloying system 0.1C–9Cr–MoVNbNiN (type 10Kh9MFB). The peculiarities of phase transformations and formation of structure of welded joints of 9 % Cr steels under the conditions typical of arc welding are studied. It was established that increase in chromium content in heat-resistant steels (from 2.5 to 12 %) results in increase of stability of austensite in overcooling, decrease in temperature of martensite transformation (from ~450 up to ~280–230 °C) and increase in hardening level. The steels with 9 % Cr are prone to the formation of martensite (with hardness of ~450 *HV*) within wide range of cooling rates, which makes them hard-to-weld and prone to cold crack formation. The conditions of possible formation of δ-ferrite in welding of steels with 9 % Cr are established. It was shown that heterophase constitution of weld metal and fusion zone can arise in welding with increased heat input as a result of development of heterogeneous distribution of elements-ferritizers (Cr, Mo, V, Nb) and carbon (at liquation and high-temperature diffusion). The formation of δ-ferrite is caused by decrease in carbon content in welds (for example during its burning out in TIG welding), and also intensification of carbon diffusion from the base metal to a side of a weld with higher chromium content, that is typical of welding of joints of chromium and austenite steels by an austenite chromium-nickel weld. The latter phenomenon is excluded in use of nickel welding consumables. The principal approach to the technology of welding joints of martensite steels with 9 % Cr is the application of conditions with a decreased heat input. The regularities of formation of stress-strain state and formation of cold cracks in welded joints of hardening steels are studied. It was experimentally shown that main factor predetermining the tendency of martensite metal to cold crack formation is the degree of strengthening in hardening. Welding (shrinkage) stresses together with stresses from external loading is an additional factor initiating the fracture process. Using developed method the thermokinetic peculiarities of delayed fracture of welded joints were investigated. It was established that tendency to cold crack formation of welded joints of martensite steels is manifested at the temperature below ~140 °C; at 80–100 °C the joints have a minimal crack resistance that is determined by maximum rate of fracture process. Basing on dilatometric investigations of specimens of hardened steels (10/40Kh9MFB, 25Kh2NMFA, 38KhN3MFA) and determination of activation energy of development of deformations in the period of tests of crack resistance it is shown that revealed differences in resistance to cold cracks formation at different temperatures can be connected with different kinetics of development of low-temperature decay (tempering) of martensite. The appeared microstructural heterogeneity determines the nature of distribution of elastic-plastic deformations in volume of metal hardened in welding and probability of formation of microareas with high local stresses, density of dislocations and hydrogen concentration where fracture initiates and develops. At the high rate of decay (within the range of 80–100 °C) the conditions for local deformations in the zone of grain boundaries and rapid fracture are created. It is proved experimentally and theoretically that the high rate of martensite decay propagation in the volume of metal at increased temperatures and also evolution of diffusive hydrogen from a welded joint are the conditions of increase of resistance to a delayed fracture. It was shown that the presence of microstructural components (δ-ferrite), more tended to deformation, in initial hard martensite structure leads to decrease in crack resistance. The concepts of mechanism of tempering brittleness become more profound and factors are established defining the possibility of formation of cracks under conditions of high-temperature relaxation of stresses in welded joints of 9 % Cr steels. The effect of dispersion hardening within the range of ~400–550 °C is revealed, the reason of which can be the precipitation of chromium carbide M_7C_3. It was established that at the presence of δ-ferrite in the structure at tempering within the range of hardening the cracks can form. The condition of high resistance against cracks formation in tempering is the providing of homogeneous martensite structure. Basing on the study of kinetics of stress relaxation in the process of high-temperature tests it was established that to relieve inner stresses more completely the tempering of welded joints should be carried out at temperatures ~750–760 °C. The level of weld metal alloying by C, Mn, Ni was defined to provide its single-phase martensite structure and obtaining of required mechanical properties after tempering of welded joints. The recommendations to the conditions of submerged manual and automatic welding are experimentally and theoretically grounded. The conditions of achievement of high resistance of welded joints against delayed fracture using thermal influence on structural and hydrogen factors are determined (limit of cooling rate of HAZ metal of $w_{6/5} \leq 8$–10 °C/c, thermal relaxation at temperatures 160–200 °C) and providing of their required mechanical properties at heat treatment (high tempering at $T \approx 750$–760 °C during not less than 2 h). New welding electrodes ANL-8 are developed, the technical documentation on main technologies of welding of typical pipe joints is worked out. The pilot-industrial verification of welding technology was performed.

TECHNOLOGICAL SEMINAR OF DELORO STELLITE IN ZAPOROZHIE

Technological Seminar «Peculiarities of Application of Deloro Stellite Equipment and Materials in Aerospace Engineering and Turbine Construction» took place in Zaporozhie, Ukraine. It was organized by specialists of Deloro Stellite (Germany) and OJSC Motor Sich (Ukraine). Specialists of Deloro Stellite and Motor Sich, as well as 46 specialists representing aircraft repair and machine building enterprises of Ukraine, Russia and Belarus took part in the Seminar.

The Seminar was opened at the conference-hall of the «Dion» hotel on November 23 with presentation of a group of the Deloro Stellite companies made by E.M. Dubunina, manager of Deloro Stellite in CIS. It was noted that Deloro Stellite is a leading company having world name, centennial history and wide experience in the field of manufacture of parts from cobalt, nickel and iron based alloys: filler materials for cladding and spraying in the form of rods, electrodes, flux-cored wires and powders, cast parts and parts produced by powder metallurgy using customers' drawings, as well as equipment for plasma-powder cladding (PTA) and supersonic spraying (Jet Kote). The group of Deloro Stellite companies consists of 14 plants in Germany, Italy, France, England, India, USA, China, Canada and Russia, the headquarters being located in Koblenz (Germany).

Activities of Deloro Stellite are oriented to protection of surfaces of super heavy-duty metallic parts from complex wear. Alloys of the Company work well under severe conditions of the influence by several wear factors at a time, for example, high temperature and impact loads, corrosion, abrasive wear, cavitations and etc.

Repair and strengthening technologies of Deloro Stellite took firm positions in different industries from airspace engineering, power generation, automotive industry, nuclear power engineering, oil and gas production and chemical engineering to medicine, etc.

Aviation, cosmonautics and turbine construction are special industries, where, as a rule, the latest achievements in materials science, application of high technologies and modern equipment are concentrated. Being a world leader in the field of the improvement of wear resistance, Deloro Stellite gives special consideration to the industries where wear protection, service life and operational reliability of equipment are tightly interrelated.

Deloro Stellite offers a wide range of wear-, heat- and corrosion-resistant alloys. The Company has in its arsenal more than 500 alloys developed to address specific technical tasks. Properties of such alloys are determined by the hard phase of carbides, intermetallics, borides and other materials contained in a tough metal matrix.

The most widespread and extensively used are cobalt-based alloys of the Stellite® series, belonging to the Co–Cr–W–C group. These alloys retain their very high abrasive and corrosion resistance at elevated tem-

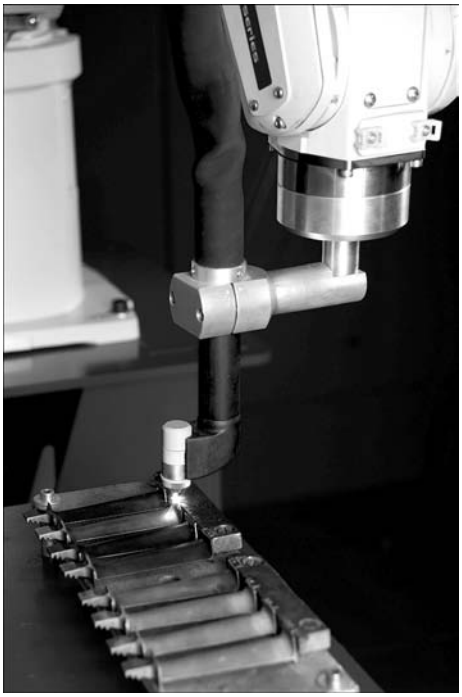

Robotic microplasma cladding of blades at «Motor Sich»

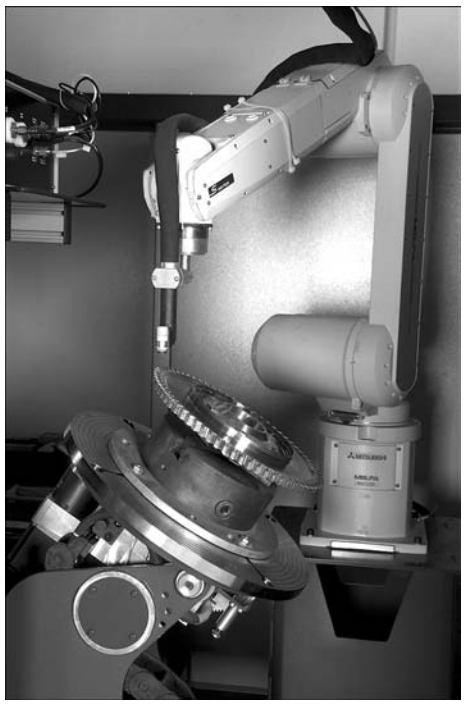

Robotic microplasma cladding of labyrinth disk at «Motor Sich»

Cladding of labyrinth disk

Weld beads on labyrinth disk

peratures and have excellent cavitation and erosion resistance, as well as high score resistance.

Deloro® series nickel-based alloys of the Ni–Cr–B–Si type provide good corrosion and abrasive wear resistance, and retain hardness at high temperatures, which in some cases allows using them instead of the Stellite® ones. These alloys are widely used for surfacing of industrial valves and elements of stop valves.

Tribaloy®, Stellite®, Deloro®, Nistelle®, Stelcar®, Jet Kote® and Delchrome® are covered by patents, and are the registered trade marks of Deloro Stellite. The Tribaloy® series cobalt-based alloys of intermetallic type contain the hard Laves phase distributed in a softer matrix of the eutectoid or solid solution type. These alloys are widely used in cases where dry metal to metal friction is combined with high temperature, corrosion and abrasive wear. The area of application is continually widening (automotive, aerospace, shipbuilding, etc.).

Nistelle® are nickel-based alloys developed for protection of surfaces from aggressive chemical environments. They also have high resistance to thermal and mechanical impacts.

Stelcar® type alloys are a mixture of carbide particles and self-fluxing nickel or cobalt powder. Because of their specific compositions, these materials are produced only in the form of composite powders for cladding and spraying.

Jet Kote® powders are applied for supersonic thermal spraying and produced in different combinations of mixtures of agglomerated and spheroidized powders, e.g. WC–Co, Cr_3C_2–NiCr, or of Stellite® and Deloro® alloys.

Delchrome® alloys are iron-based alloys. They are developed for cladding of parts working under abrasive wear conditions at low temperatures. Their corrosion resistance is relatively low, compared to cobalt and nickel alloys.

The Table gives generalized data for selection of one or other Deloro Stellite material, depending on the service conditions.

The experience accumulated by Deloro Stellite allows solving the problems of clients by selecting the required alloy or developing the new one for specific service conditions at a customer's request. For this the Company can offer manufacture of parts by the precision casting method, or it can offer a welding consumable (electrode, wire, rod, powder), necessary equipment and repair technology.

Deloro Stellite materials are used in repair and strengthening technologies by using the following methods:

- argon-arc/acetylene-oxygen cladding with rods;
- manual arc covered-electrode cladding;
- mechanized shielded-gas flux-cored wire arc cladding (MIG/MAG), submerged-arc cladding;
- plasma-powder cladding;
- laser cladding;
- flame spraying with further fusion;
- flame powder cladding;
- plasma spraying;
- supersonic flame spraying (HVOF, Jet Kote).

Selection of alloy	Alloy	Wear		
		Mechanical	Corrosion	High temperature
Low resistance +	Stellite	+++	+++	++++
	Deloro	+++	+	+
Satisfactory resistance ++	Tribaloy	+++	+++	++++
Good resistance +++	Nistelle	+	++++	+
	Delchrome	+++	+	+

The most efficient repair and strengthening technologies are based on utilization of plasma-powder cladding, i.e. PTA process, and supersonic spraying (Jet Kote).

The equipment for cladding and spraying, developed by Deloro Stellite, has a modular structure, which allows the required layout to be performed to address various practical tasks and meet requirements of a customer. For example, the robotic PTA unit for Motor Sich has the following technical capabilities and specifications:

- weld bead width — 1.2–5.0 mm;
- minimum thickness of a part — 0.8 mm;
- consistent weld bead size;
- automatic positioning of plasmatron;
- program control of all cladding parameters;
- two working positions for cladding;
- mains voltage — 3 × 400 V;
- welding current — 3–190 A;
- pilot arc current — 3–30 A;
- carrier gas flow rate — 0.5–5.0 l/min;
- shielding gas flow rate — 1.5–15.0 l/min;
- plasma gas flow rate — 0.2–5.0 l/min.

Units for supersonic spraying (Jet Kote) provide the process with minimum heating of a workpiece (cold hardening).

Utilization of agglomerated and spheroidized Deloro Stellite powders with a small amount of stellites allows achieving a high density of the surface with only 1–2 % porosity, the process characteristics being as follows:

- gas plasma jet velocity — 1500–2000 m/s;
- plasma temperature — 2700–3000 °C;
- powder particles flying velocity — 900–1200 m/s;
- spraying rate — 2–6 kg/h;
- flow rates of gases: natural gas — 100–150 l/min; oxygen — 220–330 l/min; nitrogen, argon — 25–40 l/min.

The latest supersonic spraying (HVOF) unit is operated at the venture company of Deloro Stellite and Russian partners — DS URAL Perm. The unit is robotized, having a capability of spraying of parts up to 10 m long and up to 4 t in weight.

Deloro Stellite continuously improves its products. New grades of alloys are developed, widening the technological capabilities of reconditioning of parts. This fact was told about at the Seminar by Prof. A. Pavlenko, manager of export to Europe and South-East Asia countries.

The Company offered a new process — high-temperature isostatic pressing, including heating of a cast part from the Deloro Stellite material up to a melting temperature and holding it under a super high pressure in a neutral medium. This treatment removes casting microdefects and consolidates the material, imparting it new characteristics.

700 series of Stellite alloy, doped with molybdenum instead of tungsten, was developed. It results in a higher wear resistance and corrosion resistance without reduction of hot hardness.

The Seminar was continued on November 24 at the Motor Sich Zaporozhsky plant, which was founded in 1907 and is today one of the world-biggest plants manufacturing aircraft engines. Motor Sich engines are operated in more than 100 countries of the world; every tenth aircraft and every fourth helicopter in the world is equipped with the Motor Sich engines. Products of the plant are certified by Bureau Veritas ISO 9001–2000.

Units with specific characteristics to address the problems of repair and strengthening of super thin and small parts in aerospace engineering and power generation were developed in 2007 after four years of scientific-and-technical cooperation of the specialists of Motor Sich and Deloro Stellite. In the same year, the units were supplied to a customer, and a section

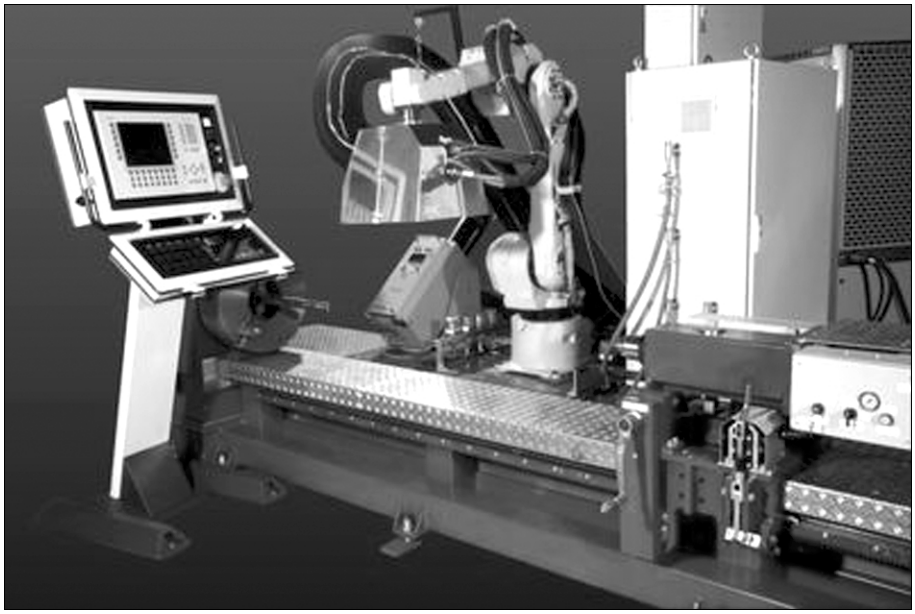

Jet Kote unit for supersonic spraying

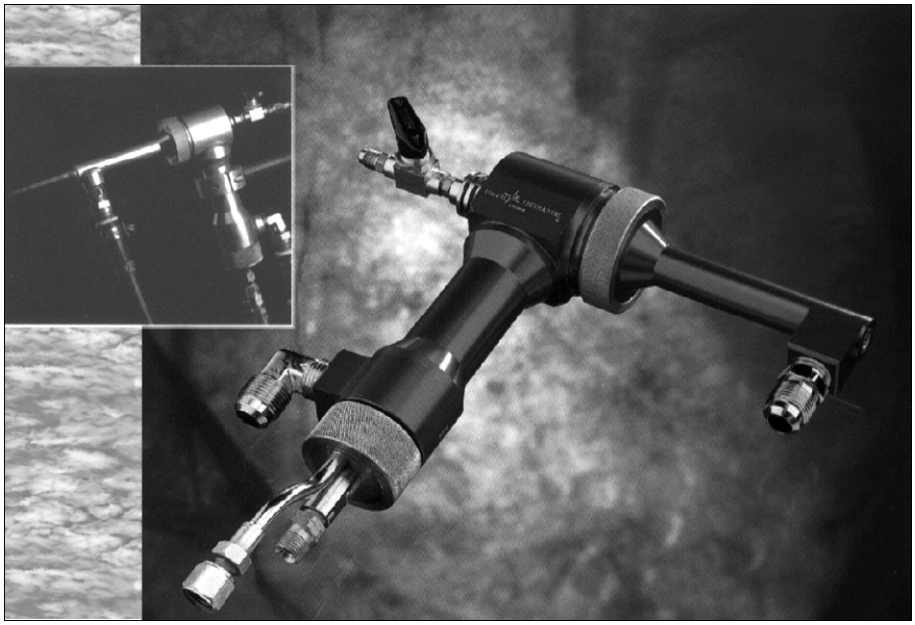

Gun for supersonic spraying

for repair of blades and disks of gas turbine engines was arranged at the plant.

Earlier, the blades were repaired at the plant by manual argon arc cladding using rods. According to I.A. Petrik, Chief Welder of Motor Sich, it took a week to clad one disk by the manual argon arc method at a rather low quality, up to 20 % of clad products were rejected (cracks, etc.). A change of the repair technology from manual argon-arc to plasma-powder allowed improving the quality and efficiency of repair. The units were repaid for two years. At present, domestic powders JS-32 and JS-6 produced by UkrNII-SpetsStal (Zaporozhie), as well as powders V3K and Stellite® produced by Deloro Stellite are used for plasma-powder cladding. The experience of utilization of the above powders showed their high quality. I.A. Petrik indicated the following advantages of the plasma-powder cladding process: low base metal with cladding alloy dilution, low temperature distortions of workpieces, decrease in the amount of machining after cladding, reduction of losses of filler powder, high repeatability of the cladding process, and easy automation. Some disadvantages were also noted: difficulties in using some types of powder in one work shift, as it is necessary to refill the powder feeder, which increases downtime of the equipment; cladding can be well performed on edges and worse — on plane surfaces; it is better to perform cladding in a vertical position.

Answering questions asked by the Seminar participants, E.M. Dubunina informed, in particular, that the Deloro Stellite PTA units can be equipped with the two feeders for different powders, which can significantly speed up changing of the powders; the angle of inclination of the plasmatron from a vertical line can be changed up to 45° and more; and cladding, if necessary, can be performed in the overhead position.

A storehouse of Deloro Stellite for direct sales to clients in the CIS countries was opened in Moscow in October 2009. GRIK Ltd. (Kiev), being a representative of Deloro Stellite in Ukraine for 10 years now, sells the Deloro Stellite goods in Ukraine.

In conclusion, participants of the Seminar pointed out that advanced technologies of Deloro Stellite can well address the problems of manufacture and repair of parts for aircraft engineering and turbine building, providing good technical and technological characteristics, and proved expediency of application of the Deloro Stellite equipment at enterprises of the aircraft and power generation complexes of Ukraine, Russia and Belarus.

Dr. A.T. Zelnichenko,
Prof. V.N. Lipodaev, PWI

4th INTERNATIONAL SEMINAR «NEW DIRECTIONS OF RESEARCH IN THE FIELD OF HIGH-FREQUENCY ELECTRIC WELDING OF SOFT LIVE TISSUES»

On November 23, 2009 the 4th International Seminar on «New Directions of Research in the Field of High-Frequency Electric Welding of Soft Live Tissues» was held in Kiev at the E.O. Paton Electric Welding Institute of NASU. More than 60 persons (doctors of surgical profile, veterinary surgeons, and specialists on medical equipment) from Ukraine, Russia, Belarus and the USA participated in it. The Seminar organizers were PWI and International Association «Welding» (IAW).

Opening the Seminar, Prof. B.E. Paton noted that its objective is exchange of general information on the achieved results in the field of high-frequency welding of soft live tissues and jointly overcoming the bottlenecks in application of this technology. The near-term goals are development of higher quality certified equipment and tools, organizing surgeon training, continuation of research and application of the technology in new areas of surgery.

During almost nine years of application of the technology of high-frequency electric welding of soft live tissues in practical surgery in Ukraine more than 50,000 operations have been performed in 80 clinics, and about 100 new surgical procedures have been developed.

Technology of high-frequency electric welding of soft live tissues is protected by patents of Ukraine, Russia, USA, Australia, European Union, Canada, China and Japan. Permissions were obtained for clinical application in Ukraine, Russia, USA and countries of the European Union. Our dream and near-term goal is fitting every surgical ward in Ukraine with equipment for welding live soft tissues; considering that there are 9,000 surgeons and about 27,000 beds in the surgical wards in Ukraine, it is necessary to annually manufacture up to 1000 EK-300M1 units with different sets of bipolar welding tools. This means that a transition from small-batch to large-batch manufacturing of equipment and tools is required.

Seminar session in progress

Let us note some of the speeches. In his presentation Prof. G.S. Marinsky (PWI) gave a retrospective analysis of the equipment and bipolar welding tools for welding soft live tissues, manufactured by PWI and IAW. Presentation of Dr. O.N. Ivanova (IAW) and D.D. Kunkin (PWI) was devoted to development of devices for recording the electric parameters in welding live tissues in order to analyze their influence on welded joint quality and selection of control algorithm of this process. In the presentation of Prof. S.E. Podpryatov (PWI/KCCH #1, Kiev) it was noted, in particular, that strength of the joint in electric welding is achieved due to welding of muscle tissues to each other and creation of new joints of collagen fibres. Performance of electric welding of various soft live tissues requires a certain combination of the value (and shape) of electric current, degree of tissue heating and pressure on the tissues. Presentation of M.P. Zakharash, Corresp. Member of AMSU (O.O. Bogomolets National Medical University, Kiev) dealt with the issues of application of electric welding technology in surgeries on patients with mechanical jaundice. Presentation of E.Yu. Aktan (Taras Shevchenko National University, Kiev) highlighted the issues of application of biophysical effects in electric welding of soft live tissues and prospects for their application in surgical practices and provided a classification of structural changes in biological tissues depending on temperature (40–45 °C — cell loss, 60–80 °C — protein denaturation, except for collagens, 80–100 °C — collagen denaturation, above 100 °C — dehydration and coagulation of the tissue). It is shown that investigation of structural changes in the collagen component during welding enables assessment of the effectiveness of the electric welding method compared to laser welding. A.F. Vozianov, academician of AMS (Institute of Urology of AMS of Ukraine, Kiev) spoke about the prospects for application of electric welding technology in urology. G.V. Bondar, academician of AMS (Donetsk Regional Antitumour Center) noted that it is very difficult to change technology in medicine, but the technology of electric welding of soft live tissues provides a significant shortening of surgery duration, reduction of blood loss, absence of either sutures or post-operation complications, high degree of tissue regeneration, etc., which, in its turn, stimulates the surgeon to quickly master the technology.

Donetsk Regional Antitumour Center has 25 operating rooms and EK-300M1 units are installed in 12 of them, and the technology is used in almost all the operations, except for lung surgery. Among the disadvantages of the technology, G.V. Bondar noted an absence of a wide range of bipolar welding tools, both as to their purpose and typesize. Yu.A. Zozulya, academician of AMS (Institute of Neurosurgery of AMS of Ukraine, Kiev) spoke about the prospects for application of electric welding technology in neurosurgery: for stopping parechymatous bleeding from brain tissue, for sealing brain system after tumour removal, for sealing the meninges.

Two presentations by V.A. Naumenko (V.P. Filatov Institute of Eye Diseases and Tissue Therapy of AMS, Odessa) were devoted to application of high-frequency electric welding technology in treatment of eye diseases, in particular, in retinopexy (retinal detachment) and eye enucleation. It is proven that application of high-frequency electric welding in eye enucleation allows preventing blood loss when crossing muscles and neurovascular bundle and achieving the necessary fastening of the muscles to Tenon's capsule and reliable joining of the conjunctiva edges to each other without suture application. In eight cases of retinopexy the chorioretinal commissure made by electric welding method, prevented development of retinal detachment beyond the experimental area. In one case separation of the retina on the boundary of chorioretinal site was noted (chorioretinal commissure made by laser coagulation, turned out to be untenable on all the eyes).

Discussion during the Seminar: *standing from left to right* Profs. M.E. Nechitajlo (A.A. Shalimov National Institute of Surgery and Transplantology) and G.V. Bondar (Donetsk Regional Anitutmour Center)

In conclusion Prof. B.E. Paton noted that many problems of the technology of electric welding of live tissues have already been solved, and this technology is already quite well-established in surgery, but there are still many tasks ahead of us. These are setting up large-scale production, manufacturing of competitive power sources and tools, certification of European level production, provision of guarantee and after-sale service, organizing surgeon training, etc.

Dr. A.T. Zelnichenko, PWI

FORUM-SEMINAR OF LIMITED LIABILITY COMPANY «BINZEL UKRAINE»

«Binzel Ukraine GmbH», which is part of the ABICOR BINZEL-group (Germany), hosted the Forum-Seminar of the Company's partners in Kiev on the 17th of December. The Seminar was arranged by Yu.A. Didus, Director General of the Company, and managers. It was attended by over 20 specialists representing trade subsidiaries of «Binzel Ukraine», as well as exclusive partners (distributors) from a number of cities and regions of Ukraine.

Agenda of the Seminar included discussion of the cooperation results in the current year, analysis of quarterly sales in 2009, their progress trends for 2010 and different factors affecting the progress, as well as presentation of new products of the ABICOR BINZEL brand, which were demonstrated in September at the «Schweissen und Schneiden 2009» Fair in Essen (Germany).

The volume of sales of the ABICOR BINZEL™ products in Ukraine was continuously growing, and at high rates, up to 2007. Actually, it doubled from year to year. This trend got broken during the economic crisis. A marked recession in sales occurred in 2008. However, positive changes in the economy of Ukraine in the second half of 2008 and active efforts of the Company allowed it to achieve the sales of a level of 2007 by the end of 2009. This was favoured to a considerable degree by the aggressive activity of external services of «Binzel Ukraine» and high investments in them.

Expectations of «Binzel Ukraine» concerning sales in 2010 are rather optimistic. They are based in many respects on appearance of new innovative products of the ABICOR BINZEL trademark on the Ukrainian market as early as in the first quarter of 2010. Among them are the following products: in the MIG/MAG segment — a new generation of torches ABIMIG® GRIP and ABIMIG® GRIP A in a set with a new generation of hose pack Low-Weight Bikox®, in the TIG segment — a new generation of torches ABITIG® GRIP and ABITIG® GRIP Little, in the line of welding post components — new product BFR (tester for forced cooling units and welding torches with liquid cooling), in the plasma cutting segment — a new generation of plasma torches ABICUT, and in the automation segment — robotic welding torches ABIROB® W.

The Seminar also comprised presentation of German Company «JAECKLE Schneid- und Schweisstechnik», which is specialising in production of a wide range of welding equipment, as well as air-plasma cutting devices. The latter are equipped with the ABICOR BINZEL™ plasma cutters.

Demonstration of the air-plasma cutting devices in operation was arranged at the end of the Seminar, and attendees were given the possibility to try them out and learn about peculiarities of their application.

The Seminar participants expressed their gratitude to the organisers for excellent conditions and effective program of the event.

Dr. A.T. Zelnichenko,
Prof. V.N. Lipodaev, PWI